METEOR-Berichte

FUNCTIONING OF LARGE FLUID ESCAPE SYSTEMS

Cruise No. M87/2

May 5 – May 27, 2012

Reykjavik (Iceland) – Stavanger (Norway)

C. Berndt

Editorial Assistance:

DFG-Senatskommission für Ozeanographie
MARUM – Zentrum für Marine Umweltwissenschaften der Universität Bremen

2014

The METEOR-Berichte are published at irregular intervals. They are working papers for people who are occupied with the respective expedition and are intended as reports for the funding institutions. The opinions expressed in the METEOR-Berichte are only those of the authors.

The METEOR expeditions are funded by the *Deutsche Forschungsgemeinschaft (DFG)* and the *Bundesministerium für Bildung und Forschung (BMBF)*.

Editor:
DFG-Senatskommission für Ozeanographie
c/o MARUM – Zentrum für Marine Umweltwissenschaften
Universität Bremen
Leobener Strasse
28359 Bremen

Author:
Prof. Dr. Christian Berndt
GEOMAR
Wischhofstraße 12,
24148 Kiel

Telefon: +49 431 600 2273
Telefax: +49 431 600 2922
e-mail: cberndt@geomar.de

Citation: C. Berndt (2014) FUNCTIONING OF LARGE FLUID ESCAPE SYSTEMS - Cruise No. M87/2 – May 5 – May 27, 2012 – Reykjavik (Iceland) – Stavanger (Norway). METEOR-Berichte, M87/2, 87 pp., DFG-Senatskommission für Ozeanographie, DOI:10.2312/cr_m87_2

ISSN 2195-8475

Table of Contents:

List of abbreviations:

DASI	Deep-towed Active Source Instrument
CSEM	Controlled-Source ElectroMagnetics
EM	ElectroMagnetic
HyBIS	Hydraulic Benthic Interactive Sampler
LEMUR	Low-frequency ElectroMagnetic Underwater Recorders
OBEM	Ocean Bottom ElectroMagnetic receiver
OBS	Ocean Bottom Seismometer
Sputnik	Electrical dipole transmitter
USBL	Ultra Short Base Line
VULCAN	Deep-towed electromagnetic receiver

1 Summary

M87/2 COSY set out to investigate the geological processes that may cause significant migration of carbon from the subsurface into the ocean and ultimately into the atmosphere. Understanding these processes is fundamental for understanding episodic climate forcing by geological processes, for assessing the role that subsurface fluid migration plays for slope stability, and for assessing the economic potential of hydrate-bearing sediments as a future energy source. As such the cruise contributed mainly to two scientific projects: the Excellence Cluster Future Ocean and here in particular the sub-project Ocean Controls, and the BMBF-funded project Sugar2.

The two main objectives of the cruise were (1) to find out if the Giant Gjallar Vent on the north-western Vøring Margin can serve as a window to the deeper structures of the Vøring Basin, which were strongly influenced by hydrothermal activity related to break-up volcanism, and (2) to provide a controlled-source electromagnetic (CSEM) data set in an area where co-existing 3D ocean bottom seismometer data exist.

We managed to achieve both objectives. Although we did not manage to collect a high-resolution 3D seismic data set because of technical problems in the beginning of the cruise and adverse weather conditions later on, we can now show that the Giant Gjallar Vent is still active to some extent, but much less than hoped before the cruise. The main phase of activity, which generated the present seafloor morphology, must have occurred during deposition of the late Kai Formation. The rugged seafloor has been draped by hemipelagic sediments ever since. However, there are strong indications for ongoing neotectonic activity, significant accumulation of free gas below the Top Kai horizon, and minor evidence for formation of seepage-related authigenic carbonates.

We also achieved the second objective of collecting a benchmark dataset of different types of controlled source electromagnetic data. We surveyed a pipe structure called CN03 which is located in the Nyegga area on the northern flank of the Storegga Slide, and which is characterized by high hydrate concentration at approximately 300 mbsl. In this area we collected high-resolution EM data with Sputnik and deep-penetration EM data with DASI as well as towed, continuously recording surface data with VULCAN. These data will keep a generation of marine electromagnetic geophysicists busy until all ways have been found to invert them jointly with the existing 3D P- and S-wave data for determining the hydrate and free gas distribution in the top 300 m of sediments.

Additionally, we managed to carry out a detailed survey of sea floor crevasses on the northern sidewall of the Storegga Slide. The excellent sub-bottom sediment profiler records obtained with the Parasound system strongly indicate very recent, i.e. post-Storegga Slide, deformation of the northern sidewall of the Storegga Slide. Although it was not possible to prove unequivocally this late age of activity by a HyBIS video survey that we carried out for this purpose, the Parasound data are strongly indicative of this late phase of activity. The high-resolution seismic, multibeam bathymetry, Parasound, and video dataset that we managed to acquire provide deep insight into the ways that continental margins fail due to gravitational forces.

Zusammenfassung

Gegenstand der auf der Ausfahrt M87/2 COSY durchgeführten Arbeiten sind die geologischen Prozesse, die große Mengen Kohlenstoff aus dem Meeresboden in die Wassersäule und weiter in die Atmosphäre transportieren können. Das Verständnis dieser Prozesse ist grundlegend für die Einschätzung, wie geologische Prozesse zeitweise das Klima verändern können, wie stabil untermeerische Hänge sind und ob Gashydrate in der Zukunft als Energiequelle genutzt werden können. Die Arbeiten tragen zu zwei Großprojekten bei: zum einen zum Kieler Exzellenzcluster Ozean der Zukunft und darin zum Forschungsthema Ocean Controls und zum anderen zum BMBF-finanzierten Projekt Sugar 2.

Die beiden Hauptziele der Ausfahrt waren (1) herauszufinden, ob der Giant Gjallar Vent am nordwestlichen Vøring-Kontinentalrand als ein Fenster in die während der Öffnung des Nordatlantiks stark durch Vulkanismus geprägten unteren Stockwerke des Vøring Beckens dienen kann, und (2) die Erhebung eines elektromagnetischen Datensatzes (CSEM) in einem Gebiet, für welches ein drei-dimensionales Netz von Ozeanbodenseismometer-Daten existiert,

Beide Arbeitsziele wurden erreicht. Obwohl wir es wegen technischer und wetterbedingter Probleme nicht schafften, einen 3D-seismischen Datensatz aufzunehmen, können wir doch mit den gewonnenen Daten zeigen, dass der Giant Gjallar Vent noch aktiv ist, aber sehr viel weniger als erwartet. Die Hauptphase seiner Aktivität scheint sich mit der Ablagerung der oberen Kai-Formation zu schneiden und muss als Ursache der heutigen Meeresbodentopographie gelten. Die damaligen Meeresbodenversätze wurden im Nachhinein von hemipelagischen Sedimenten überdeckt. Es gibt jedoch auch Hinweise auf neotektonische Aktivität und signifikante Ansammlungen von freiem Gas, das sich unter der Naust-Formation gesammelt hat. Am Meeresboden gibt es schwache Indikatoren für rezenten Fluidaufstieg.

Wir erreichten auch das zweite Ziel der Ausfahrt, die Erhebung verschiedener elektromagnetischer Daten, deren Kombination der Standard für zukünftige elektromagnetische Experimente werden dürfte. Wir haben die Fluidaustrittsstruktur namens CN03 untersucht, die sich in der Nyegga-Gegend am nördlichen Rand der Storegga-Rutschung befindet. In dieser Gegend findet man ausgeprägte geophysikalische Hinweise auf Gashydrat in etwa 300 m Tiefe unter dem Meeresboden. Hier haben wir hochauflösende elektromagnetische Daten mit dem Sputnik-System, sowie Daten mit höherer Eindringung mit dem DASI-System aufgenommen. Zusätzlich wurden noch dauerhaft die DASI-Signale mit dem VULCAN-System gemessen, welches hinter DASI hergeschleppt wird. Mit diesem Datensatz dürften sich die Konzentrationen von Gas und Gashydrat sowie deren Verteilung in den oberen 300 m unter dem Meeresboden bestimmen lassen.

Desweiteren waren wir in der Lage, eine detaillierte Studie von Meeresbodenspalten am Nordrand der Storegga-Rutschung durchzuführen. Die hervorragenden Sedimentecholot-Daten des Parasound-Systems zeigen jüngste Aktivität dieser Verwerfungen, die vermutlich noch jünger als die Storegga-Rutschung ist.

2 Participants

Name	Discipline	Institution
Berndt, Christian, Prof. Dr.	Chief Scientist	GEOMAR
Berndt, Holger	P-Cable	VBPR
Chi, Wu-Cheng, Dr.	Seismologist	SINICA
Couillard, Melanie	Sedimentology	UMont
Crutchley, Gareth, Dr.	Leader P-Cable	GEOMAR
Dumke, Ines	P-Cable	GEOMAR
Eckardt, Thomas	Watch keeper	GEOMAR
Hölz, Sebastian, Dr.	CSEM	GEOMAR
Hühnerbach, Veit	HyBIS	NOCS
Jegen-Kulcsar, Marion, Dr.	Leader CSEM	GEOMAR
Karstens, Jens	P-Cable	GEOMAR
Käufl, Johannes	Watch keeper	KIT
Kiyan, Tarik	Watch keeper	GEOMAR
Lettmann, Arno	Bathymetry	GEOMAR
Lüdemann, Moritz	Watch keeper	GEOMAR
Marín Moreno, Hector	CSEM	NOCS
Matthiessen, Torge	Seismic technician	GEOMAR
Mazzini, Adriano, Dr.	Sedimentology	UiO
Mickoleit, Anett	Meteorology	DWD
Raeke, Andreas	Meteorology	DWD
Sinha, Martin, Prof.	CSEM	NOCS
Sommer, Malte	CSEM	GEOMAR
Tan, Ian	CSEM engineer	GEOMAR
Weitemeyer, Karen, Dr.	CSEM	NOCS
Wetzel, Gero	Electronic engineer	GEOMAR
Wollatz-Vogt, Martin	CSEM engineer	GEOMAR

GEOMAR	GEOMAR | Helmholtz Centre for Ocean Research Kiel Marine Geodynamics, Wischhofstr. 1-3, 24148 Kiel, Germany
NOCS	National Oceanography Centre, University of Southampton European Way, Southampton, SO14 3ZH, U.K.
VBPR	Volcanic Basin Petroleum Research, Oslo Forskningsparken, Gaustadalleen 21, 0368 Oslo, Norway
UiO	University of Oslo Institute of Geology, Sem Saelandsvei 1, 0316 Oslo, Norway
UMont	University of Montpellier 2, Geosciences Montpellier, Place E. Bataillon, 34095 Montpellier, France

KIT	Karlsruhe Institut für Technologie Geophysikalisches Institut, Hertzstr. 16, 76187 Karlsruhe, Germany
SINICA	Academia Sinica Institute of Earth Sciences, 128 Academia Road, Taipei, Taiwan
DWD	Deutscher Wetterdienst Bernhard-Nocht-Straße 76, 20359 Hamburg, Germany

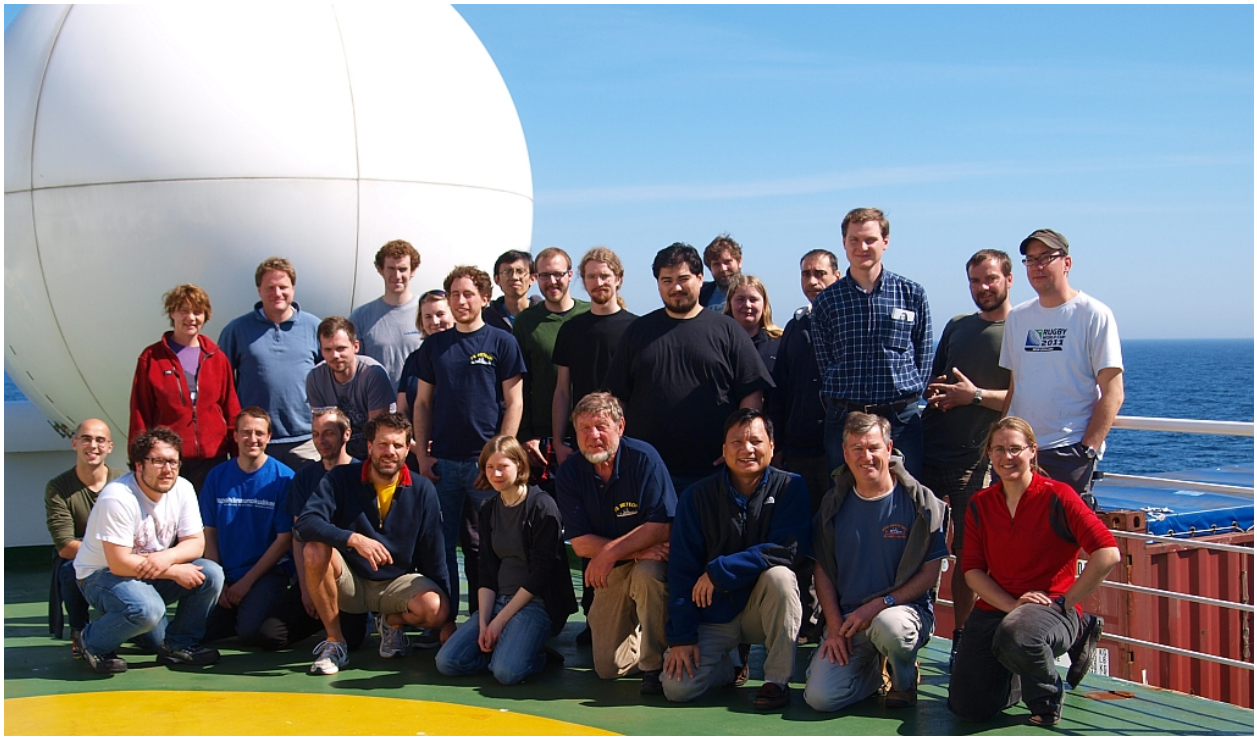

Fig. 1.1 Cruise participants.

3 Research Program

The amount of carbon entering the ocean and atmosphere from underneath the seafloor is one of the greatest uncertainties in modelling the global carbon cycle on geological time scales. Although the present day rates of carbon flux from the seafloor into the atmosphere seem to be small (Schmale et al., 2005) there is geological evidence that there were episodes in the Earth's history when these rates were significantly higher and have in fact caused rapid global warming (Zachos et al., 2001, Svensen et al., 2004).

Understanding large-scale fluid escape systems is also important for other reasons. The amount of carbon injected into the ocean can be quite large (> 2000 Gt within a few thousand years). This compares to a total carbon content of the ocean of approximately 40,000 Gt. Clearly, such sources have to be taken into consideration for an assessment of ocean oxygen starvation and ocean acidification in times of increasing carbon dioxide concentration in the ocean if one wants to put the anthropogenic carbon input into perspective of natural carbon fluxes. As the geological record indicates large variability in these sources they have to be firstly understood and secondly included when modelling the ocean's carbon cycle and possible feedback mechanisms between outer forcing and the response of the ocean.

Investigating natural fluid seeps also opens a window into the deep parts of sedimentary basins which is crucial for determining the geological processes deep within the Earth for example in subduction zones (Wallmann et al., 1997) or on passive margins (Hensen et al., 2004). For this it is crucial to be able to separate the signal produced in the uppermost sediments for example by biogenic gas production from the signals from deep below for example by diagenesis or by hydrothermal activity. This is only possible if the physical processes active in the vent systems are well constrained.

The processes associated with cold seeps such as gas hydrate formation and dissociation can create overpressured shallow gas pockets, which cause serious problems for offshore construction and exploration. Therefore further constraints on the underlying processes can facilitate safer and more economic exploitation of offshore resources. Hydrates are widespread in frontier hydrocarbon exploration provinces in deep water on continental margins, such as the Gulf of Mexico, and energy companies are increasingly drilling deepwater wells that must safely penetrate (or avoid) regions where hydrate is present to reach deeper targets. Perturbations to pressure and temperature conditions might provoke hydrate dissociation, and gas may be trapped at the base of the hydrate stability zone. Both may lead to unexpected flows into boreholes, causing costly delays, loss of the hole, or even danger to sea surface facilities through loss of buoyancy (Hovland and Gudmestad, 2001). Furthermore, dissociation of hydrate near the sea bed could lead to loss or damage of seafloor infrastructure. These hazards remain during ongoing production, because warm fluids from deep reservoirs may also destabilise hydrate. Standard industry practise has been strict avoidance of areas of hydrate hazard, but such an approach is becoming expensive. In the longer-term, methane in hydrate is also a potential energy resource in itself, and national research programs in hydrocarbon-poor countries such as Japan and India are focused on the exploitation of this resource.

The way in which large amounts (> 2000 Gt) of carbon can enter the atmosphere over short geological time scales is unclear and the hypotheses that have been proposed include rapid gas hydrate dissociation, volcanic intrusions into sedimentary basins, large-scale oxidation of sea floor through landslides or tectonic movements (Higgins and Schrag, 2006 for a review).

The most likely explanation seems to be the mobilization of hydrates as hydrate stability depends primarily on pressure and temperature and both can fluctuate rapidly. Methane hydrates form by the inclusion of methane molecules in an ice-like substance and are stable in the upper few tens to hundreds of metres of seafloor sediments in water depths greater than ~500 m. If the sea level drops or the bottom water temperature rises hydrates will start to dissociate and release the captured methane. Many hydrate provinces are characterised by gas seeps at the sea bed as a

result of methane migration. It is, however, not clear how the methane may migrate through the still existing hydrate stability zone as the gas should form new hydrate further up in the section. Several hypotheses have been proposed including temperature anomalies in the sub surface (Wood et al., 2002), salinity anomalies in the pore water (Hovland and Svensen, 2006), and dry chimneys in which the water saturation is too low to form hydrate (Westbrook et al., 2008). The first goal of the cruise was to find out which of these hypotheses is correct, because each of these processes is associated with very different rates of possible methane release to the water column. Whereas the thermal anomaly model is inherently unstable and would only allow release of carbon over short times, and the salinity anomaly model would result in relatively small advection rates due to mixing, the "dry chimney" model could potentially release very large amounts of methane only limited by the supply of gas from underneath.

The presence of hydrate within seafloor sediments causes an increase in both the bulk modulus, and hence the seismic velocity, and in the electrical resistivity. The presence of gas reduces the velocity and increases the resistivity. Seismic velocities may be measured by conventional ocean bottom cable methods (Andreassen et al., 2003) or using networks of autonomous ocean bottom instruments (Westbrook et al., 2008). The measurement of sub-sea bed electrical resistivity using marine controlled source electromagnetic techniques (CSEM) was originally pioneered in several academic institutions, including the University of Southampton, and is now a multi-million-pound industry, with a major role played by the Southampton spin-off company Offshore Hydrocarbon Mapping (OHM) Ltd. Both seismic and controlled source electromagnetic methods can and have been used to estimate hydrate and gas content (Westbrook et al., 2008; Weitemeyer et al., 2006; Schwalenberg et al., 2009a,b). However, both the seismic velocity and the electrical resistivity are sensitive also to a range of other parameters such as lithology, porosity and pore fluid salinity. Because the sensitivities are different for the two properties, determination of both velocity and resistivity for the same volume of sea bed provides a powerful tool for distinguishing the contribution of hydrate or gas from that of other parameters. Ellis et al. (2008) have developed a joint effective medium theory that allows us to invert measurements of seismic velocity and resistivity to determine hydrate and gas content. This effective medium theory will be the basis for the development of a joint inversion of CSEM and seismic data for which we have been funded through the BMBF Sugar 2 project. The second goal of the cruise was to collect a CSEM data set that can be converted jointly with the existing ocean bottom seismic data that we collected within the HERMES project at Nyegga (Fig. 1.2) to find out to what extent the quantification of gas hydrate can be improved by a joint inversion.

While hydrate dissociation seems to be the most probable explanation for large-scale carbon injection into the atmosphere during the Early Eocene, it has also been proposed that intrusive volcanic activity during the emplacement of large igneous provinces may result in the release of significant amounts of carbon (Svensen et al., 2004). During the opening of North Atlantic, volcanic intrusions affected a wide area around the break-up axis. Above the more shallow intrusions hydrothermal vent systems developed that facilitated ascent of carbon-rich pore waters to the sea bed. Such hydrothermal vent sites exist also in other large igneous provinces where it is possible to sample them in the field. Studies in the Karoo Basin have shown that the feeder systems consist of fractured host rock that was exposed to secondary high-temperature carbonate cementation (Svensen et al., 2006). On the mid-Norwegian margin alone more than 700 of these structures have been discovered yielding a total of 300-2700 Gt of carbon that was released to the atmosphere during the duration of the volcanism. Extrapolating this to the entire North Atlantic easily yields carbon volumes that would explain the Early Eocene Thermal Maximum, provided that the intrusions were emplaced during a short time. The seismic data seem to suggest this (Planke et al., 2005), but drilling is required for better dating. The seismic data indicate that most of the hydrothermal vent systems on the mid-Norwegian margin were short-lived phenomena. They consist of a feeder system rising from the sill intrusion to the paleo-sea bed where they frequently terminate in mound-like structures or craters. The third objective of the

cruise is to investigate one of these structures - the Giant Gjallar Vent at the Gjallar Ridge (Fig. 1.2) that must have been active to the recent past (Gay et al., 2012), and find out if it can be used as a geological window to the deep parts of the Vøring Basin. If that was the case future geochemical surveys could be carried out to this site to constrain the amount and timing of carbon release from the Early Eocene to today.

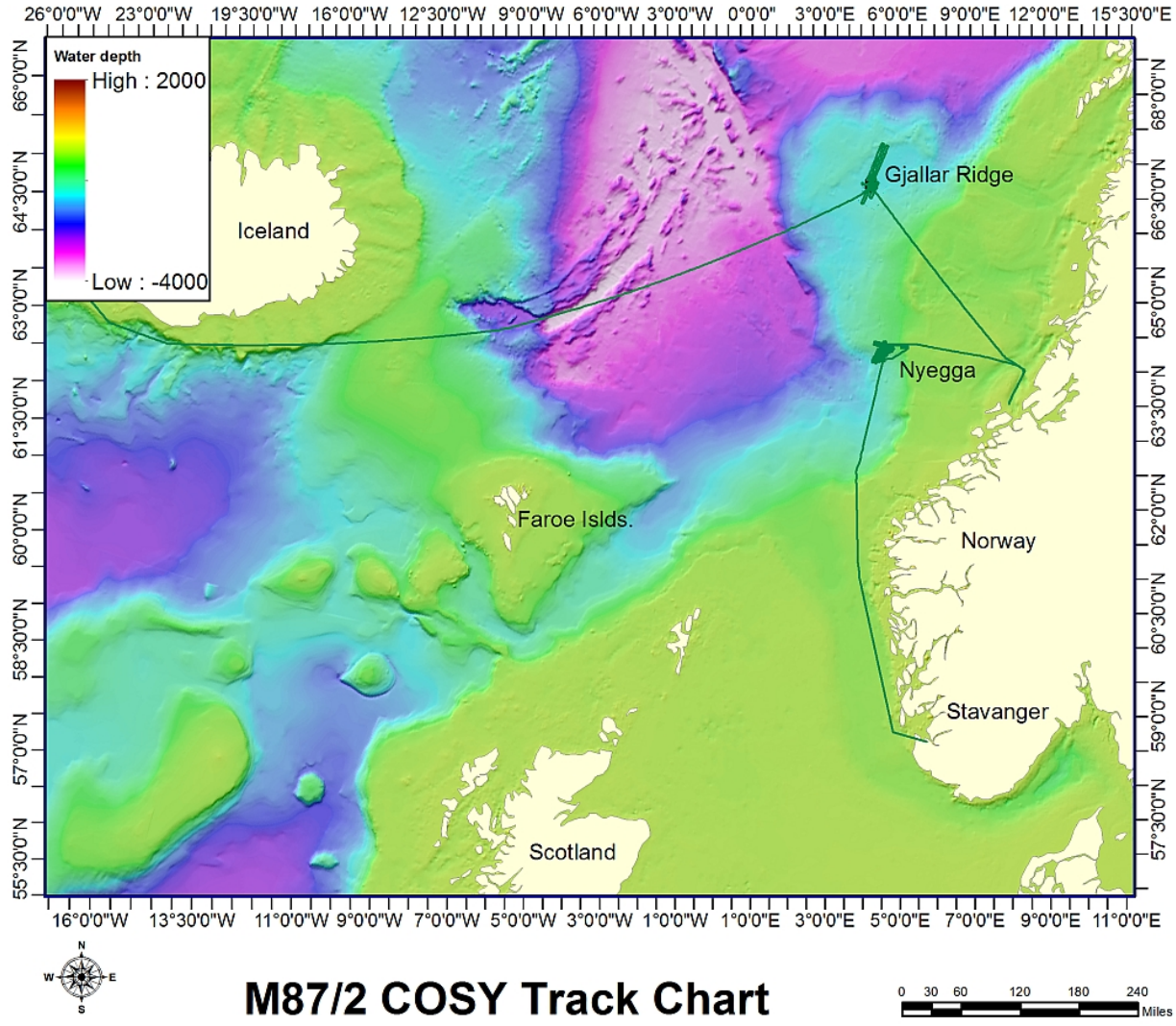

Fig. 1.2 Cruise M87/2 started from Reykjavik, Iceland on May 5th, 2012 and finished in Stavanger, Norway on May 27th, 2012. The main working areas are the Gjallar Ridge and Nyegga on the southern Vøring Plateau.

4 Narrative of the Cruise

Saturday May 5th, 2012

On May 5th, 2012 we left Reykjavik under a clear blue sky with fresh northerly winds. With the large amount of equipment to set up, everybody was busy preparing the scientific instruments. In particular the fibre optic connection between the friction winch and the DASI power supply required significant attention. Due to favourable weather forecasts we decided to sail first to the northern working area on the Gjallar Ridge in the western part of the Vøring Plateau.

Sunday May 6th and Monday May 7th, 2012
During May 6th and May 7th the transit continued without interruptions with 2 m swell and moderate northerly winds. The time was used to assemble the scientific equipment and set up the laboratories.

Tuesday May 8th, 2012
Upon arrival in the study area 1 (Gjallar Ridge, Fig. 1.2) on Tuesday, May 8th at 16:00 UTC we conducted releaser tests. First we tested the GEOMAR releasers in a steel basket and then the NOC releasers in a custom made frame. This was followed by sound velocity profile taken by the ship's crew to calibrate the multibeam echosounder. After set up of the multibeam and the Parasound system we deployed 2 ocean bottom seismometers in the southern and northern end of the planned 3D seismic cube. At 23:00 we started deployment of the P-Cable system in excellent weather conditions.

Wednesday May 9th, 2012
Deployment of the P-Cable system was completed after 3.5 hours and shooting of seismic lines began at 3 am on Wednesday, May 9th. At 07:15 something got caught in the streamer and shooting had to be discontinued. Recovery of the data cable and inspection of the seaward router and the first T-junction of the cross-cable revealed bending of the data cable at the connection point with the cross-cable and the first part of the cross-cable was replaced. After initial problems with the airguns the system was started again at 13:00 but broke down another time at 13:45. The entire system was recovered for a full inspection. Surveying with multibeam echosounder and Parasound continued and the course was changed to collect a dense grid of Parasound lines across the Gjallar Vent and then to a wider spread to obtain maximum coverage with the multibeam system.

Thursday May 10th, 2012
After finishing the multibeam transect at 13:00 we redeployed the repaired 3D seismic system. Deployment took approximately 3 hours and at 16:00 the system was working fine. However, after approximately 15 minutes seismic recording stopped again with a technical failure of the streamer power supply unit. Until 18:00 we tried to repair the seismic recording system, but when that failed we recovered the entire system. We finished recovery at approximately 20:00 and steamed back to the centre of the Giant Gjallar Vent. From 21:00 to 23:00 we tested four Posidonia receivers and collected a sound velocity profile, before beginning multibeam and Parasound profiles to map the near surface expression of the vent, which is characterized by shallow faulting.

Friday May 11th, 2012
During the morning we continued profiling and mapping while fixing the seismic acquisition system. Wind NW 4-5. From 14:00 to 17:00 we deployed the seismic system in 2D mode and at 18:00 we began shooting seismic profiles across the OBS locations. Except for an one-hour delay due to a broken part in the compressor we continued shooting during the night.

Saturday May 12th, 2012
In good weather conditions we collected several 2D seismic lines across the two ocean bottom seismometer locations. At 14:00 we retrieved the seismic equipment and steamed to the first ocean bottom seismometer location. 20 minutes after releasing the ocean bottom seismometer it surfaced and was brought on board. The data was retrieved after a GPS clock check (skew=2 ms). We then tried to release the second ocean bottom seismometer, but it did not respond. However, when steaming towards its expected position it surfaced and we recovered it at 16:30.

Also that ocean bottom seismometer acquired data and the clock worked properly (skew = +17 ms). Because of the unfavourable weather forecast for both the northern (Force 8 on Monday, Force 7 on Tuesday with expected significant wave heights in excess of 7 meters on both days) and the southern (Force 9 on Sunday-Wednesday and expected significant wave height of 7-9 meters) working areas we decided to seek shelter in the Trondheim Fjord until the weather became suitable for further work.

Sunday May 13th, 2012
With the low pressure Vera approaching and winds up to force 9 we steamed to the Trondheim Fjord, which we reached at 16:00. The rest of the day was used to process the seismic data from the Giant Gjallar Vent and wind down the P-Cable cross cable from the winch to prepare it for the DASI streamer.

Monday May 14th, 2012
During the morning we prepared the DASI streamer and put it on the P-Cable winch. This was followed by shifting the HyBIS to the back deck and terminating its cables. Unfortunately, the chief discovered that the air compressor for the seismic acquisition had a jammed piston and a spare part had to be ordered from Kiel.

Tuesday May 15th, 2012
In the morning we held a seminar on the Gjallar Vent Site, while the high voltage power test was conducted on deck. After arrival of the spare part for the compressor we left the Trondheim Fjord at 23:00. In hindsight it was good luck that we decided to steam to Trondheim instead of weathering off in working area 1. Only as a result of this decision it was possible to obtain the necessary spare part for the compressor and keep the option of further seismic work.

Wednesday May 16th, 2012
In the morning we held a seminar on the Nyegga gas hydrate province while approaching the study area. Upon arrival at noon we carried out a sound velocity profile to calibrate the mult-beam echosounder. Then we started to deploy the GEOMAR OBEM receivers. In fair weather (NW5-6) it took about eight hours to deploy the first four instruments.

Thursday May 17th, 2012
While the first four OBEM were deployed with the HyBIS vehicle over the stern of the vessel the last two were deployed with a Posidonia releaser over the starboard side of the ship. This change was necessary because the power supply of HyBIS was faulty since the early morning hours. After a successful trial of the Sputnik EM source from 07:00 to 10:00 we began to deploy the Southampton OBEM receivers again over the side of the vessel, because of their large water resistance and low weight they deployment was slower than that of the GEOMAR receivers. In parallel we started to work on the HyBIS power supply. A dirty connector in the junction box was found to cause the leakage and the system could be repaired at 18:00.

Friday May 18th, 2012
Deployment of the Southampton OBEM finished at 04:30. Until noon we collected a multibeam echo sounder and Parasound grid across the Storegga area, before starting electromagnetic soundings along a S-N profile across the centre of the CN03 structure using the Sputnik system. We collected data at four stations before we had to stop because of a technical failure in the power supply. Throughout the night we carried on surveying the area with multibeam and Parasound profiles to map out the extent of slope instabilities above the gas hydrate zone in the northern side wall of the Storegga Slide.

Saturday May 19th, 2012
The multibeam survey continued throughout the night and after a successful Posidonia transponder test at 13:00 we arrived at 14:00 at the first DASI deployment location. After powering up DASI the communication link to the system broke down. After hours of fault finding we decided to continue the Sputnik transect and moved back to transect 1. There we deployed Sputnik at 18:00.

Sunday May 20th, 2012
Throughout Sunday the Sputnik profiles continued without interruptions across the vent site CN03. The weather was fine with light northerly winds. At the same time the Southampton team carried out repairs and further tests of the DASI vehicle discovering two broken connections in the main antenna power supply which could be fixed until the evening.

Monday May 21st, 2012
We finished the third Sputnik profile at 08:00 in the morning. After recovery of the vehicle we steamed 8 miles south to the deployment position of DASI, which was deployed at noon. With fine weather we acquired data with DASI throughout the rest of the day.

Tuesday May 22nd, 2012
With fresh north-easterlies we continued DASI profiling until 15:00 in the afternoon. After retrieval of DASI we picked up the GEOMAR OBEMs which was finished at 20:00. We then used the time for a multibeam and Parasound survey along the crest of the contourite that hosts the hydrate system, while DASI was disconnected from the fibre optic cable and HyBIS was connected.

Wednesday May 23rd, 2012
At 04:00 we started to pick up the Southampton OBEMs. In ideal weather conditions this work lasted until noon. After steaming to the beginning of a video transect close to the Storegga Slide side wall we deployed HyBIS at 14:00. However, after powering it up and lowering it down to approximately 60 m the front lights came off and the vehicle had to be recovered. It turned out that there was a short circuit in one of the light power supplies that damaged a cable, requiring replacement of a fuse inside the vehicle. The repair works lasted until 17:40 when we redeployed the vehicle for a very interesting video transect through a sea floor crevasse and down the Storegga Slide side wall. This transect was completed at 20:40. At 21:40 we deployed the instrument a second time to survey another crevasse that we believed to be active. However, the results of this transect were somewhat disappointing as in spite of strong seafloor diffractions in the Parasound data only little seafloor morphology could be observed.

Thursday May 24th, 2012
HyBIS was recovered from the second transect at 00:15. Afterwards we disconnected it from the fibre optic cable and cleared the deck for acquiring more high-resolution 2D seismic data while steaming to the beginning of the first profile. Deployment of the seismic system commenced at 00:30. From 03:00 onwards we collected seven N-S seismic profiles across the area with crevasses and fluid escape structures in the Nyegga Region. In the afternoon the weather became foggy, but the sea stayed calm resulting in some exceptionally good data.

Friday May 25th, 2012
Seismic data acquisition continued without interruptions until 14:00 in calm, sunny weather. At 14:00 we retrieved the seismic equipment and end the scientific work programme with another

sound velocity profile for calibrating the multibeam echosounders. This was finished at 15:45 and we started the transit back to Stavanger.

Saturday May 26th, 2012
The transit from study area 2 (Nyegga) to Stavanger continued in exceptionally nice weather. Packing and cleaning of the laboratories took all day.

Sunday May 27th, 2012
At 06:00 we arrived at the Stavanger pilot station and moored at 08:00.

5 Preliminary Results

5.1 Giant Gjallar Vent

The third objective of the cruise was to investigate the Giant Gjallar Vent and determine if it is a suitable window to the geological processes acting in the deep parts of the Vøring Basin – in particular whether it is possible to determine the amount of carbon that was released by hydrothermal activity during the Early Eocene. During the cruise we have collected ocean bottom seismometer data as well as 2 D seismic data, multibeam bathymetry data and Parasound sub-bottom profiler data across the vent structure. Unfortunately, there was no time to collect seafloor samples using the HyBIS.

5.1.1 Bathymetry

5.1.1.1 EM122

The Kongsberg EM122 system allows an accurate bathymetric mapping down to full ocean depth. Basic components of the system are two linear transducer arrays in a Mills cross configuration with separate units for transmitting and receiving. The nominal sonar frequency is 12 kHz with an angular coverage sector of up to 150° and 288 beams per ping. The emission cone is 150° wide across track, and 1° along track direction. The reception is obtained from 191 beams, with beam widths of 2° across track and 20° along track. Thus, the actual footprint of each beam has a dimension of 1° by 2°. The achievable swath width on a flat bottom will normally be up to six times the water depth, depending on the roughness of the seafloor. The angular coverage sector and beam pointing angles may be set to vary automatically with depth according to achievable coverage. This maximizes the number of usable beams. The beam spacing is normally equidistant, but an equiangular mode is also available. For depth measurements, 288 isolated depth values are obtained perpendicular to the track for each ping. Using the detected two-way-travel-time and the beam angle known for each beam, and taking into account the ray bending due to refraction in the water column due to sound speed variations, depths are calculated for each beam. A combination of amplitude (for the central beams) and phase (slant beams) is used to provide a measurement accuracy practically independent of the beam pointing angle. Beside the depth values, the EM122 provides also backscatter information and pseudo-sidescan images.

5.1.1.2 Experiment design

The EM120 was operated almost continuously during the cruise, including transits, except when the ship was on station for a longer time. The system was also switched off during the Sputnik and DASI operations in order to avoid signal interference.

5.1.1.3 Preliminary results

The Giant Gjallar Vent is characterised by positive seafloor morphology of up to 15 m, comprising two mounds marking the locations of the two fluid pipes and a western rim structure half surrounding the pipes (Fig. 5.1). Based on previous studies, it has been assumed that the seafloor elevation results from deformation that accompanied active venting processes (Gay et al., subm.), and possibly authigenic carbonate precipitates. The presence of carbonate was suggested by significantly higher seismic amplitudes of the seafloor and Top Kai horizon in the area of the Giant Gjallar Vent.

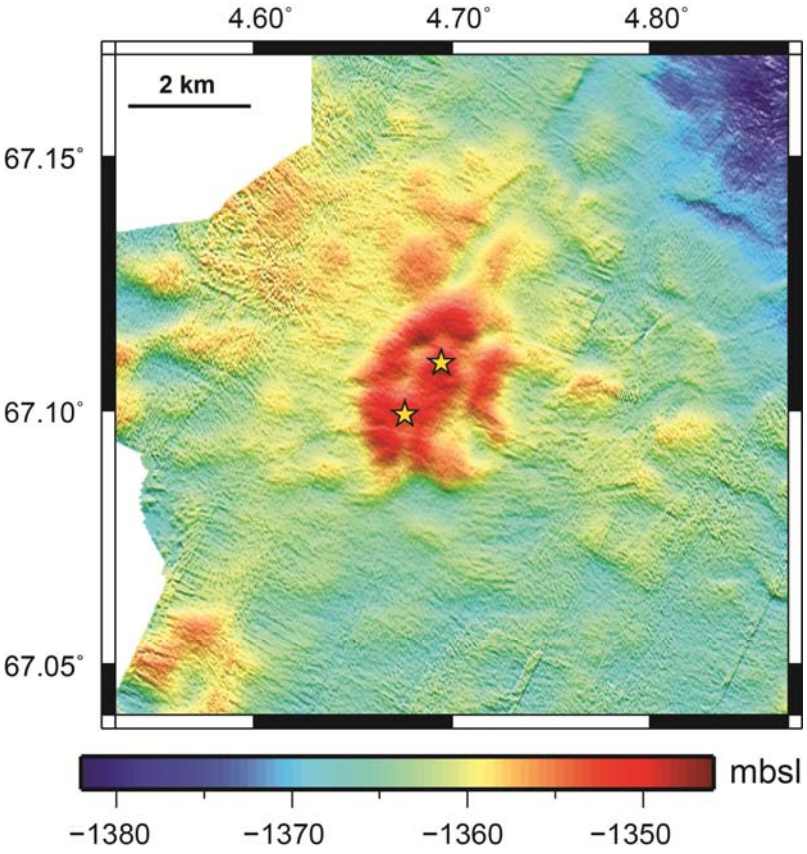

Fig. 5.1 EM122 bathymetry map of the Giant Gjallar Vent. Yellow stars mark the locations of the two fluid pipes.

5.1.2 Parasound data

5.1.2.1 Parasound system

During RV Meteor cruise M87/2, the hull-mounted parametric sub-bottom profiler Parasound P70 (ATLAS HYDROGRAPHIC) was operated to provide high-resolution data on the uppermost 50-100 m of the sediment column. Parasound P70 works as a narrow beam sediment echo sounder, providing primary frequencies of 18 (PHF) and adjustable 18.5 – 28 kHz, thus generating parametric secondary frequencies in the range of 0.5 – 10 kHz (SLF) and 36.5 – 48 kHz (SHF) respectively. The secondary frequencies develop through nonlinear acoustic interaction of the primary waves at high signal amplitudes. This interaction occurs in the emission cone of the high-frequency primary signals which is limited to an aperture angle of 4° for the Parasound P70. This narrow aperture angles is achieved by using an array of 128 transducers on a rectangular plate of approximately 1 m² surface area. Therefore the footprint size is 7% of the water depth and vertical and lateral resolution is significantly improved compared to conventional 3.5 kHz echo sounder systems. The system provides features like recording of the 18 kHz primary signal and both secondary frequencies, continuous recording of

the whole water column, beam steering, different types of source signals (continuous wave, chirp, barker coded) and signal shaping. Digitization takes place at 96 kHz to provide sufficient sampling rates for the high secondary frequency. A down-mixing algorithm in the frequency domain is used to reduce the amount of data and allow data distribution over Ethernet.

5.1.2.2 Experiment design

In order to investigate the structure of the shallow sediments and test the hypothesis of carbonate-cemented seafloor at the Giant Gjallar Vent, 24 Parasound profiles were run in the Gjallar study area. In addition to the seismic surveys during which the Parasound was operated at the same time, Parasound data were also acquired during two surveys southwest and northeast of the vent. A network of Parasound lines was run across the vent.

For the standard operation a parametric frequency of 4 kHz and a sinusoidal source wavelet of 2 periods were chosen to provide a good balance between signal penetration and vertical resolution. The 18 kHz signal was also recorded permanently. All recorded raw data were stored in the ASD data format, which contains the data of the full water column of each ping as well as the full set of system parameters. In addition, a 400 m-long reception window centred on the seafloor was recorded in the compressed PS3 data format. This format is in wide usage in the PARASOUND user community and the limited reception window provides a detailed view on the sub-bottom structures. The data were processed onboard using Seismic Unix.

5.1.2.3 Preliminary results

Parasound data do not support the idea of massive carbonates on the seafloor or above the Top Kai horizon. High signal penetration (c. 100 m) and a succession of distinct reflectors show that the vent structure is covered by stratified sediments (Fig. 5.2). If carbonate exists, it must be finely distributed within the sediment drape. A possible indicator for small carbonate occurrences are narrow vertical lenses of lower amplitudes on Parasound profiles, observed both inside and well outside of the area of elevated seafloor morphology. These features cannot be attributed to the presence of gas as in that case complete blanking of all underlying reflectors would be expected, which is not the case.

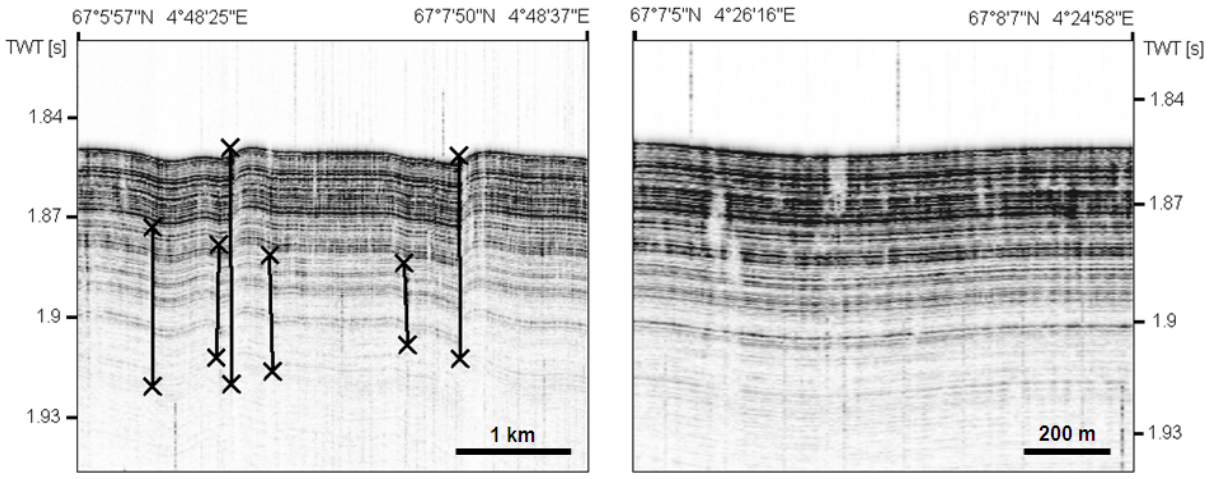

Fig. 5.2 Examples of Parasound data. Left: Vertical to sub-vertical faults through the sediment drape east of the vent structure. Right: Shallow vertical low-amplitude anomalies west of the vent structure.

The sediment drape is cut by vertical to sub-vertical faults, some of which reach the seafloor. They appear more abundant east of the vent structure, although this could also be due to a denser profile coverage compared to the western part. The faults indicate relatively recent tectonic activity in an area that is otherwise tectonically very stable – therefore, it seems likely that the

faults are the result of deformation associated with the Giant Gjallar Vent that has been proposed by Gay et al. (2012).

5.1.3 Seismic data

5.1.3.1 GI-gun

For the high-resolution seismic acquisition a GI-gun manufactured by Sercel Marine Sources Division was used. The compressed air was supplied by the super charger of RV Meteor with a pressure of 210 bar. The GI-gun was attached with chains to a steel frame and towed either from the centre or at the starboard side at 20 m behind the stern in a depth of 2 m. The setup with the floatation is shown in Figure 5.3.

Along the first profiles the gun was operated with a volume of 3.8 l (105 cinch generator chamber, 105 cinch injector chamber) as it was known for a well-balanced ratio of depth penetration and frequency content of the source signal. The shot interval was 5 s for both the 3D and 2D surveys. The injector was fired at a delay of 65 ms.

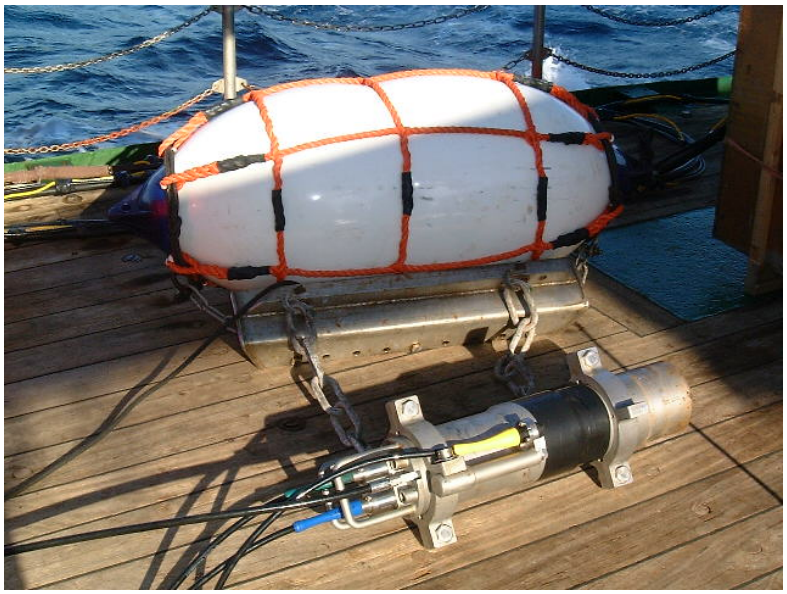

Fig. 5.3 GI-gun mounted below the carrier to which a Polyform floatation is attached.

External trigger during M87/2

With the development of the 3D P-Cable system GEOMAR has built its own GPS based trigger system. The shipboard GPS receiver delivers ZDA and PPS to a timing box. The timing box allows selecting the shot interval by a wheel switch in full second intervals. The TTL trigger pulse is delivered to a distribution box, from which the LongShot gun controller and the Geometrics streamer system receive the signal. Together with the trigger generation a time stamp is written to an internal SD memory card with shot coordinates.

To ensure all systems trigger with the same reference all trigger circuits were adjusted to work on the uprising flank (TTL+). The LongShot gun controller was set to a 40 ms aim point and adjusted later to 50 ms aim point. The automatic adjustment based on the received shot signal from the gun hydrophone usually was within +/- 1 ms.

5.1.3.1 P-Cable system

The P-Cable (VBPR patent of 2003) system design is designed to high resolution imaging of shallow horizons. GEOMAR is holding an academic license of the P-Cable system covering development and application of such a system.

Compared to standard reflection seismic applications in 2D and 3D, the basic difference is that the P-Cable is built by a cross cable towed perpendicular to the ship's heading (Fig. 5.4). Instead of a few single streamers the P-Cable uses a large number of short streamer sections towed parallel from the cross cable. Drawback is the limited depth penetration due to the short receiver offsets, which are not favourable for the removal of the multiple energy. This is well compensated by the reduced costs of the system and the ability to operate it even from small multi-purpose vessels, the usual academic platform for marine research.

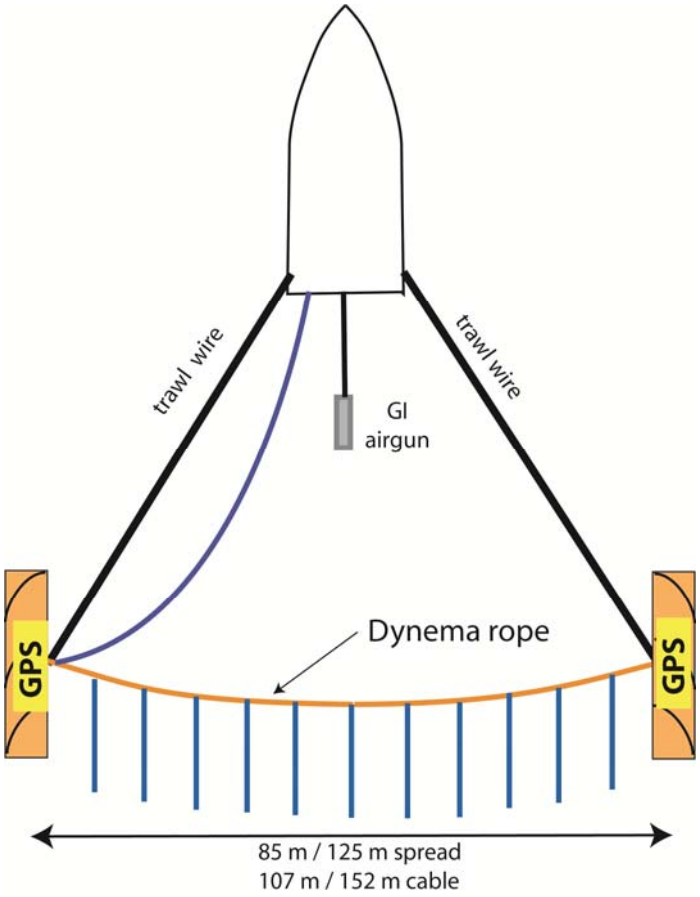

Fig. 5.4 Drawing of the P-Cable design applied during M87/2.

Figure 5.4 shows the basic principle of the P-Cable design. The advantages of the GEOMAR development are two-fold. The cross cable is based on a strength member, a Dynema rope, which takes the stretch forces of the trawl doors (Fig. 5.5). Attached to this rope is the data cable with the streamer connections. The cross cable is stretched by two trawl doors, floating at the sea surface. GEOMAR developed a modular cross cable, which allows exchange of each single streamer connector (node) in case of a malfunction. This allows easy service and reduced service costs. In addition, the modular design allows to insert connecting cables of different length between the nodes. Floats attached to each break out help to keep the streamers at 2 m depth. The current grade of the system provides 10 active nodes connected either by 14 m or 9 m long data cables. On both sides the first node is located 11.5 m off the triple point, the connection of trawl wire, cross cable and trawl door. Each one of the trawl doors provides a lifting force of 2 tons. In order to ensure continuous inline coverage the maximum shot rate of the gun (5 s / 3 s) requires a maximum speed of 3 kn or 3.5 kn.

Fig. 5.5 Photographs of the trawl doors. Left: Trawl door preparation on board. Top right: Trawl doors in rest position at the aft of RV SONNE. Bottom right: Trawl door in operation.

Upon deployment the door next to the umbilical is released from its rest position (Fig. 5.6a) while the ship sails at 1.5 kn through water against wind and waves. The door is lowered into the water while a 10 m long lead cable between door and connection point of cross cable is kept on board. Next the data cable from the recording device to the door is hooked to the connection between lead wire and cross cable. Now trawl wire, data cable and cross cable are payed out simultaneously (Fig. 5.6b). At the same time streamer sections are connected to the nodes of the cross cable. Floats are fixed to each node in order to keep the cross cable at even depth. When the entire cross cable is payed out a support rope on the support winch is used for secure transmit of the cross cable from the support winch to the lead wire of the second trawl door (Fig. 5.6c). Now both trawl wires are given out until the final length with sufficient stretch of the trawl doors is reached (Fig. 5.6d).

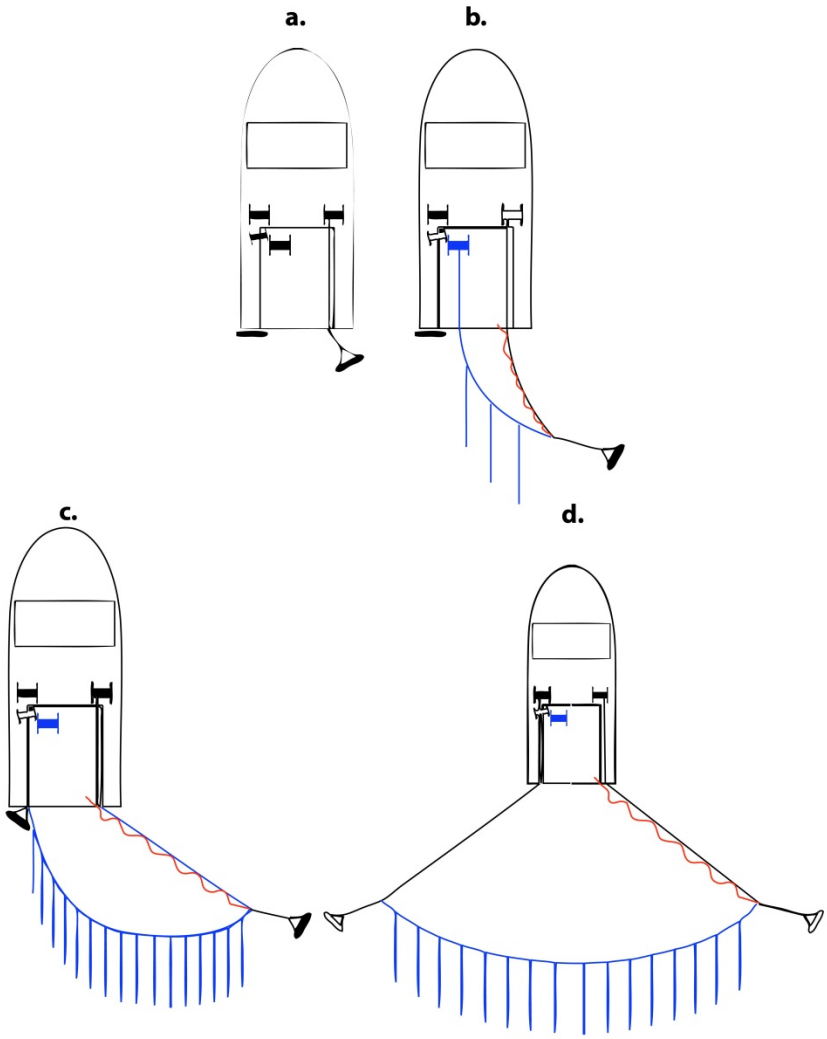

Fig. 5.6 Drawing illustration the steps during deployment of the P-Cable system.

5.1.3.2 Experiment design

The aim of the P-Cable survey was the acquisition of a 3 km by 5 km cube across the Giant Gjallar Vent. The cube was planned as 50 parallel profiles oriented in a NE-SW direction. The first deployment was completed after 3.5 hours and shooting of seismic lines began at 3 am on 09.05.2012. Acquisition parameters are given in Table 1. The system was running fine and two profiles were completed, but at 07:15 something got caught in the streamer and shooting had to be discontinued. Recovery of the data cable and inspection of the seaward router and the first T-junction of the cross-cable revealed bending of the data cable at the connection point with the cross-cable and the first part of the cross-cable was replaced. After initial problems with the airguns the system was started again at 13:00 but broke down another time at 13:45. The entire system was recovered for a full inspection.

The second deployment was completed at 16:00 on 10.05.2012. Initially the system was working fine, but after approximately 15 minutes seismic recording stopped again with a technical failure of the streamer power supply unit.

After several failed attempts of fixing the P-Cable system, the system was redeployed in 2D mode on 11.05.2012. Between 18:40 and 13:00 on 12.05.2012, seven lines were acquired across the vent structure and the two OBS locations. Shooting had to be interrupted only once due to a broken part in the compressor, which caused a 1-hour delay.

Table 1: Seismic acquisition parameters

P-Cable 3D Survey (P2100) (Gjallar Ridge)	
Number of streamers:	12
Channel interval (m):	1.5625
Recording sample rate (Hz):	2000
Recording trace length (ms):	4000

2D seismic surveys (Gjallar Ridge and Nyegga)	
Number of streamers:	12
Channel interval (m):	1.5625
Recording sample rate (Hz):	2000
Recording trace length (ms):	4000

5.1.3.3 Preliminary results

Compared to the available 3D industry-type data, the 2D seismic data (Fig. 5.7) yield higher resolution images. For example, the Top Kai horizon, which shows up-doming above the two pipes and appears as a continuous reflector in the 3D data, is disrupted above the vent structure in the 2D images. The polarity of this horizon is opposite to that of the seafloor, suggesting a layer with lower seismic impedance beneath. At the pipe structures, discontinuous high amplitude reflections are imaged just beneath the Top Kai horizon (Fig. 5.7). The high amplitudes could indicate carbonates but probably represent gas, as some reflections have negative polarity.

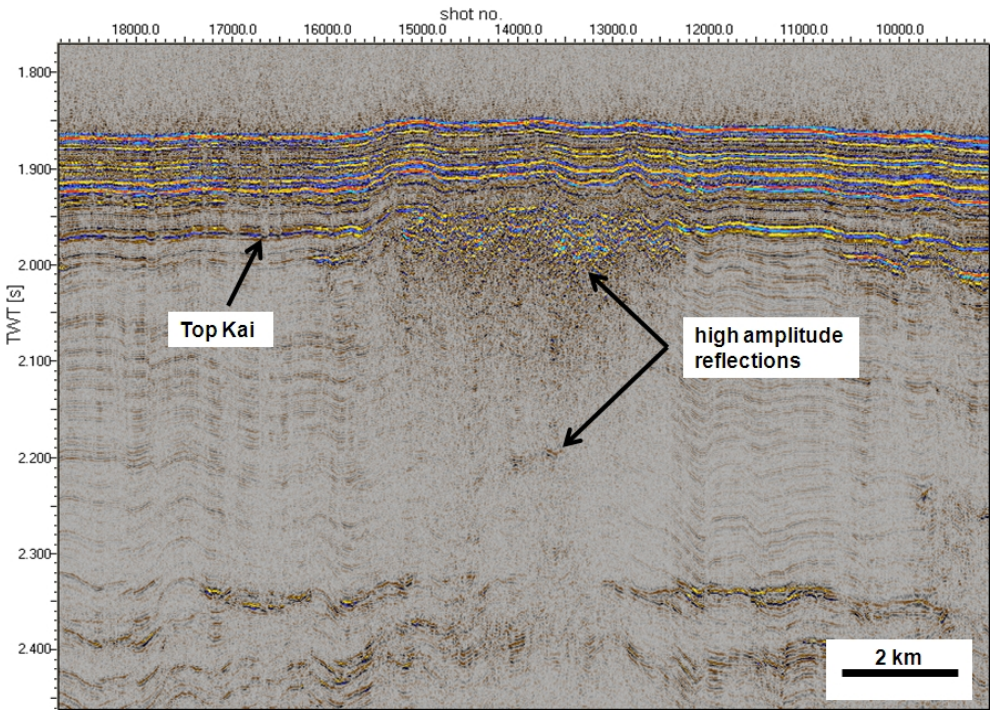

Fig. 5.7 2D seismic line across one of the two pipes, illustrating deformation and negative polarity of the Top Kai horizon and disrupted high amplitude reflections below.

The amplitude map of the Top Kai horizon (Fig. 5.8), which shows the polarity to become more negative at the Giant Gjallar Vent, also suggests the presence of gas. If carbonates were present, the polarity should become less negative. Also, if carbonates were present at Top Kai level, e.g. as the result of an intense phase of fluid venting accompanied by extensive carbonate precipitation, this would raise the question of why carbonates are only observed at this level and not anywhere else in the stratigraphy. Gas or fluids therefore constitute a more likely explanation for the high-amplitude reflections beneath Top Kai level.

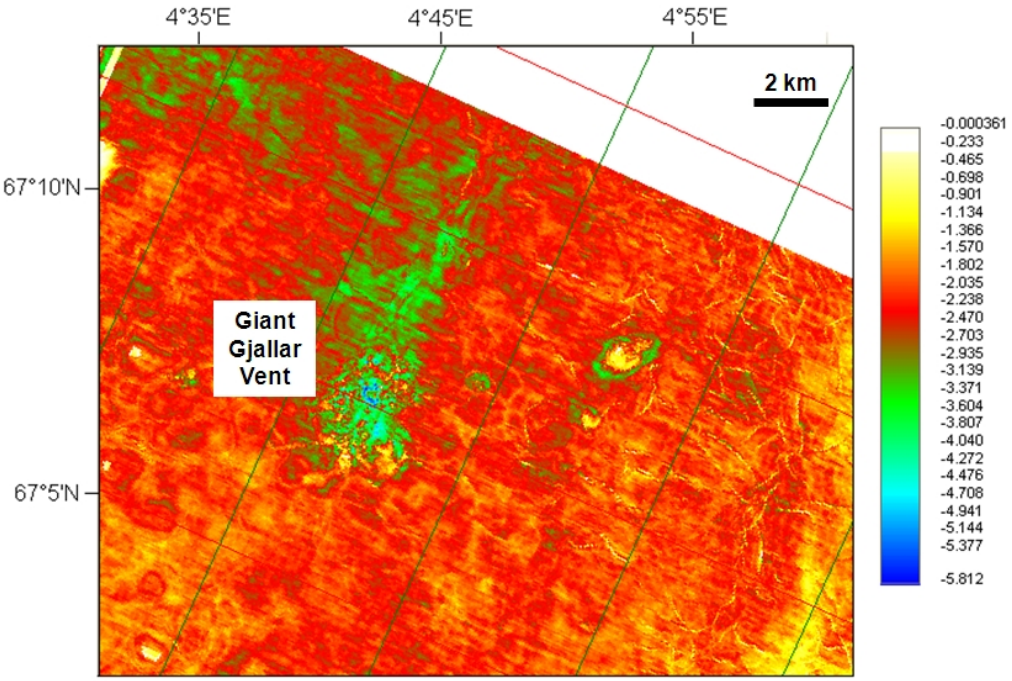

Fig. 5.8 Amplitude map of the Top Kai horizon from the industry-type 3D data. The location of the Giant Gjallar Vent is marked by increasing negative polarity suggesting the presence of gas.

The instantaneous frequency plot (Fig. 5.9) of the 3D data shows increased attenuation of higher frequencies at the vent structure below the Top Kai reflector, which is a typical characteristic if gas accumulations are present. Interestingly, less attenuation is observed in the very centre of the pipe where normally a higher amount of gas and hence stronger frequency attenuation would be expected.

The presence of gas-indicating anomalies in both the 3D data from 1996 and the new 2D data suggests that the Giant Gjallar Vent is, to a certain degree, still active in terms of vertical fluid migration. Venting activity must have been considerably more vigorous in the past when it was accompanied by intense deformation until just after deposition of the Kai formation. Deformation of the Top Kai horizon is mirrored by the sediment drape deposited during the last glaciation. The Top Kai horizon appears to constitute a seal to underlying gas, inhibiting further upward migration, which would also explain why seepage-indicating flares have not been observed in the water column anywhere in the area. However, the small, possibly carbonate-associated anomalies within the sediment drape suggest that some episodic venting must have occurred afterwards, allowing further upward migration of fluids and microbial carbonate production. Episodic seal failure and subsequent fluid migration to shallower levels have also been proposed by Hansen et al. (2005).

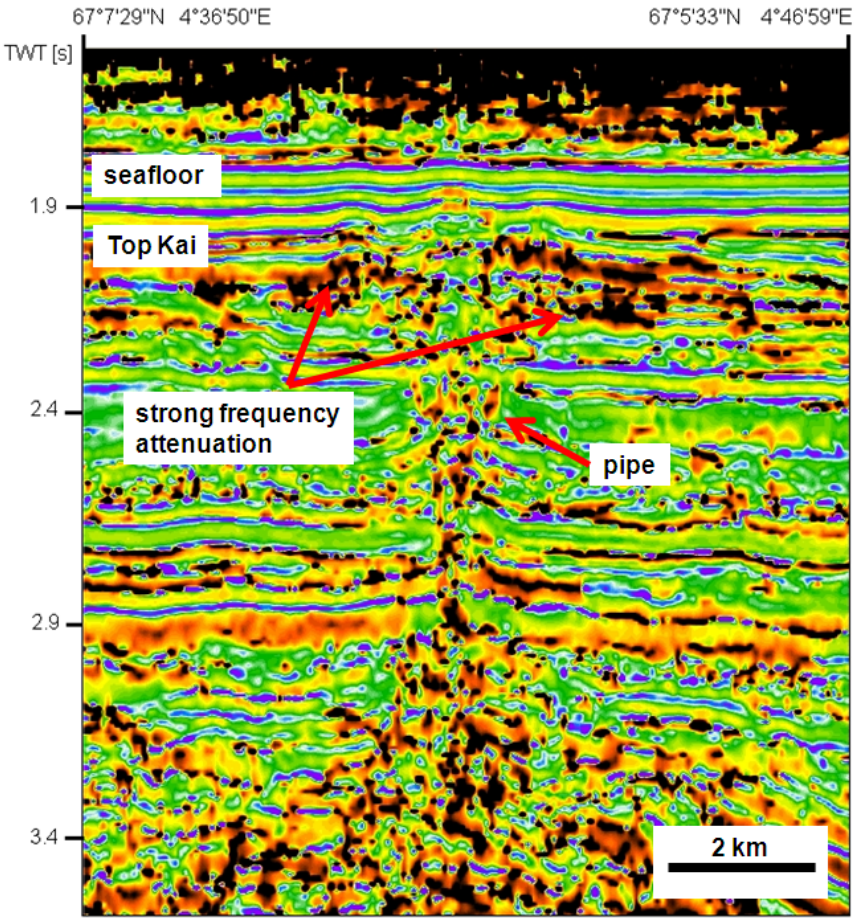

Fig. 5.9 Instantaneous frequency plot of 3D inline 11458. Strong frequency attenuation occurs at the pipe structure beneath the Top Kai horizon, indicating that gas may be trapped there.

The origin of the fluids accumulating beneath Top Kai level cannot be inferred from seismic data alone, but the fluids are probably related to migration from greater depths along the pipe structures. It does not seem likely that fluid production occurs within the Miocene formation beneath the Top Kai horizon. In that case, high-amplitude negative-polarity reflections should be observed everywhere in the area, however, they are restricted to the vent locations. Consequently, the Giant Gjallar Vent is still active, both in terms of fluid migration and tectonic deformation. The degree of activity, however, seems considerably lower compared to the past and active fluid venting at the seabed does not occur so vigorously that flares in the water column would form.

5.1.4 OBS data

5.1.4.1 Ocean bottom seismometers

To further constrain the nature of the high-amplitude reflections we have carried out an ocean bottom seismometer (OBS) survey. The OBS consists of four floats connected to frame, which carries a seismometer, a hydrophone and a data recorder cased in a high-pressure tube (Fig. 5.10). The sensors are connected to the recording unit, which continuously records the signals of the sensors. The systems itself would float at the sea surface, so in order to deploy it at the ocean bottom a weight is mounted to the frame with a releaser unit. The releaser has an acoustic communication unit, which can be addressed from the ship in order to disconnect the weight after the experiment. The OBS will then ascend to the surface and can then be recovered. A flashlight, a radio transmitter and a flag are attached to the frame in order to facilitate sighting the OBS. While the OBS measures seismic signals an additional data logger continuously records the shot times.

Fig. 5.10 Ocean bottom seismometer (OBS) before deployment.

5.1.4.2 Experiment design

The data recorders have to be programmed before the deployment of the system. The sample rate of the OBS recorders was set to 500 Hz, while the data logger recorded at a sample rate of 1000 Hz. The gain of the input channels was set to 15 for the three geophone components and 7 for the hydrophone.

Two OBS units were deployed on 08.05.2012 and recovered on 12.05.2012. The recording units were synchronized with a GPS signal before and after the recording period in order to correct the drift of the logger's internal clock. Both OBS units recorded data and did not show any error messages after recovery and synchronisation. The data have not been evaluated on board.

5.1.4.3 Outlook

Further analyses will have to be carried out to better constrain the activity history of the Gjallar Vent. For example, the OBS data which could not be processed onboard will yield velocity information that should give further indications as to the lithology beneath the Top Kai horizon. During future expeditions, seafloor video observations could be carried out at very shallow low amplitude lenses observed in the Parasound data, to look for active seepage indications such as biological communities or carbonate concretions too small to be detected by acoustic methods. Also, geochemical analyses of gravity cores would help to constrain the rates of fluid migration and the source of the fluids.

5.2 Nyegga

The Nyegga survey area was the second working area of the cruise. The region lies directly north of the Storegga Slide at approximately 5 degrees East and 65 degrees North (Fig. 1.2). The principal aim at this study area was to acquire controlled source electromagnetic data. In addition, we were also able to acquire a relatively dense network of Parasound profiles and 2D seismic data north of the Storegga Slide sidewall. It is in this area that existing studies have identified sets of shallow extension faults that result in crack-like morphological features that run sub-parallel to slope contours (Hjelstuen et al. 2010; Mienert et al. 2010). In addition to acoustic data acquisition, two HyBIS dives were carried out to film the character of the seafloor over profiles that targeted two of the crack features.

5.2.1 Electromagnetic surveys

Electromagnetic (EM) measurements determining the electrical resistivity of the seafloor were carried out at the Nyegga area (site CN03), where in previous years different types of seismic data (3D OBS and reflection seismics) had been acquired within the framework of the European funded project HERMES. The concurrent seismic and electromagnetic data will allow us, through a joint analysis, to identify and distinguish between temperature anomalies, (low resistivity anomaly), presence of highly saline water (low resistivity anomaly) and hydrate (high resistivity and high P-wave anomaly) and gas distribution (high resistivity and low P-wave anomaly).

For maximum coverage electromagnetic data on four different scales were conducted (Fig. 5.11). The chimney itself is investigated with a very high-resolution shallow, i.e. of the order of 200 to 300 m, 3D tomographic controlled source EM measurement. This data set will be used to quantify the amount of gas and methane hydrate in the chimney and its immediate surroundings. At deeper scales (on the order of a few hundred meters), intermediate-resolution controlled source EM measurements employing a towed high-voltage/current source DASI and stationary receivers is geared towards investigating the methane hydrate layers at depth over a larger regional scale. The regional data is complemented by data acquired with the VULCAN receiver, which is towed at a distance of several hundred meters behind the DASI source and delivers higher-resolution 2D information along the DASI tow-profiles.

Deep penetrating (of the order of several kilometres) low-resolution natural source magnetotelluric (MT) data complement the electromagnetic experiments and are expected to shed light on deeper fluid and temperature processes.

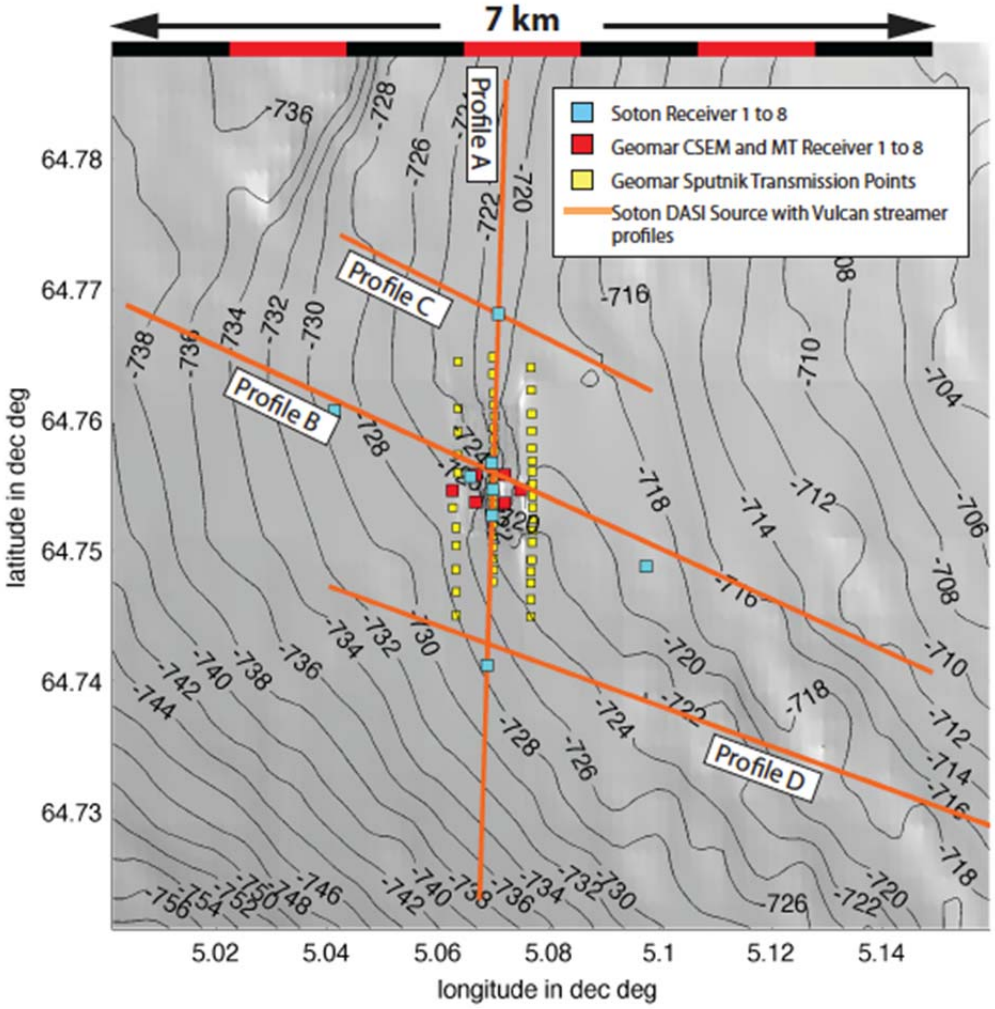

Fig. 5.11 Overview of the electromagnetic experiments conducted on Nyegga CN03 site. 1. 3D high resolution shallow penetration CSEM data (GEOMAR receiver denoted as red squares, Sputnik transmission sites as yellow squares); 2. intermediate penetration depth CSEM data (Soton receiver denoted as cyan squares, high power towed DASI profiles A to D denoted as orange lines); 3. high resolution 2D VULCAN streamer data along DASI profiles A to D; 4. deep penetration MT data (GEOMAR receiver denoted as red squares).

5.2.1.1 High-resolution 3D tomography EM Experiment (GEOMAR)

The high-resolution 3D tomographic EM experiment entails the transmission of an electromagnetic waveform from different points on the seafloor to a number of stationary ocean bottom electromagnetic (OBEM) receivers. The travel time of the signal from the transmitter to the receiver as well as the amplitude of the received signal depend on the electrical resistivity structure of the underlying seafloor and may therefore be used to derive an electrical resistivity model of the subsurface. The measurement of travel time requires a sufficiently precise knowledge of the distance between transmitter and receiver (on the range of 10 to 50 m depending on separation). For this reason the six OBEM were carefully placed on the seafloor using HyBIS or lowered on a wire equipped with a Posidonia positioned release system. The electromagnetic source (Sputnik) equipped with a Posidonia transponder is placed stationary onto the seafloor for a transmission cycle.

5.2.1.1.1 Ocean bottom electromagnetic receivers

The OBEM (Fig. 5.12) consist of a buoyant titanium frame on which two orthogonal electric dipoles with a length of 10 m are mounted, as well as a data logger with a high precision clock

and battery packs, housed in a titanium pressure cylinder. The instrument is kept on the seafloor with an anchor, which is attached to the frame by a releaser. Sampling of the electromagnetic wave occurs at a frequency of 10 kHz. The orientation of the instrument is determined through the recording of full field fluxgate magnetometer data.

Fig. 5.12 Left: GEOMAR OBEM receivers equipped with two electrical dipoles. Right: OBEM receiver mounted underneath HyBIS before deployment (prior to attachment of electric dipoles.

The electrical dipole transmitter Sputnik (Fig. 5.13) is built on a metal cage carrying 3 titanium pressure cylinders housing the wave form generator, buffer batteries and a data logger with a high precision clock. Two 9.1 m long orthogonal dipoles are attached to the cage through arms that fold up when Sputnik hangs by its own weight on the cable but drop to horizontal position once Sputnik stands on the seafloor. The folding mechanism allows easy deployment and movement on the seafloor, while maintaining a long dipole length and thereby ensuring sufficient electromagnetic power for the transmitter. Sputnik is deployed over an 18 mm coax cable over mid-ship and placed onto the seafloor for a transmission cycle.

The transmission cycle entails a current in the form of a bi-polar square wave with an amplitude of 10, 20, 30, 40 or 50 Ampere (depending on distance to receivers), which is pushed through spherical electrodes at the end of the dipoles into the water column, first for the first and then for the second dipole direction.

After transmission has ended it is heaved, depending on the topography, 10 to 30 meters over the seafloor, moved and lowered onto the seafloor at the next transmission point (time between transmission at two points approximately 20 to 40 minutes).

Fig. 5.13 Sputnik electric dipole transmitter on deck.

The system requires a one-phase voltage supply from the ship which is transformed in a deck unit to 300 V DC. The DC voltage continuously recharges the buffer batteries on the seafloor unit through the coax cable. The coax cable also serves as a DSL Ethernet connection from the ship to the microprocessor and data logger at the seafloor unit, allowing the online control over power output and data transfer of the emitted waveform, compass heading, pitch and roll of the transmitter cage as well as inclinometer data of the four arms. Online monitoring of the seafloor placement and seafloor conditions occurs through a video camera attached to the frame.

5.2.1.1.2 Experiment design

Six OBEM receivers (G01 to G06) have been placed on the seafloor using HyBIS (G01 to G03) and a wire with a Posidonia positioned release (G04 to G06). The locations of the 6 OBEM receivers as well as the 56 Sputnik transmission points are illustrated in Fig. 5.14. The OBEM were placed around the immediate vicinity of the CN03 chimney and received transmissions from 59 sites along 3 profiles. At each point a bi-polar square-wave with an amplitude of 50 A and a length of 4 seconds has been injected into the water column for a duration of 1 minute for each of the two orthogonal transmitter dipoles (see Fig. 5.13). On sites closer to the centre of the structure, an additional sequence with an amplitude of 10 A was transmitted to avoid potential clipping of the signal in the receiver electronics. For the 59 transmission sites along 3 profiles an overall period of approx. 40 hours was required. After some technical problems had been solved, Sputnik ran for approximately 30 hours continuously and 2 to 3 transmission sites were covered within one hour.

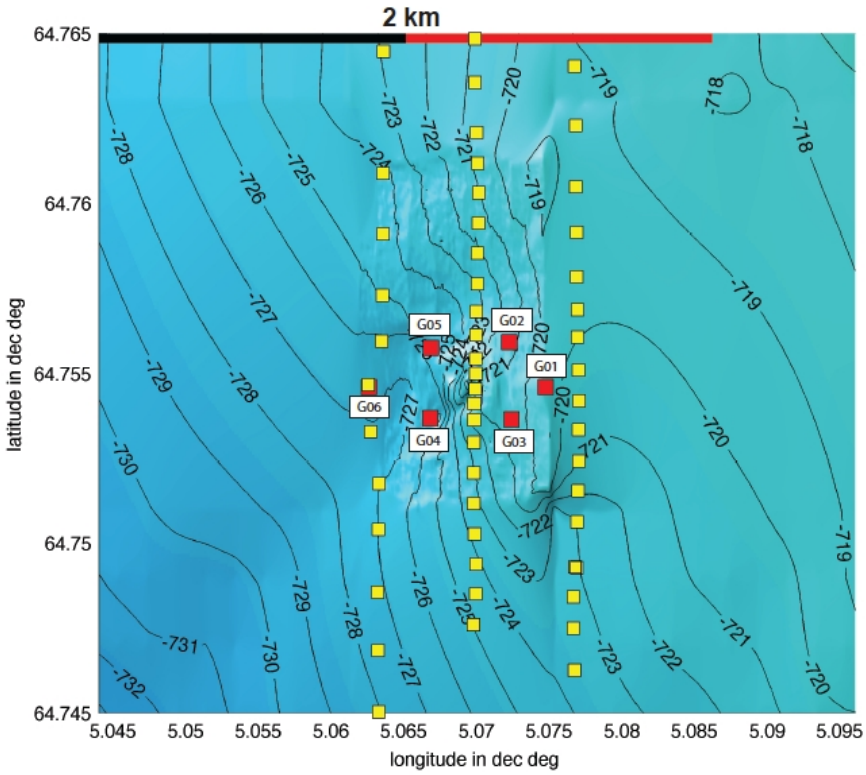

Fig. 5.14 Location of G01 to G06 OBEM stations (red boxes). Yellow boxes mark Sputnik transmission sites and DASI tracks.

5.2.1.1.3 Preliminary results

Preliminary analysis of the data showed that a clear signal has been recorded on all receivers. An example of the data is shown in Figs. 5.15 and 5.16. The transmitted wave could be recorded up to a distance of 1 km, indicating that the expected depth of penetration is on the order of 300 to 350 m and therefore down to or beyond the BSR (Fig. 5.17).

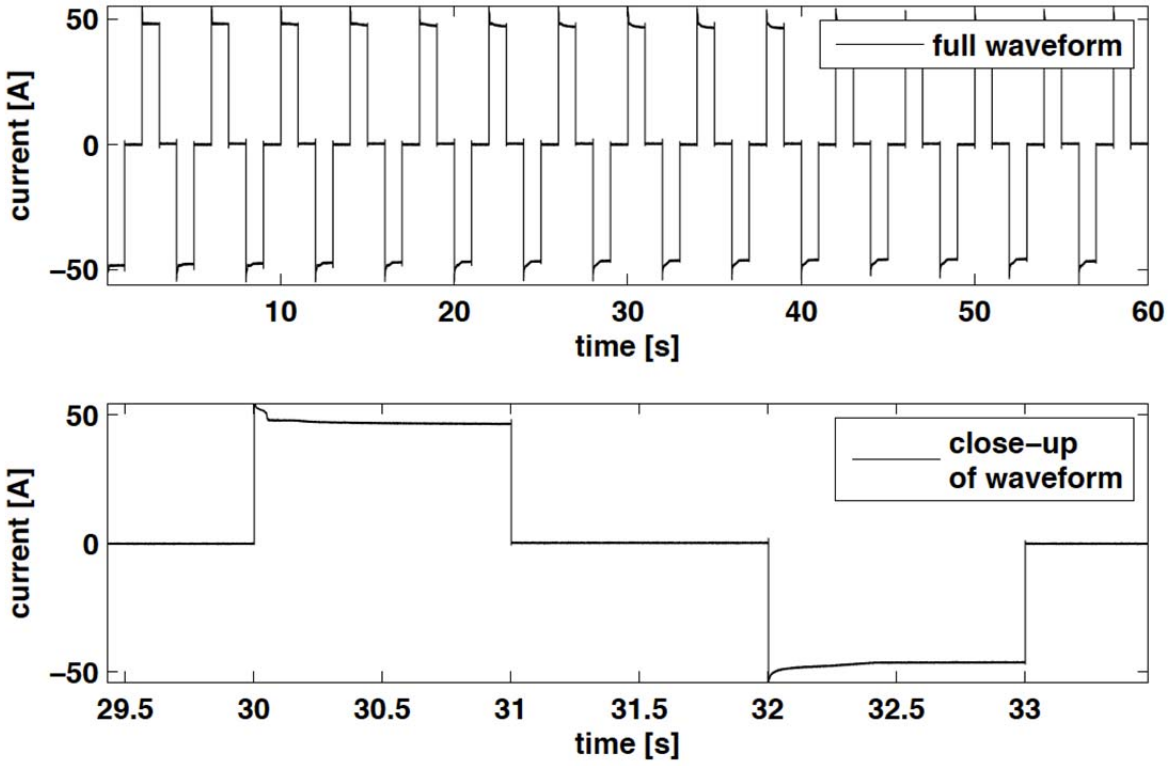

Fig. 5.15 Example of a transmitted current waveform at a transmission site.

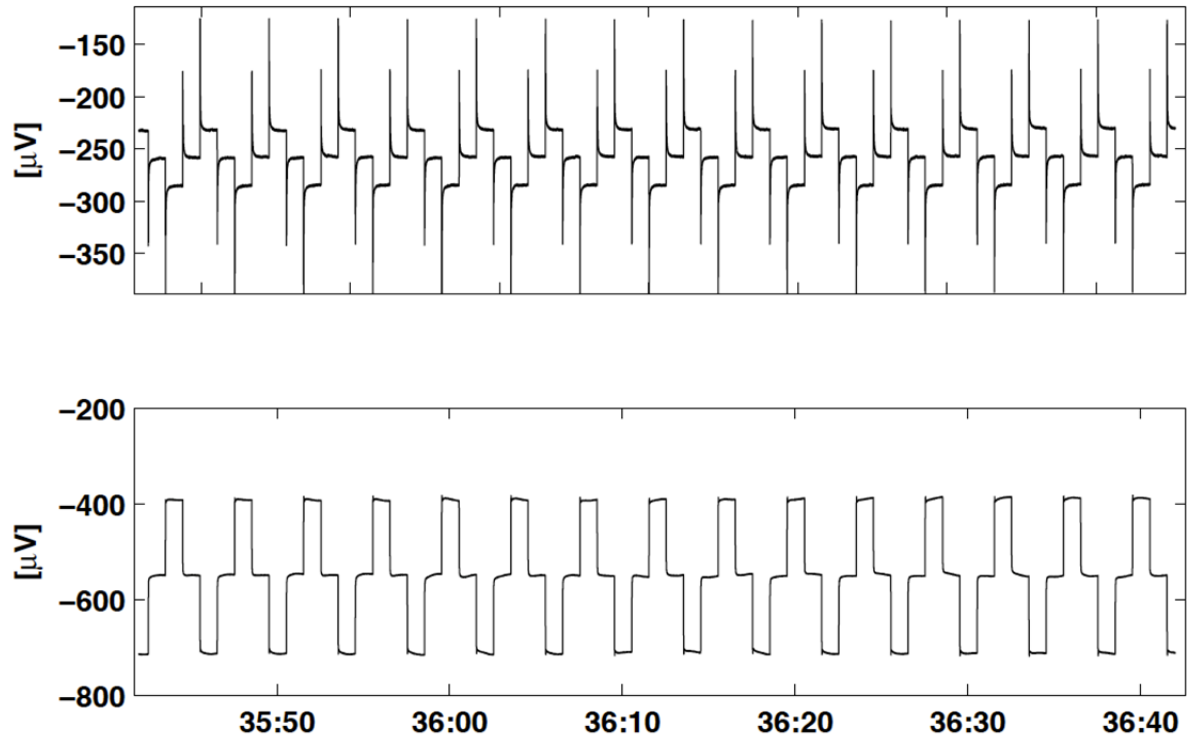

Fig. 5.16 Receiver data at G01 for transmission point 38 (approximately 200 m North of CN03 on the middle profile).

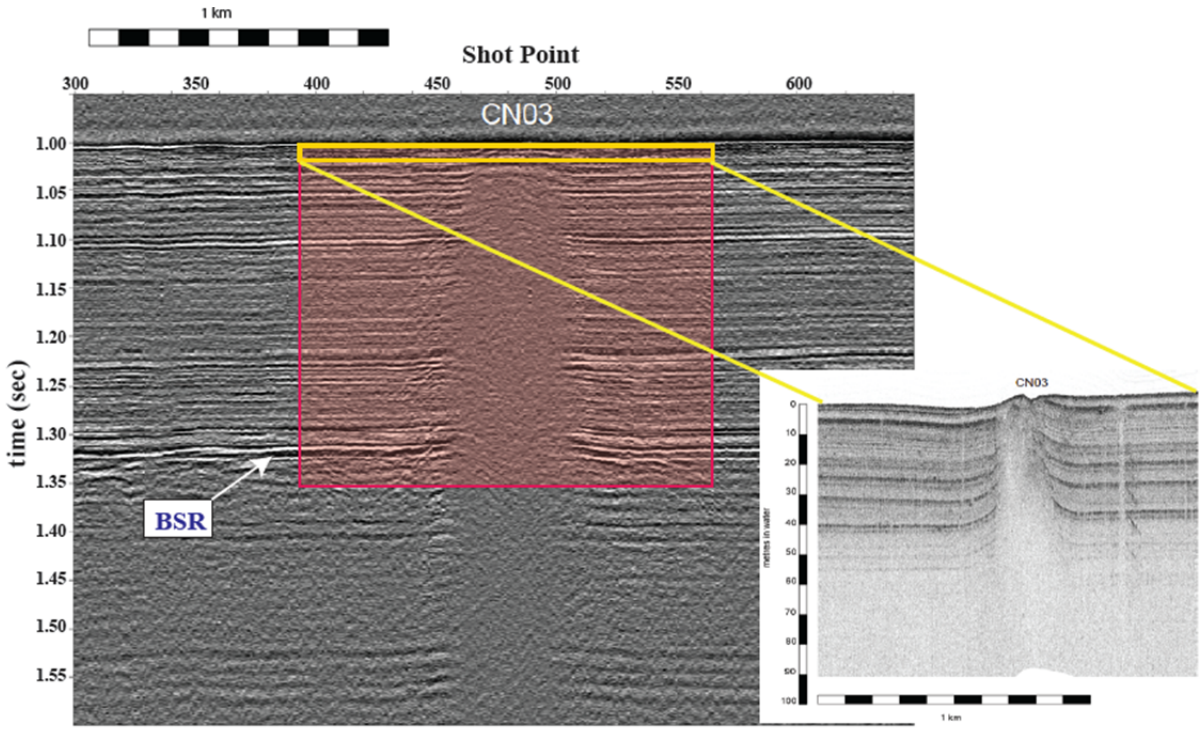

Fig. 5.17 Expected depth of investigation of the 3D tomographic EM experiment based on preliminary analysis of the data.

5.2.1.2 Intermediate depth-scale CSEM survey and 2D profile VULCAN streamer data (NOCS)

The Southampton contribution to the EM survey work made use of three types of equipment. The DASI (Deep-towed Active Source Instrument) transmitter provided frequency domain signals which were recorded by fixed sea-bottom receivers (LEMURs – Low-frequency ElectroMagnetic Underwater Recorders) and also by the deep-towed VULCAN instrument.

5.2.1.2.1 Instrument description

The DASI system (Fig. 5.18) uses a high voltage energy source provided through its umbilical tow cable, and was operated throughout M87/2 survey activities at an altitude of 50 m above the sea floor. Data from the altimeter and other key sensors (including CTD) are telemetered to operators at the surface ship through an optical fibre system embedded within the tow cable. The energy is converted in the DASI vehicle to a high current, pseudo-square wave and transmitted through a grounded dipole antenna in the form of a neutrally buoyant streamer, towed behind the DASI system. For this survey, the signal used throughout was a 1.00 Hz pseudo-square wave of approximately 100 A amplitude, and the transmitting dipole length was 100 m, giving a source dipole moment of 104 Am. Throughout the DASI survey, the DASI vehicle was positioned by Posidonia USBL acoustic navigation, using a transponder mounted in the nose of the DASI vehicle.

The fixed seabed LEMUR receivers (Fig. 5.19) record horizontal electric field data from two orthogonal channels. The sensor for each channel consists of a 12 m grounded electric dipole. The sampling rate was 125 Hz and the instruments recorded continuously from 0600UT 18/05/2012 until their recovery. The LEMURs are owned and operated by the UK Ocean Bottom Instrument Consortium (OBIC), and were provided jointly by the Universities of Durham and Southampton. Since the locations of the receivers must be known to within a few metres, it had been our intention to deploy them using the HyBIS vehicle equipped with Posidonia. However technical problems with the high voltage umbilical cable system prevented this – so the instruments were deployed from the starboard A frame on a wire, using a Posidonia beacon and an acoustic release.

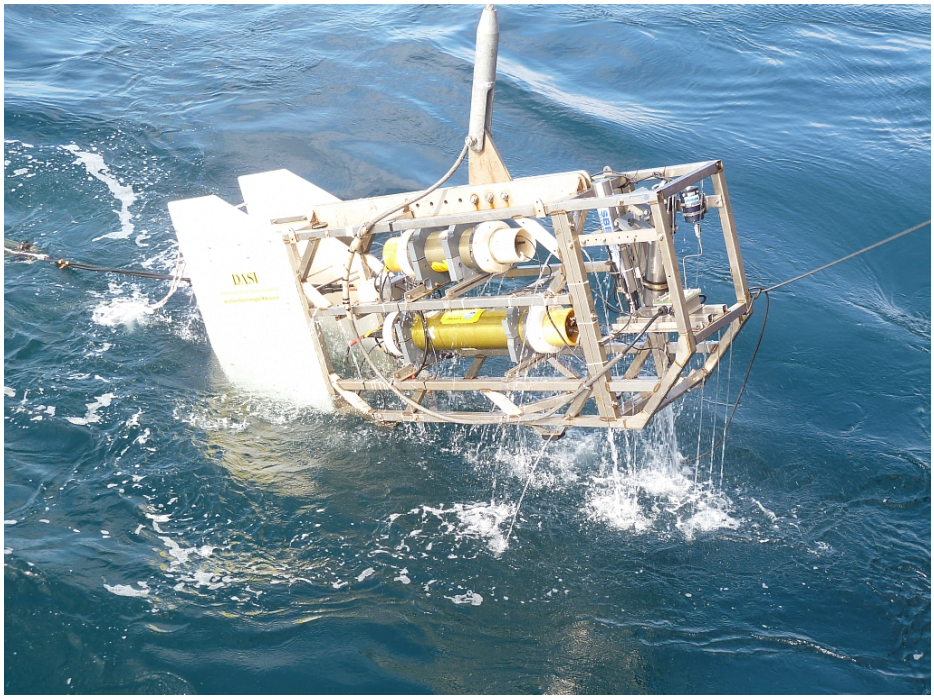

Fig. 5.18 Launching the DASI transmitter vehicle.. Photo: Chi Wu-Cheng

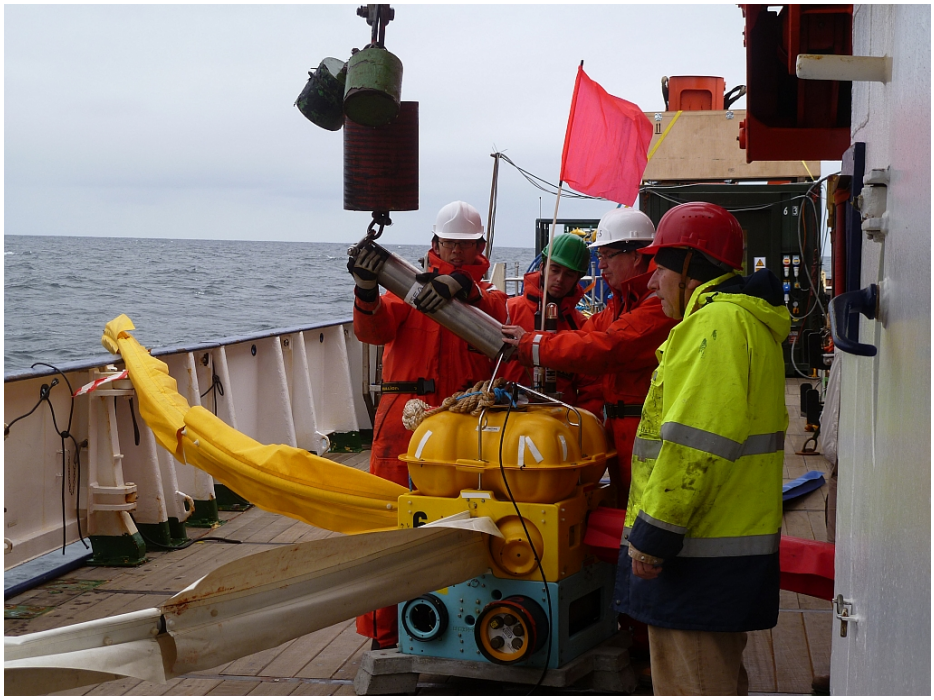

Fig. 5.19 Deployment of a LEMUR instrument, showing the acoustic release system and cable. Photo: Chi Wu-Cheng.

The third type of instrument used was the VULCAN towed receiver (Fig. 5.20). VULCAN is approximately neutrally buoyant in seawater (in fact slight positive buoyancy) and is equipped with compass and inclinometer; three channels of accelerometer; and three orthogonal channels of electric field sensor (in-line, cross-line and vertical). For this survey VULCAN was towed 300 m behind the tail end of the DASI transmitting antenna.

Fig. 5.20 Deployment of the VULCAN towed electric field receiver. Photo: Chi Wu-Cheng.

5.2.1.2.2 Experiment design

For the frequency domain CSEM survey, eight LEMUR receivers were deployed in a pattern extending up to 1.5 km from the central fluid escape feature. Four were deployed within the central zone, close to but avoiding the exact locations of the main cluster of OBSs from the

previous seismic study. The other four were placed at 1.5 km distance, along survey lines co-located with extensive airgun shooting tracks from the previous surveys. Our Line A runs N-S, and our Line B runs approximately NW-SE. The DASI system – with VULCAN – was then towed along each of these lines – first Line A from S to N, then Line B from SE to NW (see Fig. 5.11).

Two additional survey lines – C and D – were placed parallel to line B, and passing directly over the two outer LEMUR receivers on Line A. These lines are designed to provide broadside CSEM transmissions into the central group of receivers – highly desirable since a combination of broadside and in-line CSEM data, and the combination of polarization directions that it leads to, can significantly increase survey resolution; decrease ambiguities in inversion; and possibly provide some indication of any anisotropy present in the electrical resistivity structure.

On completion of Tow Lines A to D, a further survey was carried out using only the DASI-VULCAN combination. This line (E) ran from south to north across a series of seafloor fluid escape features (see Fig. 5.21) to the south and east of CN03, designated Tobic, Sharic, Bobic and Dodo (Ivanov et al., 2010).

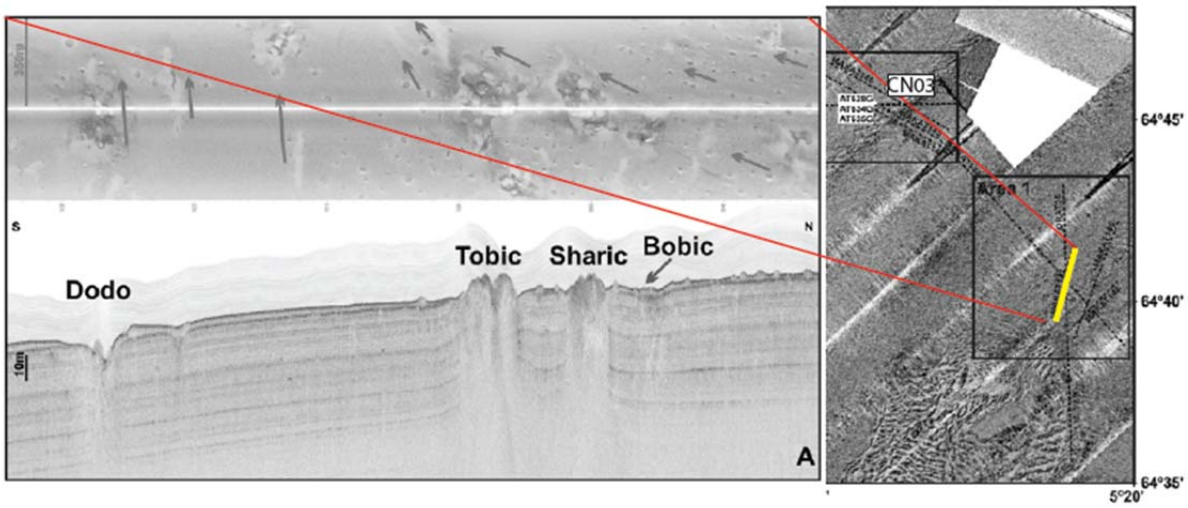

Fig. 5.21 Left: Sidescan data (upper panel) and Parasound sata (lower panel) across four fluid escape features at the northern headwall of the Storegga Slide (after Ivanaov et al., 2010). Right: Profile location (yellow line) on a sidescan sonar mosaic (Ivanaov et al., 2010); this profile corresponds to the additional Vulcan profile E.

The VULCAN receiver recorded the DASI frequency domain signal throughout DASI operations. The resulting multi-frequency data will provide a set of 2D shallow vertical high-resolution profiles of electrical resistivity along these tracks.

The LEMUR receivers recorded the DASI signals throughout most of the DASI deployment, except when the source was operating at the longest distances to the outer receivers. The resulting data set will provide a combination of 2D profiles and a 3D volume of frequency domain CSEM data, with both in-line and broadside polarizations, for inversion. The central group of LEMURs also recorded the time-domain signals from the Sputnik transmitter, and so this will provide additional data density in the central area.

The DASI signals should also have been recorded by the GEOMAR receivers, in low-frequency (10 Hz) sampling mode (as for MT). This will provide some additional data density, again within the central area, at the lowest frequencies (1 Hz and possibly 3 Hz).

Hence the combination of EM systems and survey layouts deployed here will lead to a nested set of measurements for characterising the resistivity structure beneath CN03 at a variety of scales. Firstly the MT sites (natural sources, frequency domain) will provide the vertical resistivity structure at the lowest resolution, but to a depth of several kilometres. Secondly the

LEMUR-DASI combination (controlled source in the frequency domain) will yield a background resistivity structure, over a lateral extent of up to 6 km (up to 3 km radius) and with an expected depth of penetration of up to about 700 m. Thirdly the DASI-VULCAN combination will yield a series of 2D frequency domain controlled source profiles at higher vertical and lateral resolution, but with limited depth of penetration (typically 100 - 150 m). Finally the Sputnik – GEOMAR OBEM combination, with the high frequency sampling on the OBEMs, will yield the highest resolution 3-D time domain CSEM information on the central area.

5.2.1.2.3 Preliminary results

Initial downloading and very preliminary analysis of the LEMUR and VULCAN data, carried out on board, indicates that all 8 LEMURs had recorded successfully on both channels; and that VULCAN had recorded successfully on all data channels. Initial amplitude spectrum and spectrogram plots carried out for QC purposes show good signal to noise ratios, indicated by strong peaks at the transmitter frequencies, in all cases. Time series plots of the data confirm the good signal to noise ratios achieved by the receivers (Figs. 5.22-5.25).

Fig. 5.22 Time domain plot of a sample of both channels of electric field data from all eight LEMUR recievers, during DASI transmissions. The 1 Hz signal can be seen on all channels.

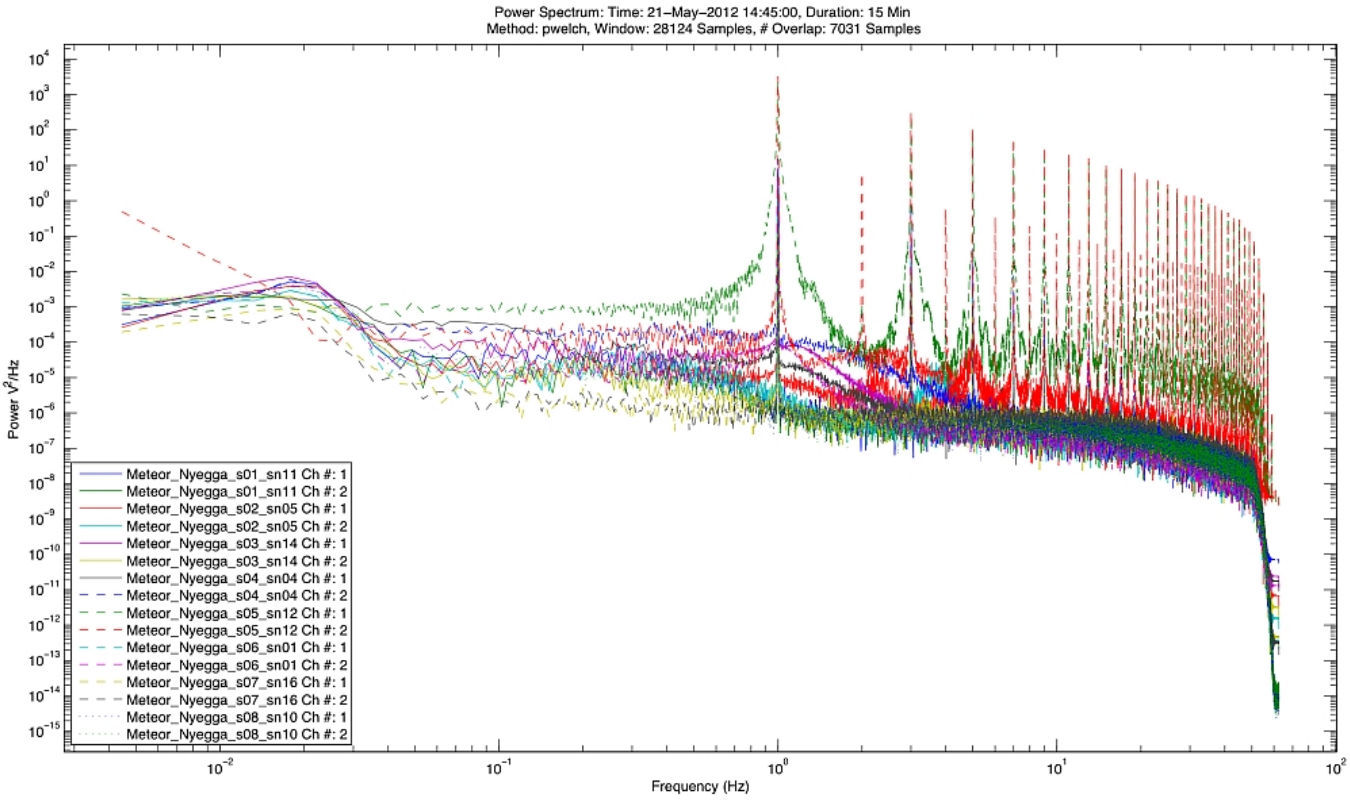

Fig. 5.23 Amplitude spectrum of both channels from all eight LEMUR instruments from a sample of data during DASI transmissions. The base frequency at 1 Hz and many higher harmonics can be seen as line peaks in the spectra. The roll off at the high frequency end corresponds to the action of the anti-alias filters in the instruments.

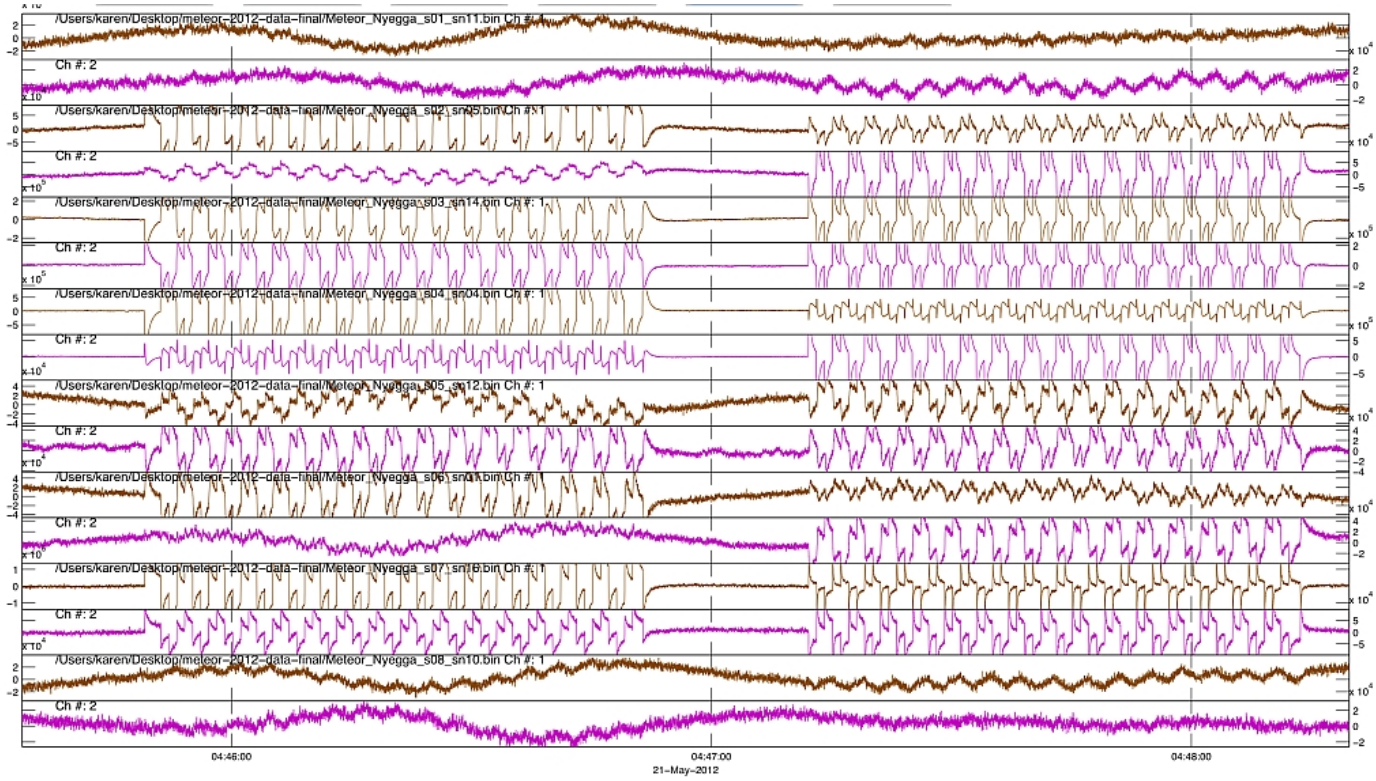

Fig. 5.24 Example of a time series section from both channels of all 8 LEMUR receivers during Sputnik time domain signal transmissions. The two intervals of data with clear signals correspond to transmissions at the two contrasting Sputnik polarizations.

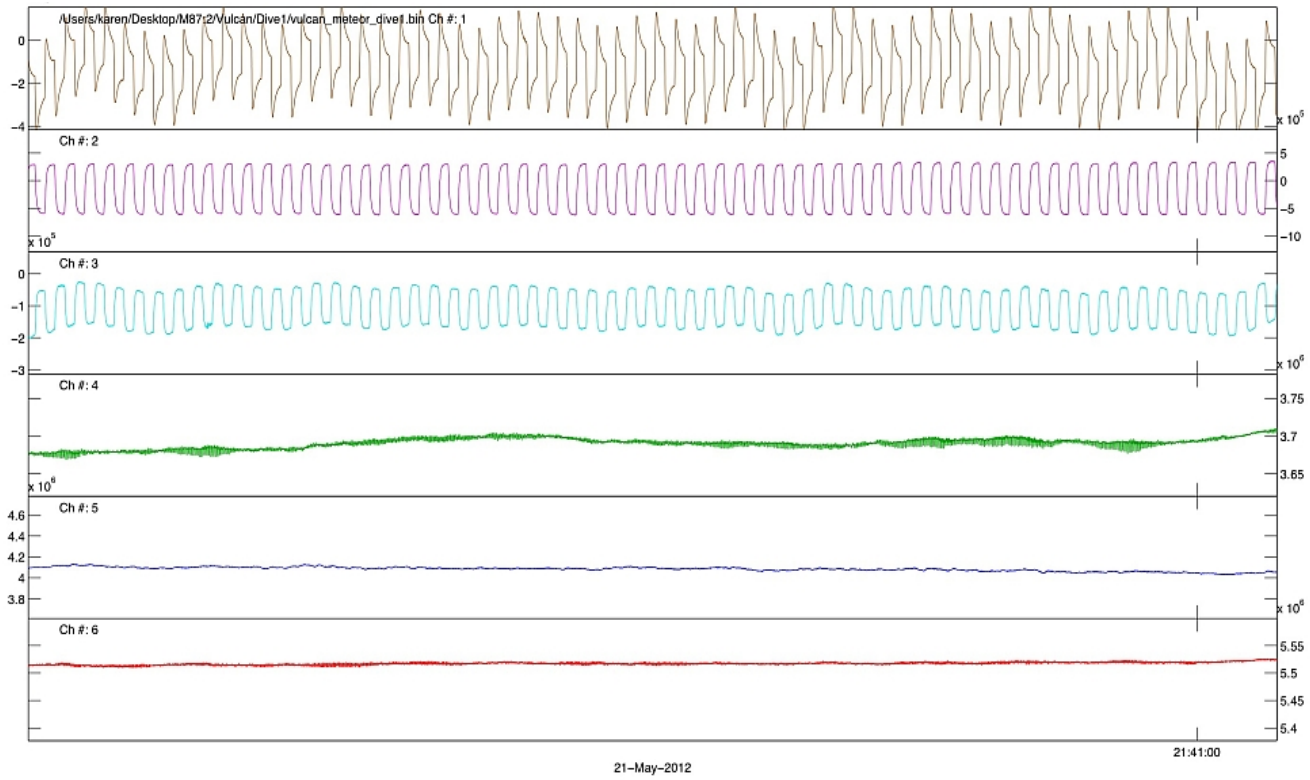

Fig. 5.25 Example time series of VULCAN receiver data during DASI operations. Upper three channels: cross-line, in-line and vertical electric field sensors respectively. Lower three channels: accelerometers.

5.2.2 Magnetotelluric data (GEOMAR)

Magnetotellurics is a passive electromagnetic geophysical method for imaging the electrical-resistivity structure (reciprocal to conductivity) of the subsurface. Naturally occurring fluctuations of the Earth's magnetic external field induce electric currents whose strength and distribution depend on the subsurface resistivity. Variations of the horizontal electric and three-component magnetic fields are recorded on the ocean bottom to derive a spectral, complex-valued impedance tensor Z given by Z Hh = Eh where Eh and Hh denote the frequency-dependent horizontal electric (Eh) and magnetic (Hh) field vectors. In a homogenous half-space, the so-called skin depth d is a crude estimate of detection depth with d = sqrt(r T) in kilometres (where T is the period in seconds and r is the bulk resistivity). At periods shorter than approximately 1 s, seafloor electromagnetic signals are very small. This is due to the high conductivity of the seawater above, which causes attenuation according to skin depth and thus reduces the resolvability of shallower sea-bottom features.

5.2.2.1 Ocean bottom magnetotelluric receivers

To allow the recording of low-frequency magnetotelluric data, the GEOMAR receivers are also equipped with a highly sensitive flux gate magnetometer and a separate low frequency ADC board. Switching from the MT modus recording low frequency (max 10 Hz) electric and magnetic fields to CSEM modus recording electric fields at 10 kHz is initiated through an acoustic transponder signal from the ship.

5.2.2.2 Experiment design

The MT signals were recorded at G01 to G06 when no transmission of an active signal occurred. Given the low resolution of the method, it would have been desirable to spread out the MT sites over several kilometres; however, this could not be done due to the limited number of instruments available. The longest section of continuous MT data was 45 hours and recorded

from the time that the instruments were placed onto the seafloor up to the first CSEM transmission.

5.2.2.3 Preliminary results

Fig. 5.26 and Fig. 5.27 show the recorded electric and magnetic field variations at station G01 over the 45 hours period. Clear magnetic and electric field amplitudes could be measured. Pitch and roll measurement show that very little movement of the instrument on the seafloor has occurred, thus indicating that the data is motion noise free.

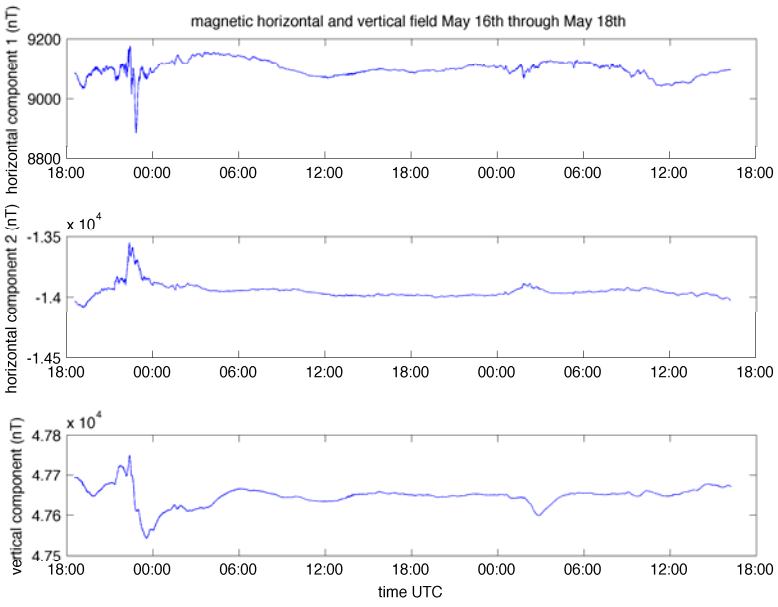

Fig. 5.26 Raw magnetic field variations recorded at OBEM station G01.

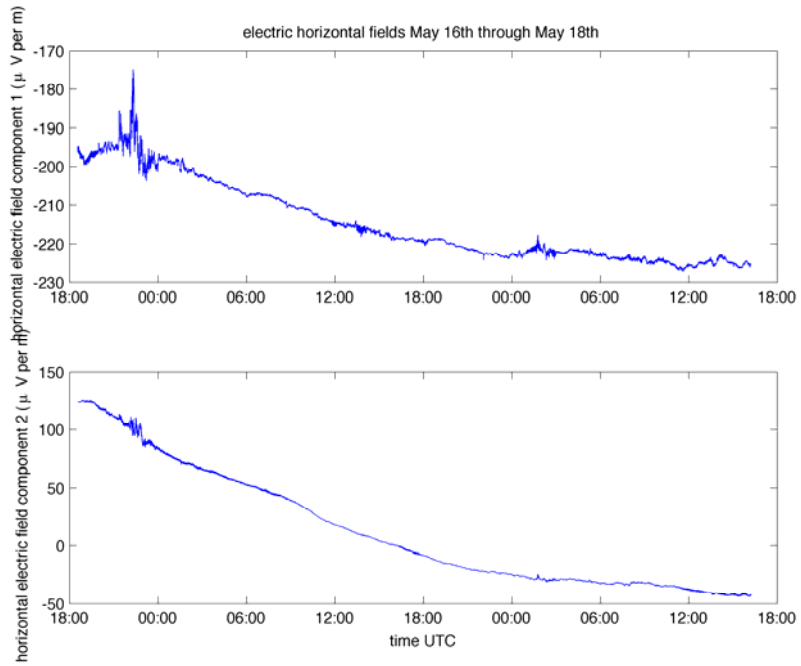

Fig. 5.27 Raw electric field variations recorded at OBEM station G01.

5.2.3 Parasound data

In order to to map out the extent of slope instabilities above the gas hydrate zone in the northern side wall of the Storegga Slide, and to determine whether the crack-bounding normal faults displace the shallowest stratigraphic horizons, within 5 m or so of the seafloor, ultra high-resolution data are required. To guide the initial Parasound survey planning, we calculated

curvature attributes from the seafloor reflection in existing industry 3D seismic data. This attribute allowed us to detect the spatial distribution of some of these cracks in the survey area.

5.2.3.1 Experiment design

A total of 26 Parasound lines were collected in the Nyegga area during four separate surveys (Fig. 5.28), with multibeam data being collected simultaneously. The first survey lasted from 03:20 to 14:10 on 18.05.2012, and the second survey was run during the night from 20:40 to 09:00 on 19.05.2012. The third survey lasted from 19:10 on 22.05.2012 to 2:10 on 23.05.2012. The fourth survey was the 2D seismic survey during which Parasound and multibeam data were collected as well. This survey was run from 01.10 on 24.05.2012 to 12:00 on 25.05.2012.

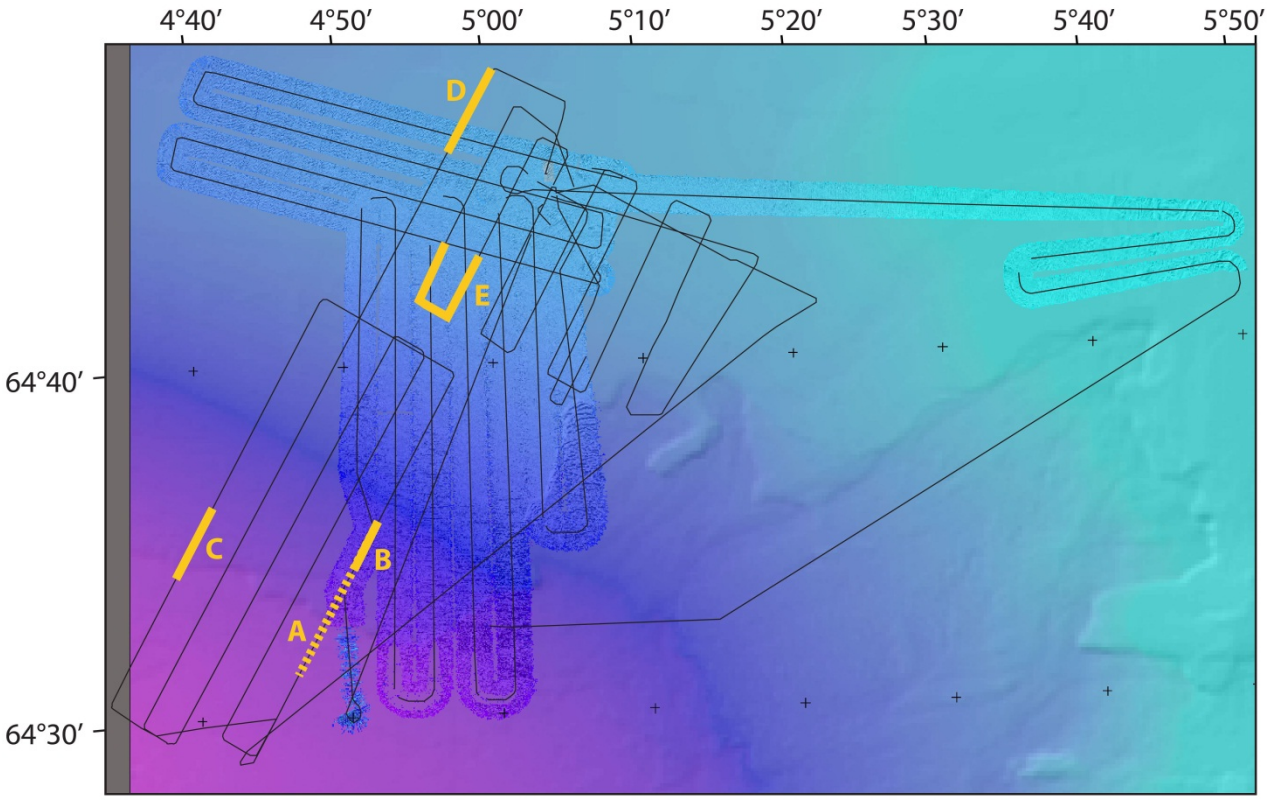

Fig. 5.28 Map of the Parasound profiles (thin black lines) acquired in the Nyegga survey area. Line segments marked in yellow shown in Fig. 5.24.

5.2.3.2 Preliminary results

We observe very good signal penetration (up to 80 m) and the vertical resolution is sufficient to delineate very small-scale stratigraphic layering. Fig. 5.29 shows a series of typical Parasound profiles, where crack features and slide deposits can be clearly mapped out. Aside from acquiring data over the cracks identified in the existing 3D seismic data, we also collected a series of lines west of the cube that revealed another two major crack systems that strike approximately E-W. Most of the surveyed cracks are characterised by one pair of conjugate normal faults that bound the down-thrown block, but we also identified systems with two sets of normal faults. In most cases the strata of the down-thrown block are characterised by approximately the same dip as the strata outside the crack system, but there are also examples of block tilting between the faults (e.g. Fig. 5.29 middle panel and lower right panel).

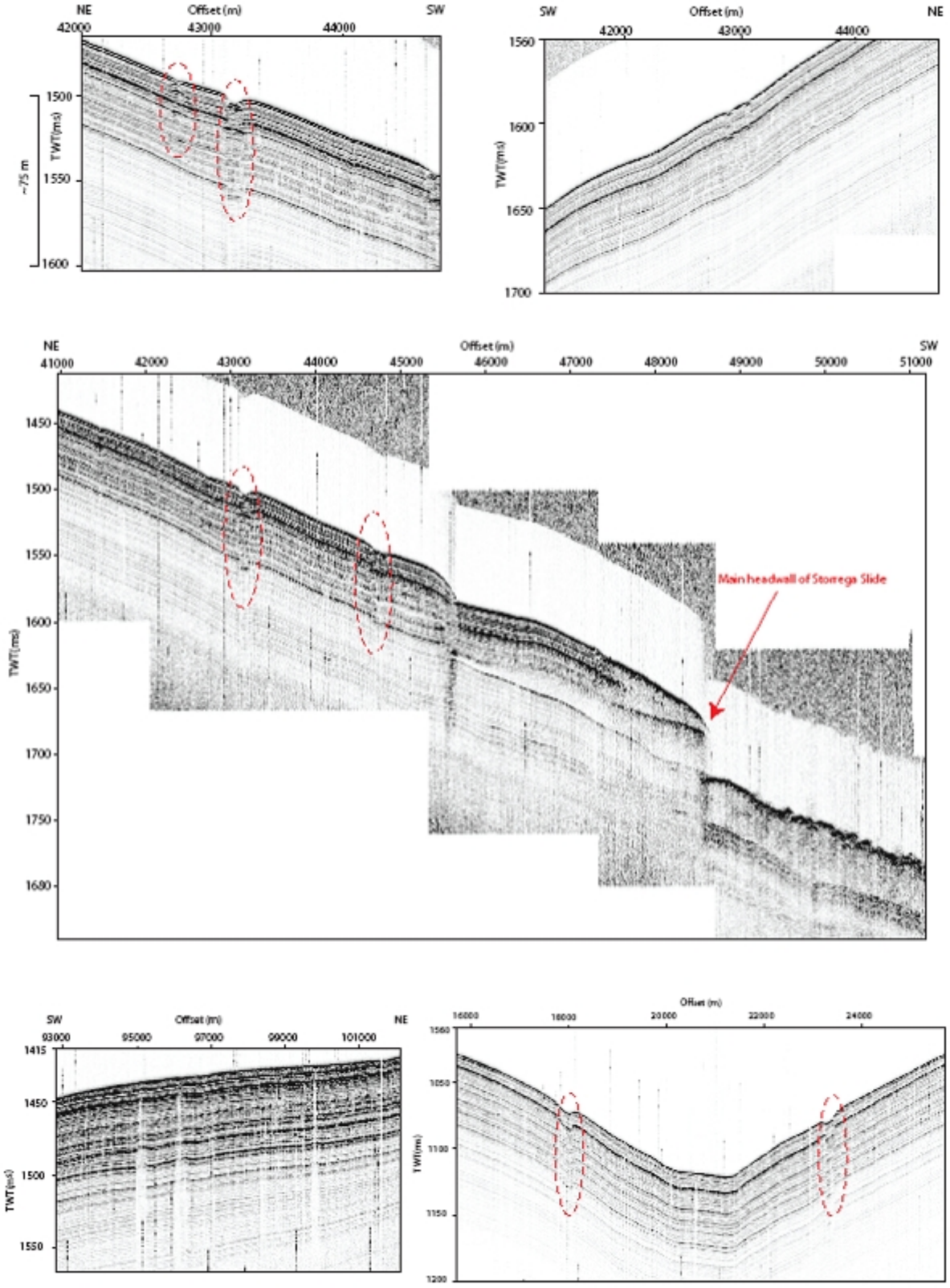

Fig. 5.29 Example Parasound profiles from the Nyegga survey area. Extensional crack systems are highlighted by the broken red ellipses in each of the different figure panels. Upper panel: Cracks (left; location A in Fig. 5.28) and normal faults (right; B in Fig. 5.28) near the Storegga sidewall. Middle panel: Cracks north of the main headwall of the Storegga slide (C in Fig. 5.28). Lower panel: Vertical chimney structures (left; D in Fig. 5.28) and crack (right; E in Fig. 5.28).

Based on an assessment of all Parasound data, we selected two cracks to be targeted by dedicated HyBIS dives. The Parasound images of these cracks show indications that deformation is likely to extend to the seafloor. Firstly, offset reflections can be observed just a few metres beneath the seafloor, and secondly, strong diffraction hyperbolae are observed originating from the seafloor reflection. This latter observation suggests that a significant discontinuity exists at the seafloor reflection, within the resolution of the data.

5.2.4 2D-Seismic data

5.2.4.1 Experiment design

At the completion of the HyBIS survey (5.2.5) the 2D seismic system was deployed and 11 profiles were acquired over a period of approximately one and a half days (Fig. 5.30). Acquisition parameters are given in Table 1. The survey was designed to image as many of the cracks as possible, extend into the Storegga slope failure, and image some of the Nyegga chimney province.

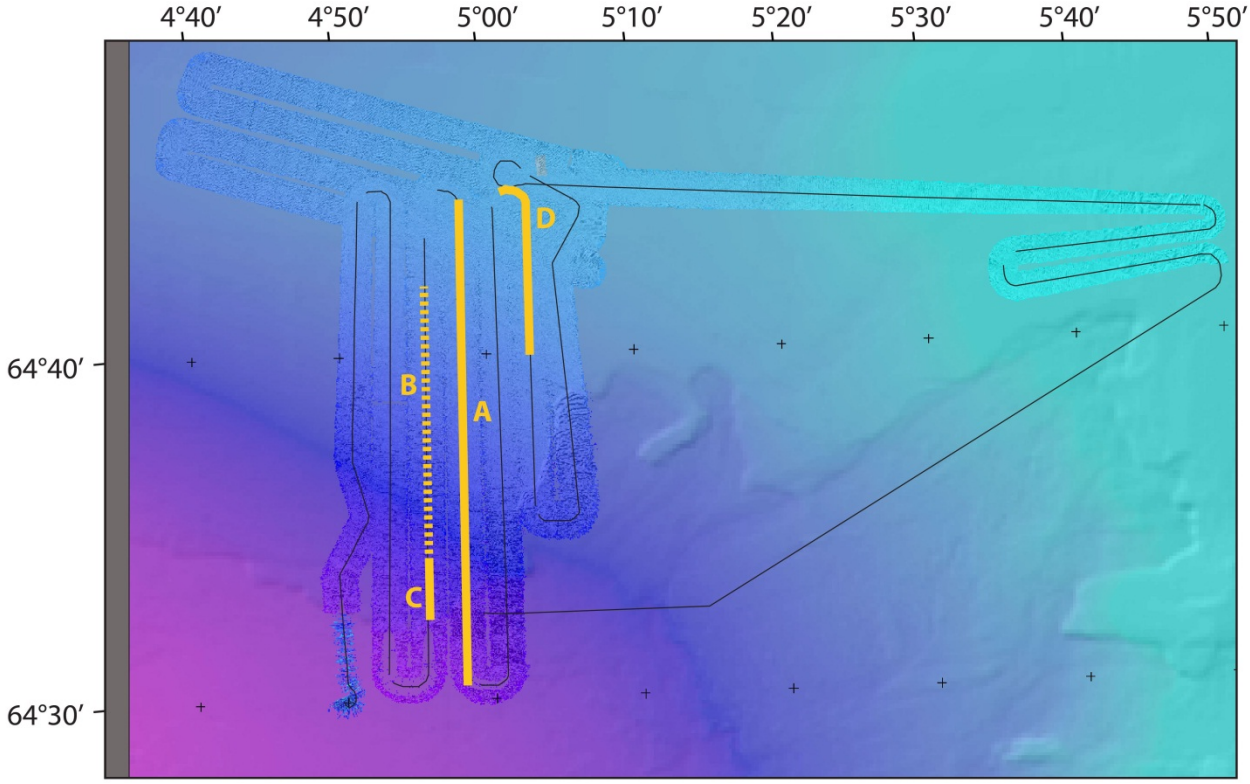

Fig. 5.30 Map of the 2D seismic profiles (thin black lines) acquired in the Nyegga survey area. Line segments marked in yellow are shown in the following figures.

5.2.4.2 Preliminary results

The seismic data are of excellent quality (e.g. Fig. 5.31), allowing the detection of fine-scale fault systems and the resolution various stratigraphic and structural relationships in very high detail. A direct comparison between existing industry 3D data and the new 2D seismic profiles is given in Fig. 5.32. The drastic improvement in both horizontal and vertical resolution is critical for determining the distribution of fine-scale faulting and offset layering.

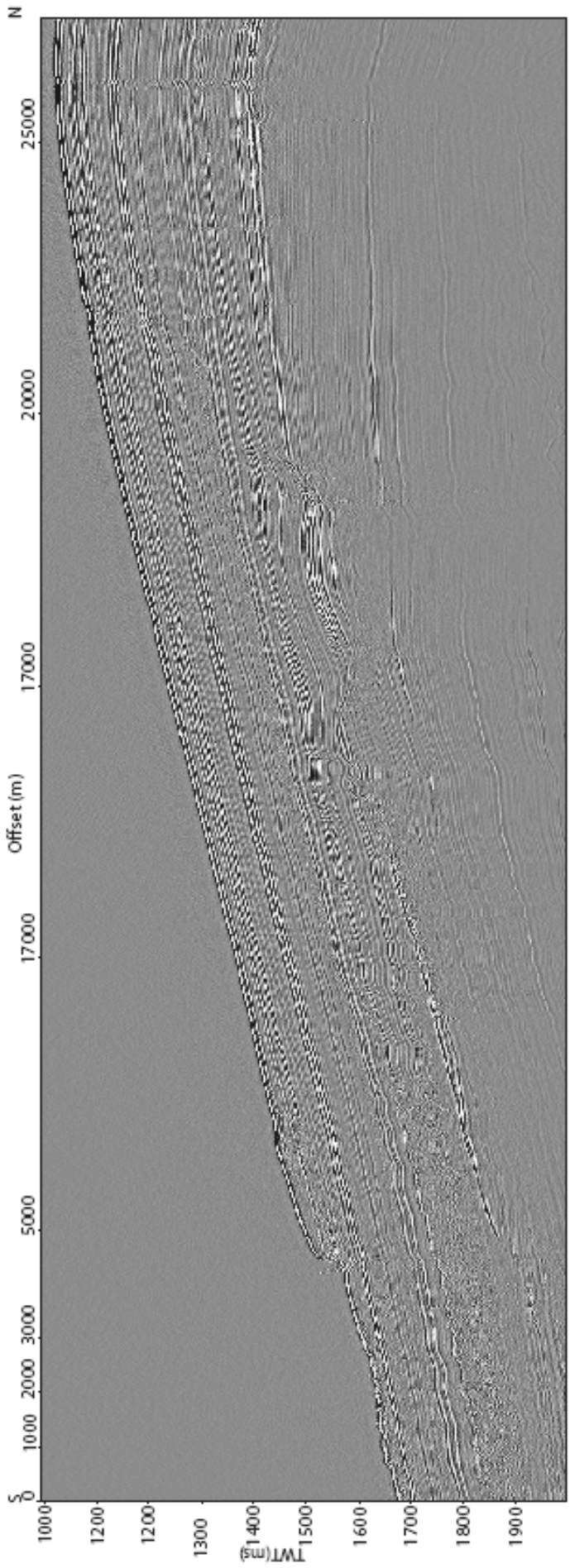

Fig. 5.31 An example 2D seismic section from the Nyegga survey area (location A in Fig. 5.30). The data are binned at 1.25 m and reveal excellent signal to noise ratio.

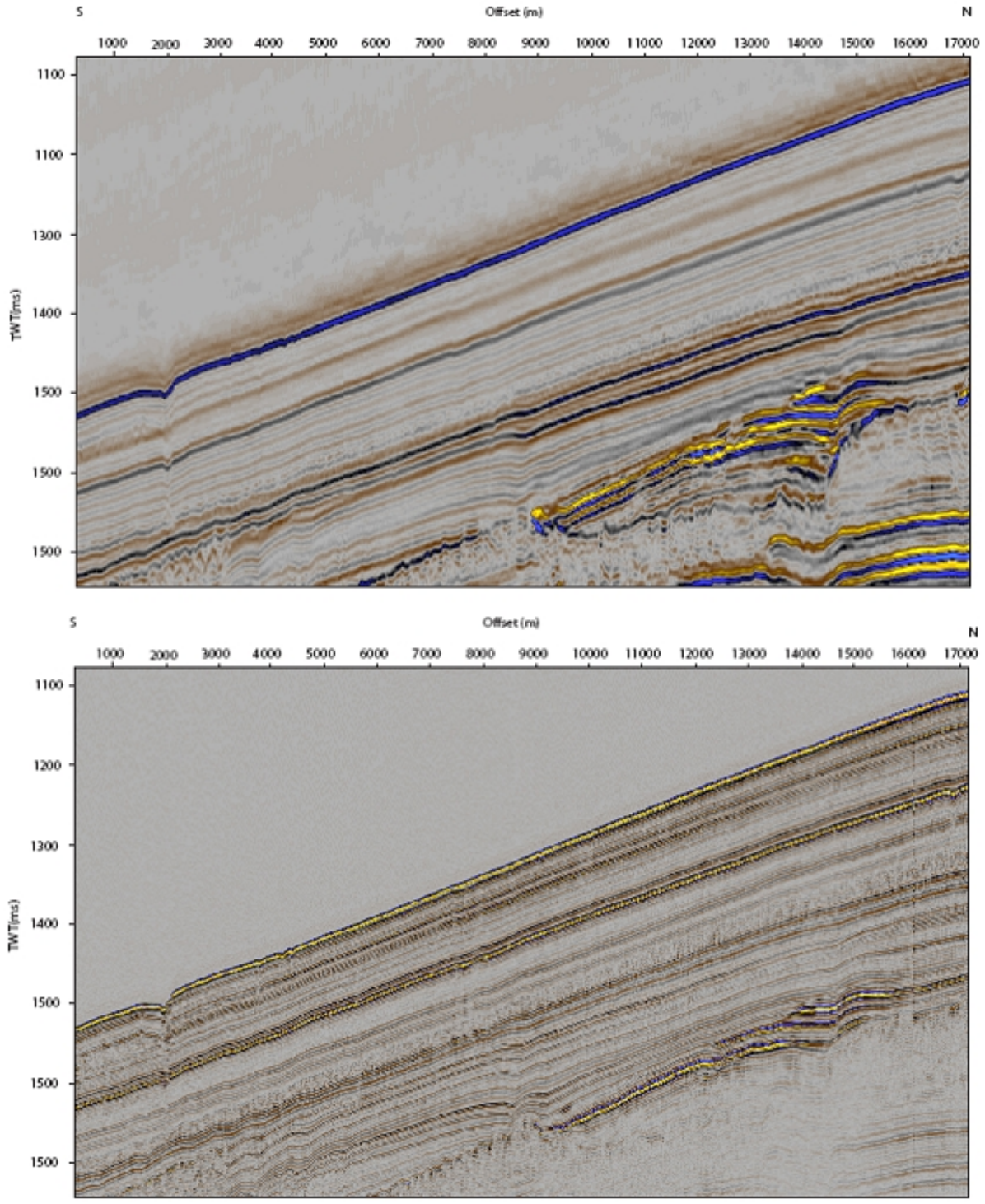

Fig. 5.32 Comparison between existing 3D seismic data (above) and the new 2D data (below), plotted at the same scale. The marked improvement in resolution in the 2D dataset is apparent. Location B in Fig. 5.30.

The crack features can be clearly mapped out in the 2D data (e.g. Fig. 5.33). One of the most striking observations with respect to the crack systems is that the bounding normal faults extend to various stratigraphic depths. Many of them, including some of those where the deformation appears to extend to the seafloor, can be traced to depths greater than the base of the Storegga slide complex. Others terminate at shallower depths above the base of the Storegga Slide.

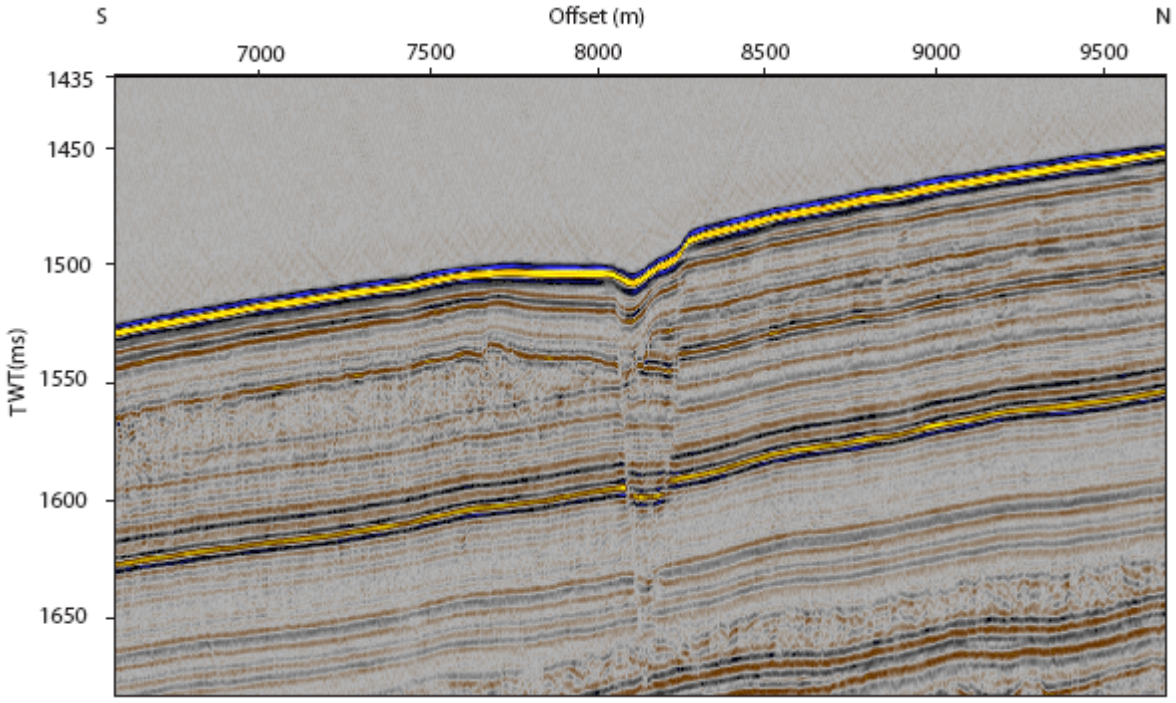

Fig. 5.33 A seismic section across one of the well-defined extensional crack features (C in Fig. 5.30). The conjugate fault set can be clearly delineated, defining the margins of a graben structure.

5.2.4.3 Outlook

More work will be required to understand the significance of these observations with respect to the history of extension along the faults. Aside from delineating the geometry of the crack systems, the 2D seismic data deliver very high resolution of some of the Nyegga chimneys that were crossed during the profiling (e.g. Fig. 5.34).

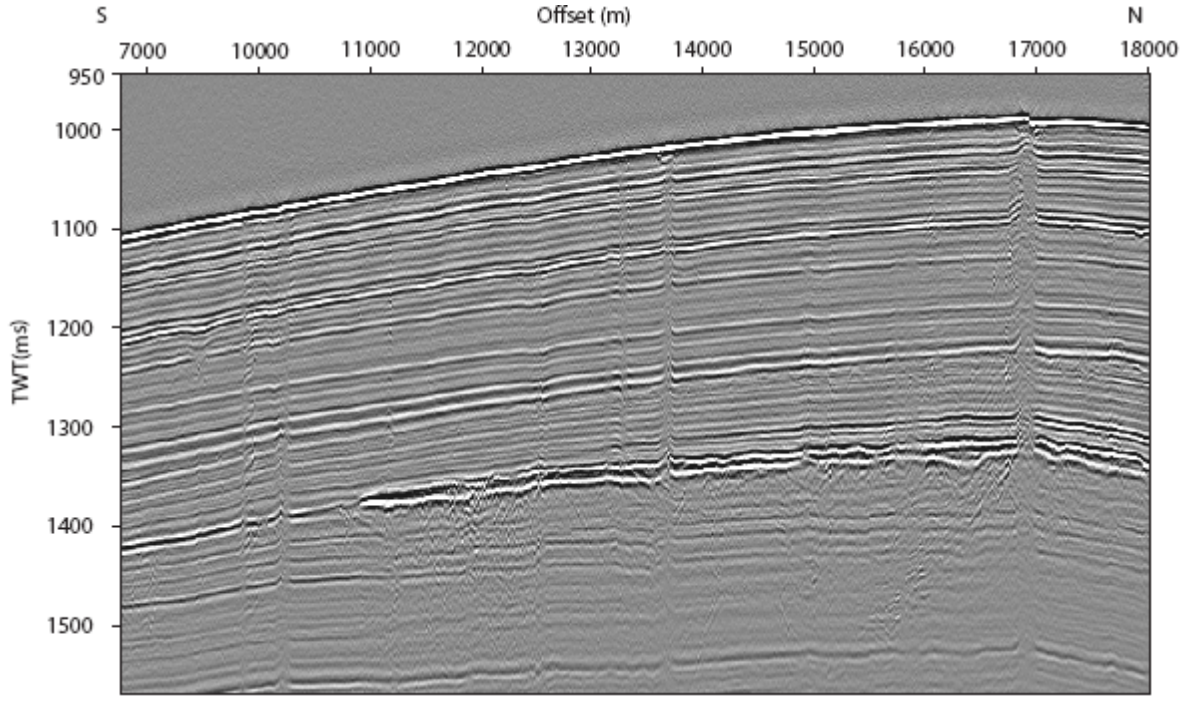

Fig. 5.34 A seismic section across a series of vertical blanking zones – some of the Nyegga chimney structures (D in Fig. 5.30). The chimney at an offset of approximately 1700 m along this profile is characterised by prominent seafloor topography and offset reflectors on either side.

5.2.5 HyBIS operations

5.2.5.1 The HyBIS vehicle

HyBIS is a simple, low-cost, multi-purpose, survey and sampling robotic underwater vehicle (RUV) with a depth capability of 6000 m (Fig. 5.35). It was designed and built in the UK by Hydro-Lek Ltd. in collaboration with the National Oceanography Centre, Southampton (NOC), back in 2008.

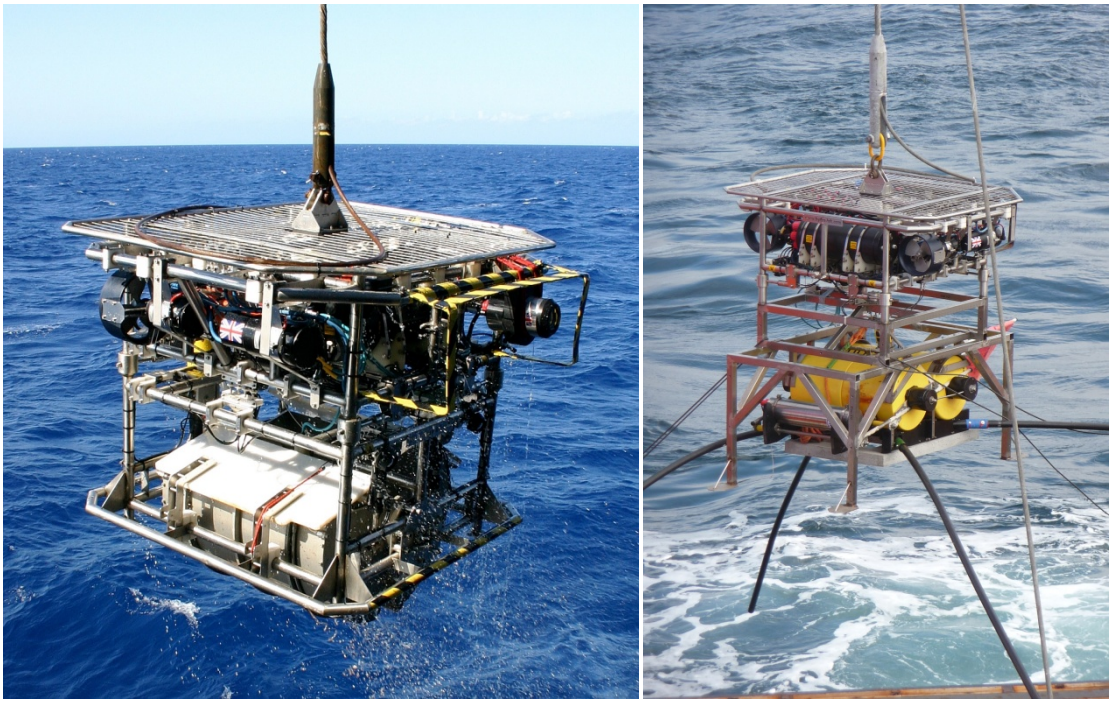

Fig. 5.35 HyBIS vehicle with grab (left) and GEOMAR OBEM deployment module (right).

The vehicle has a modular design that makes it very versatile, with the top module being a command and power system that comprises power management, cameras, lights, hydraulics, thrusters and telemetry. Telemetry is via a single-mode fibre optic link and provides 3 channels of real-time standard-definition colour video plus vehicle attitude data. Power is supplied through a single-phase 1500V ac, 8kVA umbilical and converted to 3-phase 120V on the vehicle by two silicon motor controllers, 240V ac for the lights, and 24 to 12 V dc for onboard instruments.

The easily changeable lower modules available at the moment include a clam-shell sampling grab, a 5-function manipulator-arm and tool sled, a winch with 600m rope for instrument recovery and an ocean bottom seismometer deployment module. The sampling module used during M87/2 during the video surveys comprised a 0.5 cubic metre clam-shell grab with a pay-load capacity of 750kg and closure force of 4 tonnes. No sediment sample was taken during the voyage of RV Meteor 87/2. The GEOMAR OBEM deployment module worked perfectly on the vehicle (Fig 2.26b).

Unlike a conventional ROV, HyBIS does not have any floatation or buoyancy, it is rather suspended by its umbilical cable directly from the ship which makes it slightly susceptible to ship roll and heave motion. On the positive side, the advantage of direct suspension is that HyBIS can recover or deploy a payload of up to 750kg.

Laboratory control unit setup

The top-side control centre (Fig. 5.36) was established in the wetlab, on port side, towards the aft and next to the Hatlapa deep-tow winch. This minimised the length of trailing high-voltage leads across the deck. The DASI HV container provided the access to the high-voltage junction

box. The vehicle's primary control box was supplemented with additional monitors and a relay of the USBL navigation screen. A dedicated GPS aerial was mounted on an out-rigger over the port side and provided a continuously recorded GPS string to the Garmin GPS navigation system in the control box. Winch controls were established adjacent to the vehicle pilot's position, allowing synchronisation between winch operator and pilot. Two additional television screens were installed to allow the winch driver to observe the winch drum and the friction.

Video was recorded digitally as DV and AVI formats on 2Tb hard-discs. Two cameras (forward and downward SD) were recorded continuously in standard definition. The forward looking camera with vehicle attitude data overlain was also recorded on DVDs of about one hour length. Full HD video (1080i, PAL, 30fps, AVCHD format) was not used. Back-ups of all dive data and videos were then made on regular intervals. All GPS navigation data were recorded on the top-side command unit and copied to a USB portable drive. Time codes were all set and synchronised to GMT.

Acoustic navigation was provided by the 'Ixsea' USBL system ABYSS on the RV Meteor and a mini transponder on the HyBIS vehicle. Tracking was generally good although transponder battery conditions provide a limited maximum dive time of about 8 hours until recharge becomes necessary.

Fig. 5.36 Left to right, top to bottom: Lab setup showing video screen arrangements for the winch and the HyBIS video logging system and main control box.

High-voltage power setup

Prior to the survey, the HyBIS HV transformer was installed inside the DASI power container in order to comply with UK high-voltage regulation that requires HV equipment to be stored safely in a lockable enclosure. HV safe working procedures were put in place which meant that neither HyBIS nor DASI were to be switched on prior to deployment and recovery. HV working permits were issued and signed off for each deployment.

The Hatlapa winch system

For the cruise the purpose-built containerised Hatlapa winch system was used. It consists of two standard 20' containers carrying the winch drum in one, and the friction system in the second. The cable was a 24 mm double-armoured steel cable with several cores (3 for high voltage, 3 for voltages up to 1000 V) and 6 single mode fibre optic leads. The fibre optic wires were altogether in a metal tube, but had no standard protection other than the coloured 125 micrometre coating. This resulted in the fibre being very fragile when being transferred from one vehicle to another. The winch could be operated very smoothly allowing the winch drivers to keep the vehicles at the required depth, sometimes only a couple of metres above the seabed.

Although one fibre was already connected to the slip ring, none of the 6 fibres were connected in the winch junction box on the left hand side of the drum. It took two days to connect and polish the delicate fibres. Since the winch was delivered without cable to connect it to a power source, a ~10 m section of the deep-tow cable was cut off and used to connect the DASI container to the winch.

5.2.5.2 Experiment design (dive narrative)

May 17th, 2012, HyBIS Dive #88
Nyegga Area (64° 45.29N, 05° 04.44E), water depth ~720 m
Aim: Deploy and install a GEOMAR Ocean Bottom Electromagnetic receiver (OBEM G1).
HyBIS deployed the OBEM instrument successfully. No video inspection was carried out.

May 17th, 2012, HyBIS Dive #89
Nyegga Area (64° 45.37N, 05° 04.28E), water depth ~720 m
Aim: Deploy a GEOMAR Ocean Bottom Electromagnetic receiver (OBEM G2).
The descent had to be abandoned due to the detachment of the OBEM recovery line which got entangled around the release mechanism of the instrument.

May 17th, 2012, HyBIS Dive #90
Nyegga Area (64° 45.37N, 05° 04.27E), water depth ~720 m
Aim: Re-deploy and install a GEOMAR Ocean Bottom Electromagnetic receiver (OBEM G2).
HyBIS deployed the OBEM instrument successfully. No video inspection was carried out.

May 17th, 2012, HyBIS Dive #91
Nyegga Area (64° 45.23N, 05° 04.26E), water depth ~720 m
Aim: Deploy a GEOMAR Ocean Bottom Electromagnetic receiver (OBEM G3).
HyBIS released the OBEM instrument successfully and its position and orientation on the seabed was recorded by a short video survey.

May 17th, 2012, HyBIS Dive #92
Nyegga Area (64° 45.26N, 05° 04.00E), water depth ~730 m
Aim: Deploy a GEOMAR Ocean Bottom Electromagnetic receiver (OBEM G4).
The descent had to be abandoned due to the detachment of the OBEM recovery line which got entangled around the release mechanism of the instrument.

May 17th, 2012, HyBIS Dive #93
Nyegga Area (64° 45.25N, 05° 03.98E), water depth ~730 m
Aim: Deploy a GEOMAR Ocean Bottom Electromagnetic receiver (OBEM G4).
The descent had to be abandoned due to a high-voltage power problem in the HyBIS system. The fault could not be located immediately hence all further HyBIS OBEM deployments were cancelled.

May 23rd, 2012, HyBIS Dive #94
Nyegga Area (64° 39.05N, 05° 05.26E), water depth ~830 m
Aim: Video survey in the Northern part of the Nyegga area to inspect fault structures identified on the seismic records, and take a grab sample if possible.
The dive had to be abandoned due to a light circuit failure in the forward light harness.

May 23rd, 2012, HyBIS Dive #95
Nyegga Area (64° 39.06N, 05° 05.27E), water depth ~830 m
Aim: Continue video survey of Dive 94, in the Northern part of the Nyegga area.

May 23rd, 2012, HyBIS Dive #96
Nyegga Area (64° 35.51N, 04° 51.92E), water depth ~1075 m
Aim: Video survey in the Northern part of the Nyegga area to inspect fault structures identified on the seismic records, and take a grab sample if possible.

With over 13 hours of total dive time, HyBIS played an important part of the science activity during the cruise although the available time window for HyBIS operations was small.

Due to minor technical problems which however took some time to find and rectify, not all of the OBEM receivers could be deployed using the HyBIS module. The remaining OBEM receivers had to be deployed in the old fashioned way using a small diameter winch cable and an acoustic release. A fault in the forward light harness caused a 2-hour delay in the operations on the day the video surveys were planned. Apart from this, the HyBIS vehicle itself worked without any problem.

5.2.5.3 Preliminary results

Seismic and Parasound profiles highlighted the presence of E-W oriented shallow faults that are parallel to the escarpment framing the northern part of the Storegga Slide. These structures dislocate the uppermost ~150-200 m of sediments and appear to reach the surface. Two TV lines were selected for sea floor investigations and possible sampling with HyBIS (Fig 2.31). The aim of the TV survey was to define if these faults are clearly visible on the seafloor and if there is any sign of recent activity. Additionally these zones could act as preferential pathways for the release of shallow fluids and thus possible authigenic carbonate precipitation.

Dive 95 (Station no.759 - Transect 1) This first transect aimed to investigate the southeastern margin of the escarpment (Fig. 5.37) Here the Storegga Slide forms an embayment and a distinct crevasse extends to the northwest within the escarpment. The N-S oriented dive (Fig. 5.38) aimed to cross the first crevasse and finally end within the Storegga Slide.

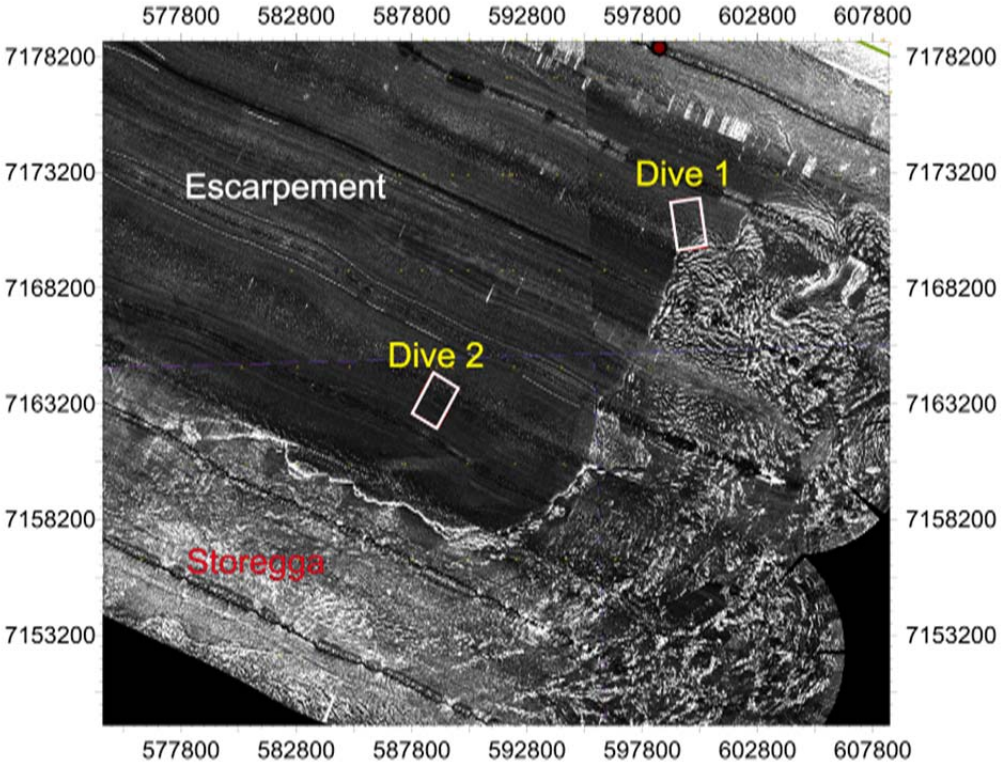

Fig. 5.37 Tobi 30 kHz sidescan sonar survey of the investigated area with the Storegga Slide in the southern part, and the escarpment in the northern part of the image. White boxes indicate the location of the two HyBIS dives. Map coordinates are in UTM zone 32.

The water column was characterized by dense clouds of plankton particles and detritus particularly between 300-500 m and between 800m to the seafloor. Shrimps were constantly present in the vicinity of the sea floor (Fig. 5.39a). The sea floor consisted of greyish brown soft clayey sediment that was heavily bioturbated throughout. Strong evidence of vertical bioturbation was visible around the burrows where lighter colored sediment from deeper non oxidized layers is expelled (Fig. 5.39b). The fauna observed consisted of numerous sea stars and/or brittle stars (of white and pink colours), occasional white bivalves, anemones, echinoderms, and a small snake fish (?) (Fig. 5.39c). The crossing of the crevasse was characterized by irregular seafloor and the dispersed alive pink coral branches (possibly *Madrepora Oculata*) that likely settled on exposed dropstones (Fig. 5.39d).

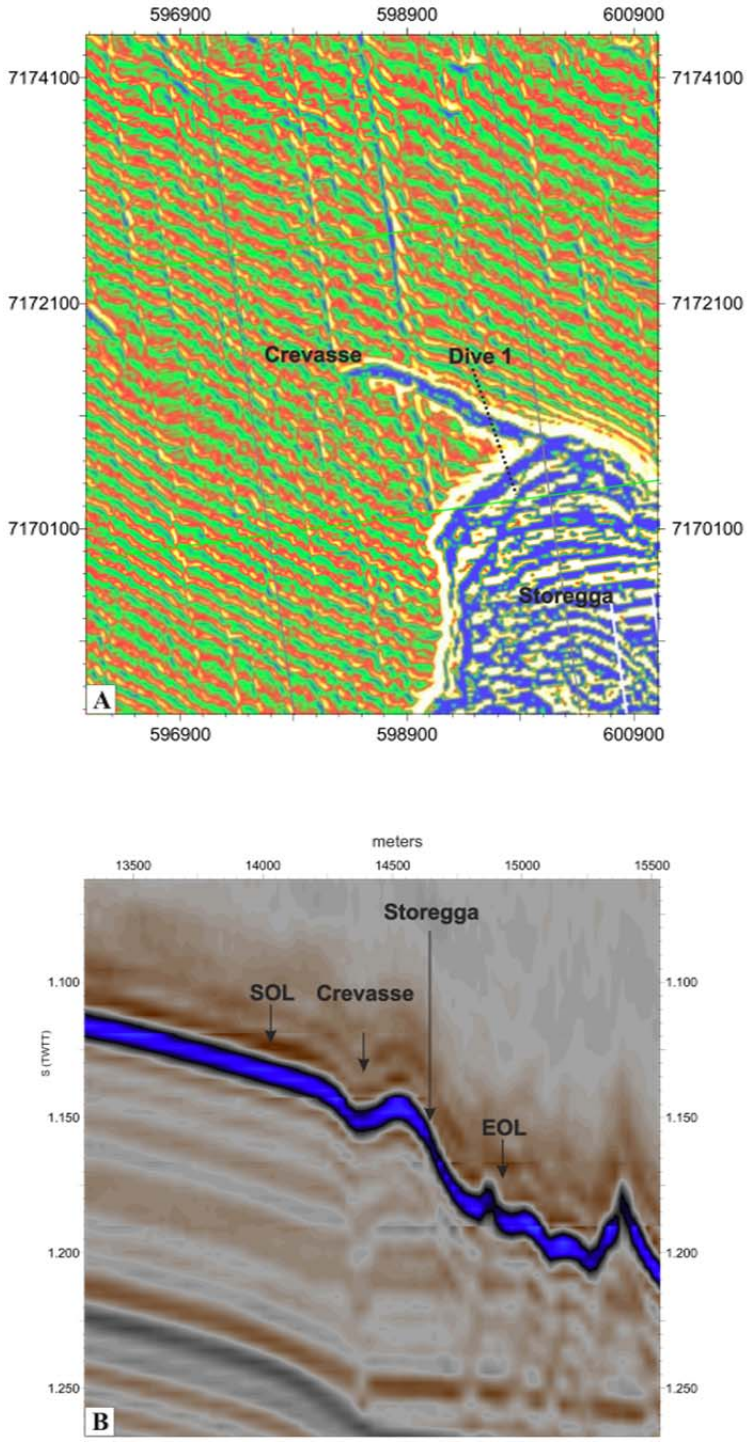

Fig. 5.38 (A) Dip curvature map of the seafloor of the Grip High 3D seismic cube indicates also the HyBIS Dive 95 crossing the crevasse and then ending in the Storegga Slide. Map coordinates are in UTM zone 32. (B) Seismic profile along HyBIS Dive 95.

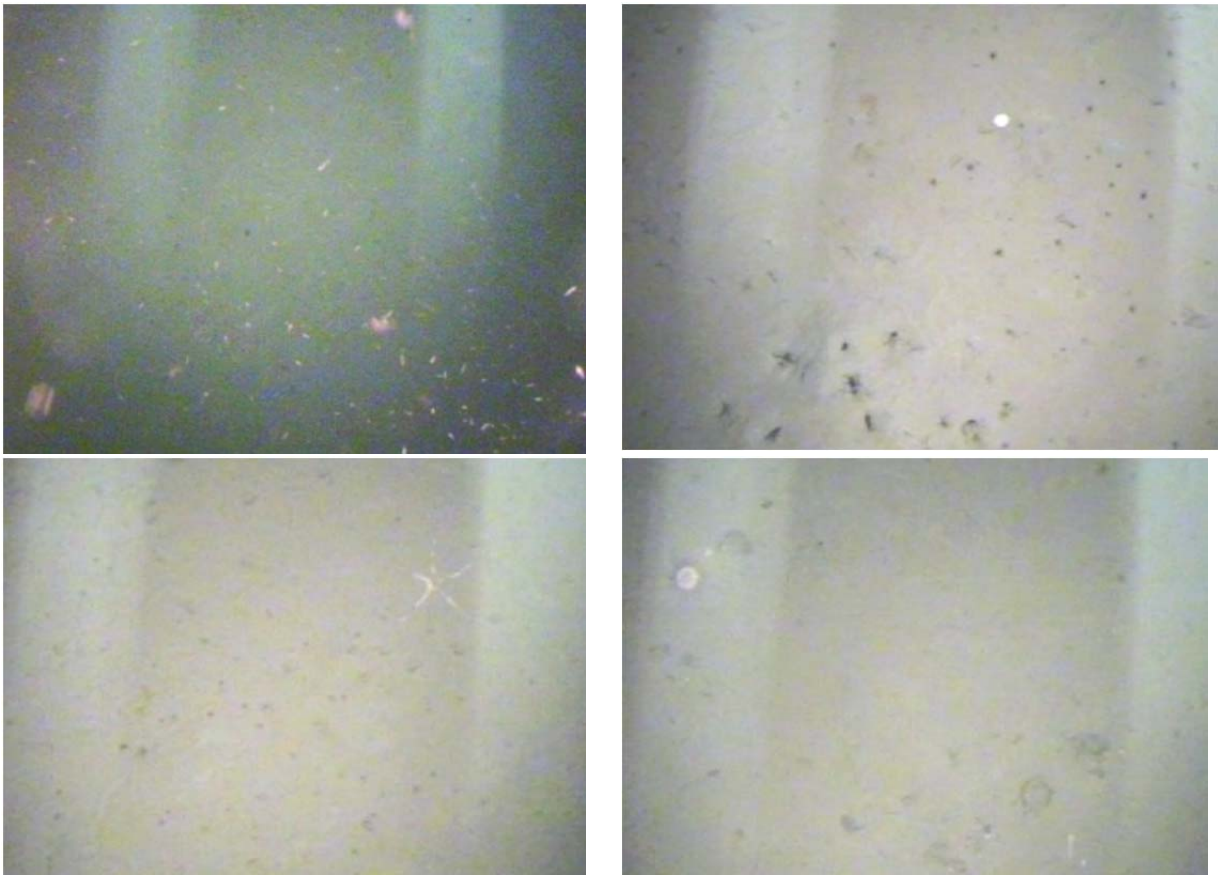

Fig. 5.39 (A) Large density of shrimps during the early portion of the profile. (B) Intensely bioturbated seafloor. (C) A sea star. (D) Small coral branches or colony observed in the crevasse characterized by irregular and rubble surface.

The last part of the survey on the Storegga slide revealed features similar to those observed in the faulted zone, with irregular seafloor, rubbles with large blocks, occasional echinoderms and bivalves and rare coral branches. The last minutes of record show a flatter sea floor with strong bioturbation similar to that observed at the beginning of the profile. This is most likely representing a depression zone within the slide that was filled by soft sediments.

In summary, TV images revealed that the crevasse is characterized by irregular sea floor with rubble. This could be related with the vertical movements of the fault. The observed alive coral branches indicate a) the presence of hard substratum for the colony to initiate the growth and b) a sufficient amount of nutrients to support these isolated colonies.

Dive 96 (Station no. 759 - Transect 2) The second dive, located to the south west of dive 1, completed a SW-NE transect through a series of E-W oriented shallow faults along the northern Storegga headwall (Fig. 5.40).

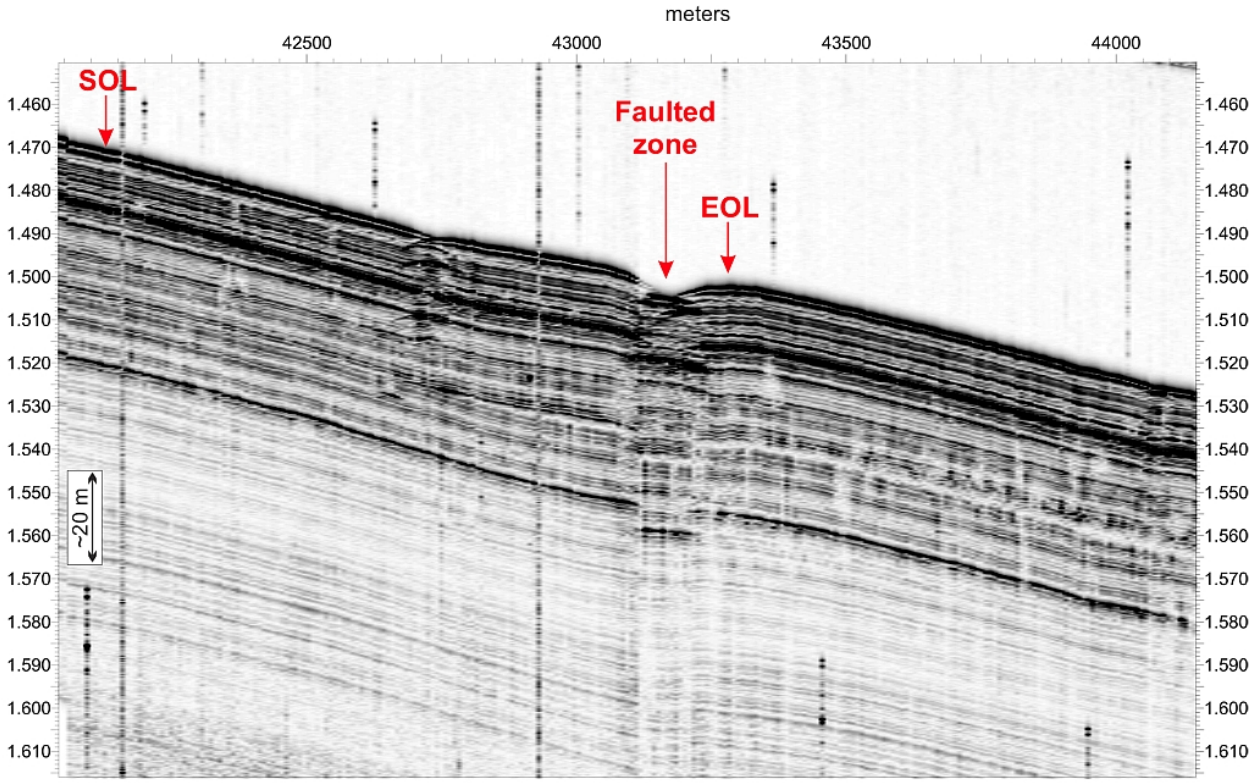

Fig. 5.40 Parasound profile along HyBIS Dive 96 intersecting the faulted zone.

The video survey revealed heavily bioturbated clayey soupy sediment with occasional sea stars of white and pink colours (Fig. 5.41a), white bivalves, several sea cucumbers, one squid, and a possible glass sponge, a fish, and a jelly fish. The amount of shrimps observed in the water column was significantly lower when compared with the images from the first dive; however dense clouds of plankton particles and detritus were also present. No significant variations in seafloor morphology or lithology were observed inside the faulted area. No clear evidence of fractures or hard substratum was seen. However, in several instances whitish and pale grey patches were observed (Fig. 5.41b). These could be interpreted as localized microbial colonies or as hard substratum, nevertheless the data collected are not sufficient to support these hypotheses. In addition, a large irregular shaped white feature was observed (Fig. 5.41c). The elongated and sharp edges suggest that this could be a bone fragment from a large fish or evidence of human impact, e.g. part of a plastic bag.

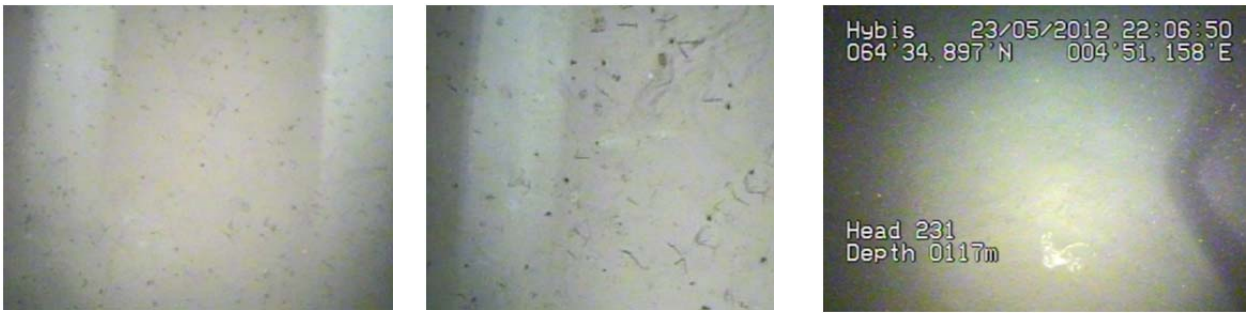

Fig. 5.41 (A) Intensely bioturbated seafloor. (B) Isolated whitish patches inside the faulted zone. (C) Large irregular shaped whitish feature.

In summary, for dive 96 the seismic and sub-bottom profiles clearly show that the fault is reaching the seafloor. However evidence of active faulting could not be observed during the TV

dive. We cannot exclude that the fault activates periodically. It is suggested that the area is currently covered by a recent hemi-pelagic veneer filling the cracks representing previous episodic vertical movements. Likewise the observations did not reveal any clear evidence of fluid seepage at this locality. The whitish patches described require further investigations to be clearly defined as microbial mats. No evidence of carbonate blocks was seen.

6 Ship's Meteorological Station

Prior to the departure from Reykjavik, it was necessary to decide which working area should be visited first. Therefore the chief scientist received weather information from the meteorological department. Due to the good weather conditions expected, the principal scientist decided on the northerly working area (Gjallar Ridge).

RV METEOR left Reykjavik port around 13:00 on 05.05.2012. During the transit the sailing area was located between a high over Greenland and a gale over the Skagerrak, which moved north. In between the pressure areas there was a northerly wind of 4 to 6 Bft. The significant wave height was about 2 m. After leaving land protection of Iceland, a south-westerly swell (oceanographic convention) of about 3 to 4 m was registered at times, caused by the mentioned gale. Water temperatures during the first two days were about 7°C. As the vessel crossed an area with colder water during transit, the temperature decreased to 2°C within a few hours. The air temperature also fell below 0°C at times. Until arrival in the first working area, the temperature slowly increased again to 7°C.

RV METEOR arrived in the first research area towards the afternoon on 08.05.2012. The first four working days were characterised by several low pressure areas, which moved from Ireland northeast into the working area or to Sweden. Thereby mainly winds between 3 and 4, at times 5 Bft., were recorded. The associated wave heights reached about 1 and 2 m. Under the influence of the low pressure systems isolated showers crossed the working area. Measured air temperatures were between 2°C and 6°C.

A large high, projected to move to Ireland, started a change in the meteorological situation around May 12th. This change only lasted for a short time, because on the northern flank of the high, a low moved from Greenland to the working area. This low deepened to a severe gale. It was situated west of Haltenbanken with its central pressure of about 973 hPa on 14.05.2012. The gale weakened only slowly and moved north.

Due to the expected wave height of about 6 m, all work was stopped on 12.05.2012 in the afternoon and RV METEOR sailed to Trondheimsfjord. The vessel left land protection again during the night of May 16th and sailed towards the southern research area.

While still under the influence of the weakening high, winds between 6 and 7 Bft were recorded during transit. The wave heights were 3 to 4 m.

The Nyegga research area was reached on 16.05.2012. The water temperatures were around 7°C and 8°C.

Until 19.05.2012, the working area was situated between low pressure over Scandinavia and high pressure over Iceland in a northerly to northwesterly current. The wind speed recorded, was about 4 and 6 Bft, and wave heights were about 3 m, decreasing to 2 m during the next days. While this low pressure system, developing into a gale, moved north, the wind backed west and decreased slightly.

In the wake of the low a new high gained influence. On 21.05.2012, this high was located over the Norwegian Sea with a central pressure of about 1027 hPa. On the southern flank of this high the wind veered already on May 20th from northwest to northeast. On the edge of the high the wind increased at times to 6-7 Bft during the night to 22.05.2012. The wave height about 3 m already decreased 2 m during the day.

During the next days the high strengthened and moved its centre first east, later south. On May 23rd its pressure centre (1033 hPa) was located over Northern Norway. Thereafter on

25.05.2012 its centre was situated over the Southern Norwegian Sea. It influenced the Norwegian Sea till the end of voyage with winds of maximum 5 Bft. RV METEOR docked in Stavanger in good weather conditions on 27.05.2012.

7 Station List M87/2

METEOR Station	Event	Time [UTC]	Latitude [°N]	Longitude [°E]	Water Depth [mbsl]	Gear	Remarks
M87/2-704-1	Releaser Test 1	2012-05-08 15:10:00.0	66°56.97’	4°16.01’	1384.8	Releaser	to water
M87/2-704-1	Releaser Test 1	2012-05-08 15:32:00.0	66°57.00’	4°15.99’	1385.4	Releaser	at depth
M87/2-704-1	Releaser Test 1	2012-05-08 16:50:00.0	66°56.99’	4°15.99’	1385	Releaser	start heaving
M87/2-704-1	Releaser Test 1	2012-05-08 17:22:00.0	66°56.99’	4°15.99’	1385	Releaser	on deck
M87/2-705-1	Releaser Test 2	2012-05-08 17:28:00.0	66°56.99’	4°15.99’	1385	Releaser	to water
M87/2-705-1	Releaser Test 2	2012-05-08 17:42:00.0	66°57.00’	4°15.99’	1385	Releaser	at depth
M87/2-705-1	Releaser Test 2	2012-05-08 18:27:00.0	66°56.99’	4°15.99’	1385	Releaser	start heaving
M87/2-705-1	Releaser Test 2	2012-05-08 18:41:00.0	66°56.99’	4°15.99’	1385	Releaser	on deck
M87/2-706-1	SVP Gjallar-1	2012-05-08 18:48:00.0	66°56.99’	4°15.99’	1385	Sound Velocity Profiler | SVP	to water
M87/2-706-1	SVP Gjallar-1	2012-05-08 19:06:00.0	66°56.99’	4°15.99’	1385	Sound Velocity Profiler | SVP	at depth
M87/2-706-1	SVP Gjallar-1	2012-05-08 19:21:00.0	66°56.99’	4°15.99’	1385	Sound Velocity Profiler | SVP	on deck
M87/2-707-1		2012-05-08 20:20:00.0	67°02.37’	4°32.50’	1393.5	Multibeam + Parasound | MB-PS	alter course
M87/2-707-1	MB-PS profile 01	2012-05-08 20:39:00.0	67°04.73’	4°39.81’	1392.8	Multibeam + Parasound | MB-PS	begin profile
M87/2-708-1	deployment OBS 1	2012-05-08 20:46:00.0	67°05.11’	4°41.03’	1393.2	Ocean Bottom Seismometer | OBS	deployment
M87/2-709-1	deployment OBS 2	2012-05-08 21:20:00.0	67°09.51’	4°43.07’	1393.7	Ocean Bottom Seismometer | OBS	deployment
M87/2-710-1	deployment	2012-05-09 01:34:00.0	67°11.43’	4°48.38’	1405.2	3D-Multi Channel Seismic | 3D-MCS [P-Cable]	surface
M87/2-710-1	3D seismic profile 01	2012-05-09 02:13:00.0	67°10.32’	4°46.98’	1399.0	3D-Multi Channel Seismic | 3D-MCS [P-Cable]	begin profile
M87/2-710-1	3D seismic profile 01	2012-05-09 04:06:00.0	67°04.41’	4°40.31’	1394.1	3D-Multi Channel Seismic | 3D-MCS [P-Cable]	end profile
M87/2-707-1	MB-PS profile 01	2012-05-09 04:06:00.0	67°04.41’	4°40.31’	1394.1	Multibeam + Parasound | MB-PS	end profile
M87/2-710-1	3D seismic profile 02	2012-05-09 04:23:00.0	67°04.71’	4°38.85’	1391.7	3D-Multi Channel Seismic | 3D-MCS [P-Cable]	begin profile
M87/2-707-1	MB-PS profile 02	2012-05-09 04:23:00.0	67°04.71’	4°38.85’	1391.7	Multibeam + Parasound | MB-PS	begin profile
M87/2-707-1	MB-PS profile 02	2012-05-09 05:56:00.0	67°10.28’	4°45.13’	1393.9	Multibeam + Parasound | MB-PS	end profile
M87/2-710-1	3D seismic profile 02	2012-05-09 05:56:00.0	67°10.28’	4°45.13’	1393.9	3D-Multi Channel Seismic | 3D-MCS [P-Cable]	end profile
M87/2-710-1	3D seismic profile 03	2012-05-09 06:12:00.0	67°09.98’	4°46.51’	1397.2	3D-Multi Channel Seismic | 3D-MCS [P-Cable]	begin profile

METEOR Station	Event	Time [UTC]	Latitude [°N]	Longitude [°E]	Water Depth [mbsl]	Gear	Remarks
M87/2-707-1	MB-PS profile 03	2012-05-09 06:12:00.0	67°09.98’	4°46.51’	1397.2	Multibeam + Parasound | MB-PS	begin profile
M87/2-710-1	3D seismic profile 03	2012-05-09 06:32:00.0	67°08.86’	4°45.26’	1393.6	3D-Multi Channel Seismic | 3D-MCS [P-Cable]	break of profile
M87/2-707-1	MB-PS profile 03	2012-05-09 09:41:00.0	67°04.27’	4°40.02’	1361.7	Multibeam + Parasound | MB-PS	alter course
M87/2-707-1	MB-PS profile 03	2012-05-09 13:00:00.0	67°10.73’	4°48.29’	1365.2	Multibeam + Parasound | MB-PS	end profile
M87/2-707-1	MB-PS profile 04	2012-05-09 15:07:00.0	67°09.82’	4°49.14’	1368.6	Multibeam + Parasound | MB-PS	begin profile
M87/2-707-1	MB-PS profile 04	2012-05-09 19:56:00.0	67°40.17’	5°25.97’	1318.6	Multibeam + Parasound | MB-PS	end profile
M87/2-707-1	MB-PS profile 05	2012-05-09 20:15:00.0	67°41.24’	5°21.07’	1249.4	Multibeam + Parasound | MB-PS	begin profile
M87/2-707-1	MB-PS profile 05	2012-05-10 00:54:00.0	67°11.70’	4°46.28’	1369.9	Multibeam + Parasound | MB-PS	end profile
M87/2-707-1	MB-PS profile 06	2012-05-10 01:16:00.0	67°12.45’	4°41.40’	1363.1	Multibeam + Parasound | MB-PS	begin profile
M87/2-707-1	MB-PS profile 06	2012-05-10 05:54:00.0	67°42.03’	5°16.11’	1199.3	Multibeam + Parasound | MB-PS	end profile
M87/2-707-1	MB-PS profile 07	2012-05-10 06:12:00.0	67°43.01’	5°10.96’	1162	Multibeam + Parasound | MB-PS	begin profile
M87/2-707-1	MB-PS profile 07	2012-05-10 10:56:00.0	67°12.96’	4°36.41’	1363.6	Multibeam + Parasound | MB-PS	end profile
M87/2-707-1		2012-05-10 12:10:00.0	67°06.84’	4°50.72’	1359.1	Multibeam + Parasound | MB-PS	alter course
M87/2-712-1	Releaser Test 3	2012-05-10 20:08:00.0	67°06.07’	4°48.24’	1358.5	Releaser	to water
M87/2-712-1	Releaser Test 3	2012-05-10 20:21:00.0	67°06.07’	4°48.24’	1357.5	Releaser	at depth
M87/2-712-1	Releaser Test 3	2012-05-10 21:19:00.0	67°06.07’	4°48.24’	1357.5	Releaser	on deck
M87/2-713-1	SVP Gjallar-2	2012-05-10 21:26:00.0	67°06.07’	4°48.24’	1358.3	Sound Velocity Profiler | SVP	to water
M87/2-713-1	SVP Gjallar-2	2012-05-10 22:00:00.0	67°06.07’	4°48.24’	1357.3	Sound Velocity Profiler | SVP	at depth
M87/2-713-1	SVP Gjallar-2	2012-05-10 22:33:00.0	67°06.07’	4°48.24’	1358	Sound Velocity Profiler | SVP	on deck
M87/2-707-1	MB-PS profile 08	2012-05-10 22:43:00.0	67°06.46’	4°48.24’	1356.7	Multibeam + Parasound | MB-PS	begin profile
M87/2-707-1	MB-PS profile 08	2012-05-10 22:48:00.0	67°07.00’	4°48.34’	1357.9	Multibeam + Parasound | MB-PS	end profile
M87/2-707-1	MB-PS profile 09	2012-05-10 22:51:00.0	67°07.13’	4°47.65’	1366.8	Multibeam + Parasound | MB-PS	begin profile
M87/2-707-1	MB-PS profile 09	2012-05-10 23:25:00.0	67°07.41’	4°37.54’	1353.6	Multibeam + Parasound | MB-PS	end profile
M87/2-707-1	MB-PS profile 10	2012-05-10 23:30:00.0	67°07.79’	4°37.18’	1360.1	Multibeam + Parasound | MB-PS	begin profile
M87/2-707-1	MB-PS profile 10	2012-05-10 23:44:00.0	67°08.73’	4°40.60’	1353	Multibeam + Parasound | MB-PS	end profile
M87/2-707-1	MB-PS profile 11	2012-05-10 23:49:00.0	67°08.59’	4°41.62’	1351.9	Multibeam + Parasound | MB-PS	begin profile
M87/2-707-1	MB-PS profile 11	2012-05-11 00:20:00.0	67°04.94’	4°41.61’	1359	Multibeam + Parasound | MB-PS	end profile
M87/2-707-1	MB-PS profile 12	2012-05-11 00:23:00.0	67°04.68’	4°42.02’	1359.7	Multibeam + Parasound | MB-PS	begin profile
M87/2-707-1	MB-PS profile 12	2012-05-11 00:31:00.0	67°04.63’	4°44.42’	1361.7	Multibeam + Parasound | MB-PS	end profile
M87/2-707-1	MB-PS profile 13	2012-05-11 00:34:00.0	67°04.80’	4°44.93’	1357.5	Multibeam + Parasound | MB-PS	begin profile
M87/2-707-1	MB-PS profile 13	2012-05-11 01:04:00.0	67°08.21’	4°44.91’	1359.4	Multibeam + Parasound | MB-PS	end profile
M87/2-707-1	MB-PS profile 14	2012-05-11 01:08:00.0	67°08.40’	4°44.15’	1355.6	Multibeam + Parasound | MB-PS	begin profile
M87/2-707-1	MB-PS profile 14	2012-05-11 01:46:00.0	67°05.27’	4°36.18’	1353.4	Multibeam + Parasound | MB-PS	end profile

METEOR Station	Event	Time [UTC]	Latitude [°N]	Longitude [°E]	Water Depth [mbsl]	Gear	Remarks
M87/2-707-1	MB-PS profile 15	2012-05-11 01:58:00.0	67°05.23’	4°36.10’	1356.5	Multibeam + Parasound | MB-PS	begin profile
M87/2-707-1	MB-PS profile 15	2012-05-11 02:40:00.0	67°07.91’	4°46.56’	1358.4	Multibeam + Parasound | MB-PS	end profile
M87/2-707-1	MB-PS profile 16	2012-05-11 02:45:00.0	67°08.29’	4°46.64’	1358	Multibeam + Parasound | MB-PS	begin profile
M87/2-707-1	MB-PS profile 16	2012-05-11 02:52:00.0	67°08.57’	4°44.84’	1357.9	Multibeam + Parasound | MB-PS	end profile
M87/2-707-1	MB-PS profile 17	2012-05-11 02:55:00.0	67°08.46’	4°44.08’	1357	Multibeam + Parasound | MB-PS	begin profile
M87/2-707-1	MB-PS profile 17	2012-05-11 03:30:00.0	67°04.84’	4°39.29’	1355.8	Multibeam + Parasound | MB-PS	end profile
M87/2-707-1	MB-PS profile 18	2012-05-11 03:38:00.0	67°04.45’	4°37.44’	1354.2	Multibeam + Parasound | MB-PS	begin profile
M87/2-707-1	MB-PS profile 18	2012-05-11 05:48:00.0	66°50.94’	4°20.42’	1319.8	Multibeam + Parasound | MB-PS	end profile
M87/2-707-1	MB-PS profile 19	2012-05-11 06:10:00.0	66°49.79’	4°25.24’	1299.1	Multibeam + Parasound | MB-PS	begin profile
M87/2-707-1	MB-PS profile 19	2012-05-11 08:20:00.0	67°03.43’	4°41.96’	1359.5	Multibeam + Parasound | MB-PS	end profile
M87/2-707-1	MB-PS profile 20	2012-05-11 08:21:00.0	67°03.53’	4°42.09’	1360.4	Multibeam + Parasound | MB-PS	begin profile
M87/2-707-1	MB-PS profile 20	2012-05-11 09:25:00.0	67°09.10’	4°55.25’	1375.6	Multibeam + Parasound | MB-PS	end profile
M87/2-707-1	MB-PS profile 21	2012-05-11 09:37:00.0	67°09.08’	4°55.25’	1377.4	Multibeam + Parasound | MB-PS	begin profile
M87/2-707-1	MB-PS profile 21	2012-05-11 11:43:00.0	66°55.82’	4°38.60’	1334.8	Multibeam + Parasound | MB-PS	end profile
M87/2-707-1	MB-PS profile 22	2012-05-11 11:47:00.0	66°55.47’	4°38.89’	1325.9	Multibeam + Parasound | MB-PS	begin profile
M87/2-707-1	MB-PS profile 22	2012-05-11 12:00:00.0	66°54.78’	4°42.46’	1306.8	Multibeam + Parasound | MB-PS	end profile
M87/2-707-1	MB-PS profile 23	2012-05-11 12:04:00.0	66°54.76’	4°43.39’	1308.2	Multibeam + Parasound | MB-PS	begin profile
M87/2-707-1	MB-PS profile 23	2012-05-11 14:14:00.0	67°08.30’	5°00.36’	1386	Multibeam + Parasound | MB-PS	end profile
M87/2-707-1	MB-PS profile 24	2012-05-11 14:19:00.0	67°08.72’	5°00.06’	1382.8	Multibeam + Parasound | MB-PS	alter course
M87/2-714-1	deployment	2012-05-11 18:00:00.0	67°07.73’	4°22.74’	1370.4	2D-Multi-Channel-Seismic | 2D-MCS	surface
M87/2-714-1	2D seismic profile 01	2012-05-11 18:40:00.0	67°07.68’	4°27.27’	1357.5	2D-Multi-Channel-Seismic | 2D-MCS	begin profile
M87/2-714-1	2D seismic profile 01	2012-05-11 20:52:00.0	67°03.43’	4°49.50’	1357.7	2D-Multi-Channel-Seismic | 2D-MCS	end profile
M87/2-714-1	2D seismic profile 02	2012-05-11 22:55:00.0	67°03.37’	4°49.46’	1361.1	2D-Multi-Channel-Seismic | 2D-MCS	begin profile
M87/2-714-1	2D seismic profile 02	2012-05-12 00:19:00.0	67°01.18’	4°34.54’	1361.8	2D-Multi-Channel-Seismic | 2D-MCS	end profile
M87/2-707-1	MB-PS profile 24	2012-05-12 00:30:00.0	67°01.59’	4°33.51’	1350.9	Multibeam + Parasound | MB-PS	alter course
M87/2-714-1	2D seismic profile 03	2012-05-12 00:30:00.0	67°01.59’	4°33.51’	1350.9	2D-Multi-Channel-Seismic | 2D-MCS [ ]	begin profile
M87/2-714-1	2D seismic profile 03	2012-05-12 03:51:00.0	67°14.74’	4°49.36’	1381.6	2D-Multi-Channel-Seismic | 2D-MCS	end profile

METEOR Station	Event	Time [UTC]	Latitude [°N]	Longitude [°E]	Water Depth [mbsl]	Gear	Remarks
M87/2-714-1	2D seismic profile 04	2012-05-12 04:00:00.0	67°15.14’	4°48.44’	1384.4	2D-Multi-Channel-Seismic | 2D-MCS	begin profile
M87/2-714-1	2D seismic profile 04	2012-05-12 05:39:00.0	67°11.74’	4°33.53’	1361.1	2D-Multi-Channel-Seismic | 2D-MCS	end profile
M87/2-714-1	2D seismic profile 05	2012-05-12 05:49:00.0	67°11.19’	4°33.66’	1358.6	2D-Multi-Channel-Seismic | 2D-MCS	begin profile
M87/2-714-1	2D seismic profile 05	2012-05-12 07:43:00.0	67°07.67’	4°53.50’	1366.6	2D-Multi-Channel-Seismic | 2D-MCS	end profile
M87/2-714-1	2D seismic profile 06	2012-05-12 07:53:00.0	67°07.93’	4°54.79’	1372.8	2D-Multi-Channel-Seismic | 2D-MCS	begin profile
M87/2-714-1	2D seismic profile 06	2012-05-12 09:26:00.0	67°14.67’	4°53.03’	1390	2D-Multi-Channel-Seismic | 2D-MCS	end profile
M87/2-714-1	2D seismic profile 07	2012-05-12 09:36:00.0	67°14.78’	4°51.56’	1387.7	2D-Multi-Channel-Seismic | 2D-MCS	begin profile
M87/2-714-1	2D seismic profile 07	2012-05-12 13:05:00.0	67°01.00’	4°36.02’	1358.1	2D-Multi-Channel-Seismic | 2D-MCS	end profile
M87/2-714-1	recovery	2012-05-12 13:35:00.0	67°01.37’	4°35.22’	1357.5	2D-Multi-Channel-Seismic | 2D-MCS	on deck
M87/2-715-1	recovery OBS 1	2012-05-12 14:16:00.0	67°04.97’	4°41.16’	1362.5	Ocean Bottom Seismometer | OBS	released
M87/2-707-1	MB-PS profile 24	2012-05-12 14:24:00.0	67°04.96’	4°41.40’	1358.9	Multibeam + Parasound | MB-PS	end profile
M87/2-715-1	recovery OBS 1	2012-05-12 14:37:00.0	67°05.01’	4°41.25’		Ocean Bottom Seismometer | OBS	surface
M87/2-715-1	recovery OBS 1	2012-05-12 14:51:00.0	67°05.16’	4°41.75’		Ocean Bottom Seismometer | OBS	on deck
M87/2-716-1	recovery OBS 2	2012-05-12 15:02:00.0	67°05.20’	4°42.15’		Ocean Bottom Seismometer | OBS	released
M87/2-716-1	recovery OBS 2	2012-05-12 15:22:00.0	67°08.14’	4°43.33’		Ocean Bottom Seismometer | OBS	at surface
M87/2-716-1	recovery OBS 2	2012-05-12 15:39:00.0	67°09.58’	4°43.62’		Ocean Bottom Seismometer | OBS	on deck
M87/2-717-1	SVP Nyegga-1	2012-05-16 12:46:00.0	64°45.27’	5°04.92’		Sound Velocity Profiler | SVP	to water
M87/2-717-1	SVP Nyegga-1	2012-05-16 13:02:00.0	64°45.27’	5°04.93’	716.4	Sound Velocity Profiler | SVP	at depth
M87/2-717-1	SVP Nyegga-1	2012-05-16 13:32:00.0	64°45.27’	5°04.93’	721.4	Sound Velocity Profiler | SVP	on deck
M87/2-718-1	OBEM G1	2012-05-16 14:56:00.0	64°45.29’	5°04.44’	716.6	Ocean bottom electro-magnetic receiver | OBEM	surface

METEOR Station	Event	Time [UTC]	Latitude [°N]	Longitude [°E]	Water Depth [mbsl]	Gear	Remarks
M87/2-718-1	OBEM G1	2012-05-16 16:02:00.0	64°45.29’	5°04.43’	716.6	Ocean bottom electro-magnetic receiver | OBEM	seabottom visible
M87/2-718-1	OBEM G1	2012-05-16 16:07:00.0	64°45.29’	5°04.42’	718.8	Ocean bottom electro-magnetic receiver | OBEM	on seabottom
M87/2-718-1	OBEM G1	2012-05-16 16:44:00.0	64°45.28’	5°04.42’	717.4	Ocean bottom electro-magnetic receiver | OBEM	on deck
M87/2-719-1	OBEM G2	2012-05-16 17:16:00.0	64°45.37’	5°04.28’	717.1	Ocean bottom electro-magnetic receiver | OBEM	surface
M87/2-719-1	OBEM G2	2012-05-16 17:47:00.0	64°45.37’	5°04.27’	724.6	Ocean bottom electro-magnetic receiver | OBEM	on deck (problems)
M87/2-719-1	OBEM G2	2012-05-16 18:22:00.0	64°45.37’	5°04.27’	728.4	Ocean bottom electro-magnetic receiver | OBEM	surface
M87/2-719-1	OBEM G2	2012-05-16 19:11:00.0	64°45.37’	5°04.27’	730.4	Ocean bottom electro-magnetic receiver | OBEM	on seabottom
M87/2-719-1	OBEM G2	2012-05-16 19:50:00.0	64°45.36’	5°04.26’	726.2	Ocean bottom electro-magnetic receiver | OBEM	on deck
M87/2-720-1	OBEM G3	2012-05-16 20:08:00.0	64°45.23’	5°04.26’	716.8	Ocean bottom electro-magnetic receiver | OBEM	surface
M87/2-720-1	OBEM G3	2012-05-16 20:53:00.0	64°45.24’	5°04.27’	718.7	Ocean bottom electro-magnetic receiver | OBEM	seabottom visible
M87/2-720-1	OBEM G3	2012-05-16 20:55:00.0	64°45.24’	5°04.27’	728.9	Ocean bottom electro-magnetic receiver | OBEM	released
M87/2-720-1	OBEM G3	2012-05-16 21:25:00.0	64°45.15’	5°04.05’	719.9	Ocean bottom electro-magnetic receiver | OBEM	on deck
M87/2-721-1	OBEM G4	2012-05-16 21:45:00.0	64°45.26’	5°04.00’	730.9	Ocean bottom electro-magnetic receiver | OBEM	surface
M87/2-721-1	OBEM G4	2012-05-16 22:14:00.0	64°45.26’	5°04.05’	720.2	Ocean bottom electro-magnetic receiver | OBEM	on deck (problems)
M87/2-721-1	OBEM G4	2012-05-16 22:30:00.0	64°45.25’	5°03.98’	731.8	Ocean bottom electro-magnetic receiver | OBEM	surface
M87/2-721-1	OBEM G4	2012-05-16 23:15:00.0	64°45.25’	5°03.99’	723.2	Ocean bottom electro-magnetic receiver | OBEM	on deck (problems)
M87/2-722-1	OBEM G4	2012-05-17 00:20:00.0	64°45.36’	5°03.99’	733	Ocean bottom electro-magnetic receiver | OBEM	surface
M87/2-722-1	OBEM G4	2012-05-17 01:11:00.0	64°45.36’	5°03.99’	728.8	Ocean bottom electro-magnetic receiver | OBEM	on seabottom
M87/2-722-1	OBEM G4	2012-05-17 01:45:00.0	64°45.36’	5°03.99’	730.9	Ocean bottom electro-magnetic receiver | OBEM	on deck

METEOR Station	Event	Time [UTC]	Latitude [°N]	Longitude [°E]	Water Depth [mbsl]	Gear	Remarks
M87/2-723-1	OBEM G5	2012-05-17 02:06:00.0	64°45.23’	5°04.01’	724.6	Ocean bottom electro-magnetic receiver | OBEM	surface
M87/2-723-1	OBEM G5	2012-05-17 03:09:00.0	64°45.23’	5°03.98’	729.6	Ocean bottom electro-magnetic receiver | OBEM	on seabottom
M87/2-723-1	OBEM G5	2012-05-17 03:24:00.0	64°45.23’	5°03.98’	725.1	Ocean bottom electro-magnetic receiver | OBEM	on deck
M87/2-724-1	OBEM G6	2012-05-17 03:36:00.0	64°45.29’	5°03.69’	726.2	Ocean bottom electro-magnetic receiver | OBEM	surface
M87/2-724-1	OBEM G6	2012-05-17 04:16:00.0	64°45.28’	5°03.72’	732	Ocean bottom electro-magnetic receiver | OBEM	on seabottom
M87/2-724-1	OBEM G6	2012-05-17 04:36:00.0	64°45.28’	5°03.72’	729.5	Ocean bottom electro-magnetic receiver | OBEM	on deck
M87/2-725-1	Sputnik Test	2012-05-17 05:23:00.0	64°45.28’	5°03.73’	730.2	Sputnik Electromagnetic Dipole Transmitter | Sputnik	surface
M87/2-725-1	Sputnik Test	2012-05-17 06:22:00.0	64°45.28’	5°03.73’	731.8	Sputnik Electromagnetic Dipole Transmitter | Sputnik	seafloor contact
M87/2-725-1	Sputnik Test	2012-05-17 06:41:00.0	64°45.28’	5°03.73’	731.9	Sputnik Electromagnetic Dipole Transmitter | Sputnik	start heaving
M87/2-725-1	Sputnik Test	2012-05-17 07:11:00.0	64°45.28’	5°03.73’	729.1	Sputnik Electromagnetic Dipole Transmitter | Sputnik	on deck
M87/2-726-1	OBEM S1	2012-05-17 09:25:00.0	64°44.48’	5°04.11’	725.2	Ocean bottom electro-magnetic receiver | OBEM	surface
M87/2-726-1	OBEM S1	2012-05-17 10:00:00.0	64°44.48’	5°04.11’	731	Ocean bottom electro-magnetic receiver | OBEM	on deck (problems)
M87/2-726-1	OBEM S1	2012-05-17 10:10:00.0	64°44.48’	5°04.11’	730.6	Ocean bottom electro-magnetic receiver | OBEM	fieren
M87/2-726-1	OBEM S1	2012-05-17 11:15:00.0	64°44.49’	5°04.09’	723.6	Ocean bottom electro-magnetic receiver | OBEM	released
M87/2-726-1	OBEM S1	2012-05-17 11:34:00.0	64°44.49’	5°04.09’	728	Ocean bottom electro-magnetic receiver | OBEM	on deck
M87/2-727-1	OBEM S2	2012-05-17 12:00:00.0	64°45.17’	5°04.17’	721.9	Ocean bottom electro-magnetic receiver | OBEM	surface
M87/2-727-1	OBEM S2	2012-05-17 13:29:00.0	64°45.18’	5°04.17’	723.3	Ocean bottom electro-magnetic receiver | OBEM	released
M87/2-727-1	OBEM S2	2012-05-17 13:47:00.0	64°45.18’	5°04.17’	721.2	Ocean bottom electro-magnetic receiver | OBEM	on deck
M87/2-728-1	OBEM S3	2012-05-17 14:00:00.0	64°45.29’	5°04.17’	717.5	Ocean bottom electro-magnetic receiver | OBEM	surface

METEOR Station	Event	Time [UTC]	Latitude [°N]	Longitude [°E]	Water Depth [mbsl]	Gear	Remarks
M87/2-728-1	OBEM S3	2012-05-17 15:18:00.0	64°45.29’	5°04.18’	717.7	Ocean bottom electro-magnetic receiver | OBEM	on seabottom
M87/2-728-1	OBEM S3	2012-05-17 15:41:00.0	64°45.29’	5°04.18’	715.9	Ocean bottom electro-magnetic receiver | OBEM	on deck
M87/2-729-1	OBEM S4	2012-05-17 16:00:00.0	64°45.41’	5°04.17’	723.2	Ocean bottom electro-magnetic receiver | OBEM	surface
M87/2-729-1	OBEM S4	2012-05-17 17:22:00.0	64°45.42’	5°04.17’	728.2	Ocean bottom electro-magnetic receiver | OBEM	on seabottom
M87/2-729-1	OBEM S4	2012-05-17 17:47:00.0	64°45.42’	5°04.17’	725.2	Ocean bottom electro-magnetic receiver | OBEM	on deck
M87/2-730-1	OBEM S5	2012-05-17 18:07:00.0	64°46.08’	5°04.24’	721.9	Ocean bottom electro-magnetic receiver | OBEM	surface
M87/2-730-1	OBEM S5	2012-05-17 19:14:00.0	64°46.10’	5°04.23’	720.3	Ocean bottom electro-magnetic receiver | OBEM	released
M87/2-730-1	OBEM S5	2012-05-17 19:34:00.0	64°46.10’	5°04.23’	719.8	Ocean bottom electro-magnetic receiver | OBEM	on deck
M87/2-731-1	OBEM S6	2012-05-17 20:00:00.0	64°45.65’	5°02.46’	726	Ocean bottom electro-magnetic receiver | OBEM	surface
M87/2-731-1	OBEM S6	2012-05-17 20:04:00.0	64°45.65’	5°02.46’	727.5	Ocean bottom electro-magnetic receiver | OBEM	on deck (problems)
M87/2-731-1	OBEM S6	2012-05-17 20:06:00.0	64°45.65’	5°02.47’	726.4	Ocean bottom electro-magnetic receiver | OBEM	surface
M87/2-731-1	OBEM S6	2012-05-17 21:20:00.0	64°45.66’	5°02.46’	730.4	Ocean bottom electro-magnetic receiver | OBEM	released
M87/2-731-1	OBEM S6	2012-05-17 21:42:00.0	64°45.67’	5°02.48’	728.5	Ocean bottom electro-magnetic receiver | OBEM	on deck
M87/2-732-1	OBEM S7	2012-05-17 22:47:00.0	64°45.35’	5°03.93’	729.2	Ocean bottom electro-magnetic receiver | OBEM	surface
M87/2-732-1	OBEM S7	2012-05-18 00:06:00.0	64°45.35’	5°03.93’	725.2	Ocean bottom electro-magnetic receiver | OBEM	released
M87/2-732-1	OBEM S7	2012-05-18 00:25:00.0	64°45.35’	5°03.93’	730	Ocean bottom electro-magnetic receiver | OBEM	on deck
M87/2-733-1	OBEM S8	2012-05-18 00:58:00.0	64°44.92’	5°05.81’	717.3	Ocean bottom electro-magnetic receiver | OBEM	surface
M87/2-733-1	OBEM S8	2012-05-18 02:23:00.0	64°44.94’	5°05.82’	716.4	Ocean bottom electro-magnetic receiver | OBEM	on seabottom
M87/2-733-1	OBEM S8	2012-05-18 02:46:00.0	64°44.94’	5°05.83’	722.3	Ocean bottom electro-magnetic receiver | OBEM	on deck

METEOR Station	Event	Time [UTC]	Latitude [°N]	Longitude [°E]	Water Depth [mbsl]	Gear	Remarks
M87/2-734-1	MB-PS profile 25	2012-05-18 03:20:00.0	64°47.00’	5°01.49’	735.3	Multibeam + Parasound | MB-PS	begin profile
M87/2-734-1	MB-PS profile 25	2012-05-18 04:07:00.0	64°42.07’	4°55.27’	827	Multibeam + Parasound | MB-PS	end profile
M87/2-734-1	MB-PS profile 26	2012-05-18 04:16:00.0	64°41.43’	4°57.27’	820.5	Multibeam + Parasound | MB-PS	begin profile
M87/2-734-1	MB-PS profile 26	2012-05-18 05:01:00.0	64°46.18’	5°03.28’	719.1	Multibeam + Parasound | MB-PS	end profile
M87/2-734-1	MB-PS profile 27	2012-05-18 05:09:00.0	64°45.82’	5°05.39’	713.6	Multibeam + Parasound | MB-PS	begin profile
M87/2-734-1	MB-PS profile 27	2012-05-18 05:56:00.0	64°40.90’	4°59.27’	828	Multibeam + Parasound | MB-PS	end profile
M87/2-734-1	MB-PS profile 28	2012-05-18 06:05:00.0	64°40.45’	5°01.59’	819.5	Multibeam + Parasound | MB-PS	begin profile
M87/2-734-1	MB-PS profile 28	2012-05-18 06:52:00.0	64°45.28’	5°07.59’	711.1	Multibeam + Parasound | MB-PS	end profile
M87/2-734-1	MB-PS profile 29	2012-05-18 07:00:00.0	64°44.82’	5°09.95’	707.8	Multibeam + Parasound | MB-PS	begin profile
M87/2-734-1	MB-PS profile 29	2012-05-18 07:50:00.0	64°39.68’	5°03.60’	828.8	Multibeam + Parasound | MB-PS	end profile
M87/2-734-1	MB-PS profile 30	2012-05-18 07:58:00.0	64°39.10’	5°06.02’	831.8	Multibeam + Parasound | MB-PS	begin profile
M87/2-734-1	MB-PS profile 30	2012-05-18 08:48:00.0	64°44.26’	5°12.16’	708.5	Multibeam + Parasound | MB-PS	end profile
M87/2-734-1	MB-PS profile 31	2012-05-18 08:57:00.0	64°43.80’	5°14.78’	695	Multibeam + Parasound | MB-PS	begin profile
M87/2-734-1	MB-PS profile 31	2012-05-18 09:46:00.0	64°38.71’	5°08.89’	841.7	Multibeam + Parasound | MB-PS	end profile
M87/2-734-1	MB-PS profile 32	2012-05-18 09:54:00.0	64°38.39’’	5°11.04’	854.4	Multibeam + Parasound | MB-PS	begin profile
M87/2-734-1	MB-PS profile 32	2012-05-18 10:38:00.0	64°42.57’	5°17.78’	690.5	Multibeam + Parasound | MB-PS	end profile
M87/2-735-1	MB-PS profile 33	2012-05-18 13:00:00.0	64°44.41’	5°04.62’	727.7	Multibeam + Parasound | MB-PS	begin profile
M87/2-735-1	MB-PS profile 33	2012-05-18 13:22:00.0	64°42.09’	5°07.25’	743.1	Multibeam + Parasound | MB-PS	end profile
M87/2-735-1	MB-PS profile 34	2012-05-18 13:24:00.0	64°41.89’	5°07.22’	745	Multibeam + Parasound | MB-PS	begin profile
M87/2-735-1	MB-PS profile 34	2012-05-18 13:51:00.0	64°39.13’	5°03.83’	850.3	Multibeam + Parasound | MB-PS	end profile
M87/2-735-1	MB-PS profile 35	2012-05-18 13:57:00.0	64°38.81’	5°04.57’	851	Multibeam + Parasound | MB-PS	begin profile
M87/2-735-1	MB-PS profile 35	2012-05-18 14:11:00.0	64°40.27’	5°06.35’	813.1	Multibeam + Parasound | MB-PS	end profile
M87/2-736-1	Sputnik P1 position 1	2012-05-18 14:53:00.0	64°44.71’	5°04.14’		Sputnik Electromagnetic Dipole Transmitter | Sputnik	surface
M87/2-736-1	Sputnik P1 position 1	2012-05-18 16:00:00.0	64°44.71’	5°04.15’	727	Sputnik Electromagnetic Dipole Transmitter | Sputnik	max. depth
M87/2-736-1	Sputnik P1 position 1	2012-05-18 16:19:00.0	64°44.71’	5°04.15’	727	Sputnik Electromagnetic Dipole Transmitter | Sputnik	start transmitting
M87/2-736-1	Sputnik P1 position 1	2012-05-18 16:37:00.0	64°44.71’	5°04.15’		Sputnik Electromagnetic Dipole Transmitter | Sputnik	end transmitting
M87/2-736-1	Sputnik P1 position 2	2012-05-18 16:59:00.0	64°44.75’	5°04.15’		Sputnik Electromagnetic Dipole Transmitter | Sputnik	start transmitting
M87/2-736-1	Sputnik P1 position 2	2012-05-18 16:59:00.0	64°44.75’	5°04.15’		Sputnik Electromagnetic Dipole Transmitter | Sputnik	max. depth

METEOR Station	Event	Time [UTC]	Latitude [°N]	Longitude [°E]	Water Depth [mbsl]	Gear	Remarks
M87/2-736-1	Sputnik P1 position 2	2012-05-18 17:17:00.0	64°44.75’	5°04.15’		Sputnik Electromagnetic Dipole Transmitter | Sputnik	end transmitting
M87/2-736-1	Sputnik P1 position 3	2012-05-18 17:46:00.0	64°44.79’	5°04.15’		Sputnik Electromagnetic Dipole Transmitter | Sputnik	max. depth
M87/2-736-1	Sputnik P1 position 3	2012-05-18 17:47:00.0	64°44.79’	5°04.15’		Sputnik Electromagnetic Dipole Transmitter | Sputnik	start transmitting
M87/2-736-1	Sputnik P1 position 3	2012-05-18 18:20:00.0	64°44.79’	5°04.15’		Sputnik Electromagnetic Dipole Transmitter | Sputnik	start heaving (problems)
M87/2-736-1	Sputnik P1 position 3	2012-05-18 18:46:00.0	64°44.79’	5°04.14’		Sputnik Electromagnetic Dipole Transmitter | Sputnik	on deck
M87/2-737-1	MB-PS profile 36	2012-05-18 20:36:00.0	64°47.35’	5°05.37’	718.8	Multibeam + Parasound | MB-PS	begin profile
M87/2-737-1	MB-PS profile 36	2012-05-18 23:59:00.0	64°30.03’	4°36.20’	1419.3	Multibeam + Parasound | MB-PS	alter course
M87/2-737-1	MB-PS profile 36	2012-05-19 00:07:00.0	64°29.41’	4°37.59’	1417.5	Multibeam + Parasound | MB-PS	alter course
M87/2-737-1	MB-PS profile 36	2012-05-19 02:03:00.0	64°40.80’	4°53.46’	870.4	Multibeam + Parasound | MB-PS	alter course
M87/2-737-1	MB-PS profile 36	2012-05-19 02:10:00.0	64°40.21’	4°55.35’	873.5	Multibeam + Parasound | MB-PS	alter course
M87/2-737-1	MB-PS profile 36	2012-05-19 03:45:00.0	64°29.73’	4°41.45’	1376.9	Multibeam + Parasound | MB-PS	alter course
M87/2-737-1	MB-PS profile 36	2012-05-19 03:54:00.0	64°29.12’	4°43.72’	1365.3	Multibeam + Parasound | MB-PS	alter course
M87/2-737-1	MB-PS profile 36	2012-05-19 04:08:00.0	64°29.93’	4°44.77’	1337.4	Multibeam + Parasound | MB-PS	break of profile
M87/2-737-1	MB-PS profile 36	2012-05-19 04:44:00.0	64°30.62’	4°34.06’	1422.4	Multibeam + Parasound | MB-PS	continue profile
M87/2-737-1	MB-PS profile 36	2012-05-19 06:33:00.0	64°41.93’	4°48.87’	863.5	Multibeam + Parasound | MB-PS	alter course
M87/2-737-1	MB-PS profile 36	2012-05-19 07:10:00.0	64°39.67’	4°57.31’	876.9	Multibeam + Parasound | MB-PS	alter course
M87/2-737-1	MB-PS profile 36	2012-05-19 08:55:00.0	64°28.89’	4°43.39’	1371.3	Multibeam + Parasound | MB-PS	end profile
M87/2-738-1	Releaser Test 3	2012-05-19 09:06:00.0	64°28.74’	4°42.76’	1377.6	Releaser	to water
M87/2-738-1	Releaser Test 3	2012-05-19 09:44:00.0	64°28.74’	4°42.76’	1375.3	Releaser	at depth
M87/2-738-1	Releaser Test 3	2012-05-19 10:08:00.0	64°28.74’	4°42.76’	1375.6	Releaser	on deck
M87/2-739-1	Sputnik P1 position 3	2012-05-19 16:26:00.0	64°44.79’	5°04.16’	725.9	Sputnik Electromagnetic Dipole Transmitter | Sputnik	Surface
M87/2-739-1	Sputnik P1 position 3	2012-05-19 17:15:00.0	64°44.80’	5°04.16’	725.9	Sputnik Electromagnetic Dipole Transmitter | Sputnik	max. depth
M87/2-739-1	Sputnik P1 position 3	2012-05-19 17:16:00.0	64°44.80’	5°04.17’	725.9	Sputnik Electromagnetic Dipole Transmitter | Sputnik	start transmitting
M87/2-739-1	Sputnik P1 position 3	2012-05-19 17:25:00.0	64°44.80’	5°04.16’	725.9	Sputnik Electromagnetic Dipole Transmitter | Sputnik	end transmitting
M87/2-739-1	Sputnik P1 position 3	2012-05-19 17:26:00.0	64°44.79’	5°04.16’	725.9	Sputnik Electromagnetic Dipole Transmitter | Sputnik	start heaving

METEOR Station	Event	Time [UTC]	Latitude [°N]	Longitude [°E]	Water Depth [mbsl]	Gear	Remarks
M87/2-739-1	Sputnik P1 position 4	2012-05-19 17:44:00.0	64°44.85’	5°04.16’		Sputnik Electromagnetic Dipole Transmitter | Sputnik	position 4
M87/2-739-1	Sputnik P1 position 4	2012-05-19 17:50:00.0	64°44.85’	5°04.16’		Sputnik Electromagnetic Dipole Transmitter | Sputnik	start transmitting
M87/2-739-1	Sputnik P1 position 4	2012-05-19 18:37:00.0	64°44.85’	5°04.16’		Sputnik Electromagnetic Dipole Transmitter | Sputnik	start heaving
M87/2-739-1	Sputnik P1 position 4	2012-05-19 18:37:00.0	64°44.85’	5°04.16’		Sputnik Electromagnetic Dipole Transmitter | Sputnik	end transmitting
M87/2-739-1	Sputnik P1 position 5	2012-05-19 18:56:00.0	64°44.90’	5°04.16’		Sputnik Electromagnetic Dipole Transmitter | Sputnik	position 5
M87/2-739-1	Sputnik P1 position 5	2012-05-19 19:01:00.0	64°44.90’	5°04.17’		Sputnik Electromagnetic Dipole Transmitter | Sputnik	start transmitting
M87/2-739-1	Sputnik P1 position 5	2012-05-19 19:20:00.0	64°44.90’	5°04.16’		Sputnik Electromagnetic Dipole Transmitter | Sputnik	end transmitting
M87/2-739-1	Sputnik P1 position 6	2012-05-19 19:36:00.0	64°44.95’	5°04.16’		Sputnik Electromagnetic Dipole Transmitter | Sputnik	position 6
M87/2-739-1	Sputnik P1 position 6	2012-05-19 19:42:00.0	64°44.95’	5°04.16’		Sputnik Electromagnetic Dipole Transmitter | Sputnik	start transmitting
M87/2-739-1	Sputnik P1 position 6	2012-05-19 19:58:00.0	64°44.95’	5°04.16’		Sputnik Electromagnetic Dipole Transmitter | Sputnik	end transmitting
M87/2-739-1	Sputnik P1 position 6	2012-05-19 20:23:00.0	64°44.95’	5°04.16’		Sputnik Electromagnetic Dipole Transmitter | Sputnik	on deck
M87/2-739-1	Sputnik P1 position 6	2012-05-19 23:02:00.0	64°44.96’	5°04.17’		Sputnik Electromagnetic Dipole Transmitter | Sputnik	Surface
M87/2-739-1	Sputnik P1 position 6	2012-05-19 23:50:00.0	64°44.96’	5°04.17’		Sputnik Electromagnetic Dipole Transmitter | Sputnik	max. depth
M87/2-739-1	Sputnik P1 position 6	2012-05-19 23:51:00.0	64°44.96’	5°04.17’		Sputnik Electromagnetic Dipole Transmitter | Sputnik	start transmitting
M87/2-739-1	Sputnik P1 position 6	2012-05-20 00:14:00.0	64°44.96’	5°04.17’		Sputnik Electromagnetic Dipole Transmitter | Sputnik	end transmitting
M87/2-739-1	Sputnik P1 position 6	2012-05-20 00:14:00.0	64°44.96’	5°04.17’		Sputnik Electromagnetic Dipole Transmitter | Sputnik	start heaving
M87/2-739-1	Sputnik P1 position 7	2012-05-20 00:30:00.0	64°45.01’	5°04.17’		Sputnik Electromagnetic Dipole Transmitter | Sputnik	position 7
M87/2-739-1	Sputnik P1 position 7	2012-05-20 00:35:00.0	64°45.01’	5°04.17’		Sputnik Electromagnetic Dipole Transmitter | Sputnik	max. depth
M87/2-739-1	Sputnik P1 position 7	2012-05-20 00:36:00.0	64°45.01’	5°04.17’		Sputnik Electromagnetic Dipole Transmitter | Sputnik	start transmitting

METEOR Station	Event	Time [UTC]	Latitude [°N]	Longitude [°E]	Water Depth [mbsl]	Gear	Remarks
M87/2-739-1	Sputnik P1 position 7	2012-05-20 00:44:00.0	64°45.01’	5°04.16’		Sputnik Electromagnetic Dipole Transmitter | Sputnik	end transmitting
M87/2-739-1	Sputnik P1 position 7	2012-05-20 00:44:00.0	64°45.01’	5°04.16’		Sputnik Electromagnetic Dipole Transmitter | Sputnik	start heaving
M87/2-739-1	Sputnik P1 position 8	2012-05-20 01:00:00.0	64°45.06’	5°04.17’		Sputnik Electromagnetic Dipole Transmitter | Sputnik	position 8
M87/2-739-1	Sputnik P1 position 8	2012-05-20 01:06:00.0	64°45.06’	5°04.17’		Sputnik Electromagnetic Dipole Transmitter | Sputnik	max. depth
M87/2-739-1	Sputnik P1 position 8	2012-05-20 01:07:00.0	64°45.06’	5°04.16’		Sputnik Electromagnetic Dipole Transmitter | Sputnik	start transmitting
M87/2-739-1	Sputnik P1 position 8	2012-05-20 01:17:00.0	64°45.06’	5°04.16’		Sputnik Electromagnetic Dipole Transmitter | Sputnik	end transmitting
M87/2-739-1	Sputnik P1 position 8	2012-05-20 01:17:00.0	64°45.06’	5°04.16’		Sputnik Electromagnetic Dipole Transmitter | Sputnik	start heaving
M87/2-739-1	Sputnik P1 position 9	2012-05-20 01:33:00.0	64°45.12’	5°04.17’		Sputnik Electromagnetic Dipole Transmitter | Sputnik	position 9
M87/2-739-1	Sputnik P1 position 9	2012-05-20 01:38:00.0	64°45.12’	5°04.16’		Sputnik Electromagnetic Dipole Transmitter | Sputnik	max. depth
M87/2-739-1	Sputnik P1 position 9	2012-05-20 01:39:00.0	64°45.12’	5°04.17’		Sputnik Electromagnetic Dipole Transmitter | Sputnik	start transmitting
M87/2-739-1	Sputnik P1 position 9	2012-05-20 01:52:00.0	64°45.12’	5°04.17’		Sputnik Electromagnetic Dipole Transmitter | Sputnik	start heaving
M87/2-739-1	Sputnik P1 position 9	2012-05-20 01:52:00.0	64°45.12’	5°04.17’		Sputnik Electromagnetic Dipole Transmitter | Sputnik	end transmitting
M87/2-739-1	Sputnik P1 position 10	2012-05-20 02:06:00.0	64°45.17’	5°04.17’		Sputnik Electromagnetic Dipole Transmitter | Sputnik	position 10
M87/2-739-1	Sputnik P1 position 10	2012-05-20 02:12:00.0	64°45.17’	5°04.17’		Sputnik Electromagnetic Dipole Transmitter | Sputnik	max. depth
M87/2-739-1	Sputnik P1 position 10	2012-05-20 02:12:00.0	64°45.17’	5°04.17’		Sputnik Electromagnetic Dipole Transmitter | Sputnik	start transmitting
M87/2-739-1	Sputnik P1 position 10	2012-05-20 02:23:00.0	64°45.17’	5°04.16’		Sputnik Electromagnetic Dipole Transmitter | Sputnik	end transmitting
M87/2-739-1	Sputnik P1 position 10	2012-05-20 02:23:00.0	64°45.17’	5°04.16’		Sputnik Electromagnetic Dipole Transmitter | Sputnik	start heaving
M87/2-739-1	Sputnik P1 position 11	2012-05-20 02:37:00.0	64°45.21’	5°04.17’		Sputnik Electromagnetic Dipole Transmitter | Sputnik	position 11
M87/2-739-1	Sputnik P1 position 11	2012-05-20 02:46:00.0	64°45.21’	5°04.17’		Sputnik Electromagnetic Dipole Transmitter | Sputnik	start transmitting

METEOR Station	Event	Time [UTC]	Latitude [°N]	Longitude [°E]	Water Depth [mbsl]	Gear	Remarks
M87/2-739-1	Sputnik P1 position 11	2012-05-20 02:46:00.0	64°45.21’	5°04.17’		Sputnik Electromagnetic Dipole Transmitter | Sputnik	max. depth
M87/2-739-1	Sputnik P1 position 11	2012-05-20 02:59:00.0	64°45.21’	5°04.17’		Sputnik Electromagnetic Dipole Transmitter | Sputnik	start heaving
M87/2-739-1	Sputnik P1 position 11	2012-05-20 02:59:00.0	64°45.21’	5°04.17’		Sputnik Electromagnetic Dipole Transmitter | Sputnik	end transmitting
M87/2-739-1	Sputnik P1 position 12	2012-05-20 03:11:00.0	64°45.24’	5°04.17’		Sputnik Electromagnetic Dipole Transmitter | Sputnik	position 12
M87/2-739-1	Sputnik P1 position 12	2012-05-20 03:14:00.0	64°45.24’	5°04.17’		Sputnik Electromagnetic Dipole Transmitter | Sputnik	max. depth
M87/2-739-1	Sputnik P1 position 12	2012-05-20 03:15:00.0	64°45.24’	5°04.17’		Sputnik Electromagnetic Dipole Transmitter | Sputnik	start transmitting
M87/2-739-1	Sputnik P1 position 12	2012-05-20 03:25:00.0	64°45.24’	5°04.17’		Sputnik Electromagnetic Dipole Transmitter | Sputnik	start heaving
M87/2-739-1	Sputnik P1 position 12	2012-05-20 03:25:00.0	64°45.24’	5°04.17’		Sputnik Electromagnetic Dipole Transmitter | Sputnik	end transmitting
M87/2-739-1	Sputnik P1 position 13	2012-05-20 03:36:00.0	64°45.26’	5°04.17’		Sputnik Electromagnetic Dipole Transmitter | Sputnik	position 13
M87/2-739-1	Sputnik P1 position 13	2012-05-20 03:46:00.0	64°45.27’	5°04.17’		Sputnik Electromagnetic Dipole Transmitter | Sputnik	start transmitting
M87/2-739-1	Sputnik P1 position 13	2012-05-20 03:46:00.0	64°45.27’	5°04.17’		Sputnik Electromagnetic Dipole Transmitter | Sputnik	max. depth
M87/2-739-1	Sputnik P1 position 13	2012-05-20 03:51:00.0	64°45.27’	5°04.17’		Sputnik Electromagnetic Dipole Transmitter | Sputnik	start heaving
M87/2-739-1	Sputnik P1 position 14	2012-05-20 04:02:00.0	64°45.29’	5°04.17’		Sputnik Electromagnetic Dipole Transmitter | Sputnik	position 14
M87/2-739-1	Sputnik P1 position 14	2012-05-20 04:12:00.0	64°45.29’	5°04.17’		Sputnik Electromagnetic Dipole Transmitter | Sputnik	start transmitting
M87/2-739-1	Sputnik P1 position 14	2012-05-20 04:12:00.0	64°45.29’	5°04.17’		Sputnik Electromagnetic Dipole Transmitter | Sputnik	max. depth
M87/2-739-1	Sputnik P1 position 14	2012-05-20 04:21:00.0	64°45.29’	5°04.17’		Sputnik Electromagnetic Dipole Transmitter | Sputnik	start heaving
M87/2-739-1	Sputnik P1 position 15	2012-05-20 04:33:00.0	64°45.32’	5°04.17’		Sputnik Electromagnetic Dipole Transmitter | Sputnik	position 15
M87/2-739-1	Sputnik P1 position 15	2012-05-20 04:41:00.0	64°45.32’	5°04.17’		Sputnik Electromagnetic Dipole Transmitter | Sputnik	max. depth
M87/2-739-1	Sputnik P1 position 15	2012-05-20 04:42:00.0	64°45.32’	5°04.17’		Sputnik Electromagnetic Dipole Transmitter | Sputnik	start transmitting

METEOR Station	Event	Time [UTC]	Latitude [°N]	Longitude [°E]	Water Depth [mbsl]	Gear	Remarks
M87/2-739-1	Sputnik P1 position 15	2012-05-20 04:49:00.0	64°45.32’	5°04.17’		Sputnik Electromagnetic Dipole Transmitter | Sputnik	start heaving
M87/2-739-1	Sputnik P1 position 16	2012-05-20 05:03:00.0	64°45.36’	5°04.17’		Sputnik Electromagnetic Dipole Transmitter | Sputnik	position 16
M87/2-739-1	Sputnik P1 position 16	2012-05-20 05:09:00.0	64°45.36’	5°04.16’		Sputnik Electromagnetic Dipole Transmitter | Sputnik	start transmitting
M87/2-739-1	Sputnik P1 position 16	2012-05-20 05:09:00.0	64°45.36’	5°04.16’		Sputnik Electromagnetic Dipole Transmitter | Sputnik	max. depth
M87/2-739-1	Sputnik P1 position 16	2012-05-20 05:15:00.0	64°45.36’	5°04.17’		Sputnik Electromagnetic Dipole Transmitter | Sputnik	end transmitting
M87/2-739-1	Sputnik P1 position 16	2012-05-20 05:16:00.0	64°45.36’	5°04.17’		Sputnik Electromagnetic Dipole Transmitter | Sputnik	start heaving
M87/2-739-1	Sputnik P1 position 17	2012-05-20 05:28:00.0	64°45.40’	5°04.16’		Sputnik Electromagnetic Dipole Transmitter | Sputnik	position 17
M87/2-739-1	Sputnik P1 position 17	2012-05-20 05:33:00.0	64°45.40’	5°04.17’		Sputnik Electromagnetic Dipole Transmitter | Sputnik	max. depth
M87/2-739-1	Sputnik P1 position 17	2012-05-20 05:34:00.0	64°45.40’	5°04.17’		Sputnik Electromagnetic Dipole Transmitter | Sputnik	start transmitting
M87/2-739-1	Sputnik P1 position 17	2012-05-20 05:37:00.0	64°45.40’	5°04.17’		Sputnik Electromagnetic Dipole Transmitter | Sputnik	end transmitting
M87/2-739-1	Sputnik P1 position 17	2012-05-20 05:38:00.0	64°45.40’	5°04.17’		Sputnik Electromagnetic Dipole Transmitter | Sputnik	start heaving
M87/2-739-1	Sputnik P1 position 18	2012-05-20 05:51:00.0	64°45.45’	5°04.17’		Sputnik Electromagnetic Dipole Transmitter | Sputnik	position 18
M87/2-739-1	Sputnik P1 position 18	2012-05-20 05:56:00.0	64°45.46’	5°04.17’		Sputnik Electromagnetic Dipole Transmitter | Sputnik	max. depth
M87/2-739-1	Sputnik P1 position 18	2012-05-20 05:57:00.0	64°45.46’	5°04.17’		Sputnik Electromagnetic Dipole Transmitter | Sputnik	start transmitting
M87/2-739-1	Sputnik P1 position 18	2012-05-20 06:01:00.0	64°45.46’	5°04.17’		Sputnik Electromagnetic Dipole Transmitter | Sputnik	end transmitting
M87/2-739-1	Sputnik P1 position 18	2012-05-20 06:01:00.0	64°45.46’	5°04.17’		Sputnik Electromagnetic Dipole Transmitter | Sputnik	start heaving
M87/2-739-1	Sputnik P1 position 19	2012-05-20 06:15:00.0	64°45.51’	5°04.17’		Sputnik Electromagnetic Dipole Transmitter | Sputnik	position 19
M87/2-739-1	Sputnik P1 position 19	2012-05-20 06:20:00.0	64°45.51’	5°04.17’		Sputnik Electromagnetic Dipole Transmitter | Sputnik	start transmitting
M87/2-739-1	Sputnik P1 position 19	2012-05-20 06:20:00.0	64°45.51’	5°04.17’		Sputnik Electromagnetic Dipole Transmitter | Sputnik	max. depth

METEOR Station	Event	Time [UTC]	Latitude [°N]	Longitude [°E]	Water Depth [mbsl]	Gear	Remarks
M87/2-739-1	Sputnik P1 position 19	2012-05-20 06:25:00.0	64°45.51’	5°04.17’		Sputnik Electromagnetic Dipole Transmitter | Sputnik	start heaving
M87/2-739-1	Sputnik P1 position 19	2012-05-20 06:25:00.0	64°45.51’	5°04.17’		Sputnik Electromagnetic Dipole Transmitter | Sputnik	end transmitting
M87/2-739-1	Sputnik P1 position 20	2012-05-20 06:38:00.0	64°45.56’	5°04.17’		Sputnik Electromagnetic Dipole Transmitter | Sputnik	position 20
M87/2-739-1	Sputnik P1 position 20	2012-05-20 06:46:00.0	64°45.56’	5°04.17’		Sputnik Electromagnetic Dipole Transmitter | Sputnik	max. depth
M87/2-739-1	Sputnik P1 position 20	2012-05-20 06:46:00.0	64°45.56’	5°04.17’		Sputnik Electromagnetic Dipole Transmitter | Sputnik	start transmitting
M87/2-739-1	Sputnik P1 position 20	2012-05-20 06:49:00.0	64°45.56’	5°04.17’		Sputnik Electromagnetic Dipole Transmitter | Sputnik	end transmitting
M87/2-739-1	Sputnik P1 position 20	2012-05-20 06:49:00.0	64°45.56’	5°04.17’		Sputnik Electromagnetic Dipole Transmitter | Sputnik	start heaving
M87/2-739-1	Sputnik P1 position 21	2012-05-20 07:06:00.0	64°45.62’	5°04.17’		Sputnik Electromagnetic Dipole Transmitter | Sputnik	position 21
M87/2-739-1	Sputnik P1 position 21	2012-05-20 07:14:00.0	64°45.62’	5°04.17’		Sputnik Electromagnetic Dipole Transmitter | Sputnik	max. depth
M87/2-739-1	Sputnik P1 position 21	2012-05-20 07:21:00.0	64°45.62’	5°04.17’		Sputnik Electromagnetic Dipole Transmitter | Sputnik	start heaving
M87/2-739-1	Sputnik P1 position 21	2012-05-20 07:21:00.0	64°45.62’	5°04.17’		Sputnik Electromagnetic Dipole Transmitter | Sputnik	start transmitting
M87/2-739-1	Sputnik P1 position 22	2012-05-20 07:35:00.0	64°45.67’	5°04.17’		Sputnik Electromagnetic Dipole Transmitter | Sputnik	position 22
M87/2-739-1	Sputnik P1 position 22	2012-05-20 07:40:00.0	64°45.68’	5°04.17’		Sputnik Electromagnetic Dipole Transmitter | Sputnik	max. depth
M87/2-739-1	Sputnik P1 position 22	2012-05-20 07:40:00.0	64°45.68’	5°04.17’		Sputnik Electromagnetic Dipole Transmitter | Sputnik	start transmitting
M87/2-739-1	Sputnik P1 position 22	2012-05-20 07:43:00.0	64°45.67’	5°04.17’		Sputnik Electromagnetic Dipole Transmitter | Sputnik	end transmitting
M87/2-739-1	Sputnik P1 position 22	2012-05-20 07:44:00.0	64°45.67’	5°04.17’		Sputnik Electromagnetic Dipole Transmitter | Sputnik	start heaving
M87/2-739-1	Sputnik P1 position 23	2012-05-20 07:45:00.0	64°45.68’	5°04.17’		Sputnik Electromagnetic Dipole Transmitter | Sputnik	position 23
M87/2-739-1	Sputnik P1 position 23	2012-05-20 07:45:00.0	64°45.68’	5°04.17’		Sputnik Electromagnetic Dipole Transmitter | Sputnik	max. depth
M87/2-739-1	Sputnik P1 position 23	2012-05-20 08:05:00.0	64°45.73’	5°04.16’		Sputnik Electromagnetic Dipole Transmitter | Sputnik	start heaving

METEOR Station	Event	Time [UTC]	Latitude [°N]	Longitude [°E]	Water Depth [mbsl]	Gear	Remarks
M87/2-739-1	Sputnik P1 position 23	2012-05-20 08:05:00.0	64°45.73’	5°04.16’		Sputnik Electromagnetic Dipole Transmitter | Sputnik	end transmitting
M87/2-739-1	Sputnik P1 position 24	2012-05-20 08:19:00.0	64°45.81’	5°04.16’		Sputnik Electromagnetic Dipole Transmitter | Sputnik	position 24
M87/2-739-1	Sputnik P1 position 24	2012-05-20 08:24:00.0	64°45.81’	5°04.16’		Sputnik Electromagnetic Dipole Transmitter | Sputnik	start heaving
M87/2-739-1	Sputnik P1 position 24-2	2012-05-20 08:30:00.0	64°45.82’	5°04.16’		Sputnik Electromagnetic Dipole Transmitter | Sputnik	position 24-2
M87/2-739-1	Sputnik P1 position 24-2	2012-05-20 08:33:00.0	64°45.82’	5°04.16’		Sputnik Electromagnetic Dipole Transmitter | Sputnik	max. depth
M87/2-739-1	Sputnik P1 position 24-2	2012-05-20 08:33:00.0	64°45.82’	5°04.16’		Sputnik Electromagnetic Dipole Transmitter | Sputnik	start transmitting
M87/2-739-1	Sputnik P1 position 24-2	2012-05-20 08:37:00.0	64°45.82’	5°04.16’		Sputnik Electromagnetic Dipole Transmitter | Sputnik	end transmitting
M87/2-739-1	Sputnik P1 position 24-2	2012-05-20 08:37:00.0	64°45.82’	5°04.16’		Sputnik Electromagnetic Dipole Transmitter | Sputnik	start heaving
M87/2-739-1	Sputnik P1 position 25	2012-05-20 08:53:00.0	64°45.90’	5°04.16’		Sputnik Electromagnetic Dipole Transmitter | Sputnik	position 25
M87/2-739-1	Sputnik P1 position 25	2012-05-20 08:57:00.0	64°45.90’	5°04.17’		Sputnik Electromagnetic Dipole Transmitter | Sputnik	start transmitting
M87/2-739-1	Sputnik P1 position 25	2012-05-20 08:57:00.0	64°45.90’	5°04.17’		Sputnik Electromagnetic Dipole Transmitter | Sputnik	max. depth
M87/2-739-1	Sputnik P1 position 25	2012-05-20 09:07:00.0	64°45.90’	5°04.16’		Sputnik Electromagnetic Dipole Transmitter | Sputnik	start heaving
M87/2-739-1	Sputnik P1 position 25	2012-05-20 09:07:00.0	64°45.90’	5°04.16’		Sputnik Electromagnetic Dipole Transmitter | Sputnik	end transmitting
M87/2-740-1	Sputnik P1 position 25	2012-05-20 09:30:00.0	64°45.90’	5°04.17’		Sputnik Electromagnetic Dipole Transmitter | Sputnik	on deck
M87/2-740-1	Sputnik P2 position 1	2012-05-20 10:20:00.0	64°44.70’	5°04.58’		Sputnik Electromagnetic Dipole Transmitter | Sputnik	surface
M87/2-740-1	Sputnik P2 position 1	2012-05-20 10:48:00.0	64°44.70’	5°04.58’		Sputnik Electromagnetic Dipole Transmitter | Sputnik	start heaving (problems)
M87/2-740-1	Sputnik P2 position 1	2012-05-20 11:07:00.0	64°44.70’	5°04.58’		Sputnik Electromagnetic Dipole Transmitter | Sputnik	on deck
M87/2-740-1	Sputnik P2 position 1	2012-05-20 12:26:00.0	64°44.70’	5°04.58’		Sputnik Electromagnetic Dipole Transmitter | Sputnik	surface
M87/2-740-1	Sputnik P2 position 1	2012-05-20 13:19:00.0	64°44.70’	5°04.58’		Sputnik Electromagnetic Dipole Transmitter | Sputnik	max. depth

METEOR Station	Event	Time [UTC]	Latitude [°N]	Longitude [°E]	Water Depth [mbsl]	Gear	Remarks
M87/2-740-1	Sputnik P2 position 1	2012-05-20 13:20:00.0	64°44.70’	5°04.58’		Sputnik Electromagnetic Dipole Transmitter | Sputnik	start transmitting
M87/2-740-1	Sputnik P2 position 1	2012-05-20 13:22:00.0	64°44.70’	5°04.58’		Sputnik Electromagnetic Dipole Transmitter | Sputnik	end transmitting
M87/2-740-1	Sputnik P2 position 1	2012-05-20 13:22:00.0	64°44.70’	5°04.58’		Sputnik Electromagnetic Dipole Transmitter | Sputnik	start heaving
M87/2-740-1	Sputnik P2 position 1	2012-05-20 13:45:00.0	64°44.70’	5°04.58’		Sputnik Electromagnetic Dipole Transmitter | Sputnik	max. depth
M87/2-740-1	Sputnik P2 position 1	2012-05-20 13:46:00.0	64°44.70’	5°04.58’		Sputnik Electromagnetic Dipole Transmitter | Sputnik	start transmitting
M87/2-740-1	Sputnik P2 position 1	2012-05-20 13:50:00.0	64°44.70’	5°04.58’		Sputnik Electromagnetic Dipole Transmitter | Sputnik	end transmitting
M87/2-740-1	Sputnik P2 position 1	2012-05-20 13:50:00.0	64°44.70’	5°04.58’		Sputnik Electromagnetic Dipole Transmitter | Sputnik	start heaving
M87/2-740-1	Sputnik P2 position 2	2012-05-20 14:06:00.0	64°44.78’	5°04.59’		Sputnik Electromagnetic Dipole Transmitter | Sputnik	position 2
M87/2-740-1	Sputnik P2 position 2	2012-05-20 14:12:00.0	64°44.78’	5°04.58’		Sputnik Electromagnetic Dipole Transmitter | Sputnik	max. depth
M87/2-740-1	Sputnik P2 position 2	2012-05-20 14:12:00.0	64°44.78’	5°04.58’		Sputnik Electromagnetic Dipole Transmitter | Sputnik	start transmitting
M87/2-740-1	Sputnik P2 position 2	2012-05-20 14:17:00.0	64°44.78’	5°04.58’		Sputnik Electromagnetic Dipole Transmitter | Sputnik	start heaving
M87/2-740-1	Sputnik P2 position 2	2012-05-20 14:17:00.0	64°44.78’	5°04.58’		Sputnik Electromagnetic Dipole Transmitter | Sputnik	end transmitting
M87/2-740-1	Sputnik P2 position 3	2012-05-20 14:37:00.0	64°44.86’	5°04.59’		Sputnik Electromagnetic Dipole Transmitter | Sputnik	position 3
M87/2-740-1	Sputnik P2 position 3	2012-05-20 14:42:00.0	64°44.86’	5°04.59’		Sputnik Electromagnetic Dipole Transmitter | Sputnik	max. depth
M87/2-740-1	Sputnik P2 position 3	2012-05-20 14:42:00.0	64°44.86’	5°04.59’		Sputnik Electromagnetic Dipole Transmitter | Sputnik	start transmitting
M87/2-740-1	Sputnik P2 position 3	2012-05-20 14:46:00.0	64°44.86’	5°04.59’		Sputnik Electromagnetic Dipole Transmitter | Sputnik	end transmitting
M87/2-740-1	Sputnik P2 position 3	2012-05-20 14:46:00.0	64°44.86’	5°04.59’		Sputnik Electromagnetic Dipole Transmitter | Sputnik	start heaving
M87/2-740-1	Sputnik P2 position 4	2012-05-20 14:56:00.0	64°44.91’	5°04.59’		Sputnik Electromagnetic Dipole Transmitter | Sputnik	position 4
M87/2-740-1	Sputnik P2 position 4	2012-05-20 15:02:00.0	64°44.91’	5°04.59’		Sputnik Electromagnetic Dipole Transmitter | Sputnik	max. depth

METEOR Station	Event	Time [UTC]	Latitude [°N]	Longitude [°E]	Water Depth [mbsl]	Gear	Remarks
M87/2-740-1	Sputnik P2 position 4	2012-05-20 15:03:00.0	64°44.91’	5°04.59’		Sputnik Electromagnetic Dipole Transmitter | Sputnik	start transmitting
M87/2-740-1	Sputnik P2 position 4	2012-05-20 15:15:00.0	64°44.91’	5°04.59’		Sputnik Electromagnetic Dipole Transmitter | Sputnik	end transmitting
M87/2-740-1	Sputnik P2 position 4	2012-05-20 15:16:00.0	64°44.91’	5°04.59’		Sputnik Electromagnetic Dipole Transmitter | Sputnik	start heaving
M87/2-740-1	Sputnik P2 position 5	2012-05-20 15:49:00.0	64°44.97’	5°04.59’		Sputnik Electromagnetic Dipole Transmitter | Sputnik	position 5
M87/2-740-1	Sputnik P2 position 5	2012-05-20 15:55:00.0	64°44.97’	5°04.59’		Sputnik Electromagnetic Dipole Transmitter | Sputnik	start transmitting
M87/2-740-1	Sputnik P2 position 5	2012-05-20 15:55:00.0	64°44.97’	5°04.59’		Sputnik Electromagnetic Dipole Transmitter | Sputnik	max. depth
M87/2-740-1	Sputnik P2 position 5	2012-05-20 15:58:00.0	64°44.97’	5°04.59’		Sputnik Electromagnetic Dipole Transmitter | Sputnik	end transmitting
M87/2-740-1	Sputnik P2 position 5	2012-05-20 15:59:00.0	64°44.97’	5°04.59’		Sputnik Electromagnetic Dipole Transmitter | Sputnik	start heaving
M87/2-740-1	Sputnik P2 position 5	2012-05-20 16:07:00.0	64°44.97’	5°04.59’		Sputnik Electromagnetic Dipole Transmitter | Sputnik	break of station (problems)
M87/2-740-1	Sputnik P2 position 5	2012-05-20 16:29:00.0	64°44.97’	5°04.59’		Sputnik Electromagnetic Dipole Transmitter | Sputnik	on deck
M87/2-741-1	Sputnik P2 position 5	2012-05-20 16:41:00.0	64°44.97’	5°04.59’		Sputnik Electromagnetic Dipole Transmitter | Sputnik	surface
M87/2-741-1	Sputnik P2 position 5	2012-05-20 17:28:00.0	64°44.97’	5°04.59’		Sputnik Electromagnetic Dipole Transmitter | Sputnik	start transmitting
M87/2-741-1	Sputnik P2 position 5	2012-05-20 17:28:00.0	64°44.97’	5°04.59’		Sputnik Electromagnetic Dipole Transmitter | Sputnik	max. depth
M87/2-741-1	Sputnik P2 position 5	2012-05-20 17:35:00.0	64°44.97’	5°04.59’		Sputnik Electromagnetic Dipole Transmitter | Sputnik	end transmitting
M87/2-741-1	Sputnik P2 position 5	2012-05-20 17:35:00.0	64°44.97’	5°04.59’		Sputnik Electromagnetic Dipole Transmitter | Sputnik	start heaving
M87/2-741-1	Sputnik P2 position 6	2012-05-20 17:48:00.0	64°45.05’	5°04.59’		Sputnik Electromagnetic Dipole Transmitter | Sputnik	position 6
M87/2-741-1	Sputnik P2 position 6	2012-05-20 18:02:00.0	64°45.05’	5°04.59’		Sputnik Electromagnetic Dipole Transmitter | Sputnik	start transmitting
M87/2-741-1	Sputnik P2 position 6	2012-05-20 18:02:00.0	64°45.05’	5°04.59’		Sputnik Electromagnetic Dipole Transmitter | Sputnik	max. depth
M87/2-741-1	Sputnik P2 position 6	2012-05-20 18:07:00.0	64°45.05’	5°04.59’		Sputnik Electromagnetic Dipole Transmitter | Sputnik	end transmitting

METEOR Station	Event	Time [UTC]	Latitude [°N]	Longitude [°E]	Water Depth [mbsl]	Gear	Remarks
M87/2-741-1	Sputnik P2 position 6	2012-05-20 18:07:00.0	64°45.05’	5°04.59’		Sputnik Electromagnetic Dipole Transmitter | Sputnik	start heaving
M87/2-741-1	Sputnik P2 position 7	2012-05-20 18:19:00.0	64°45.10’	5°04.59’		Sputnik Electromagnetic Dipole Transmitter | Sputnik	position 7
M87/2-741-1	Sputnik P2 position 7	2012-05-20 18:26:00.0	64°45.10’	5°04.59’		Sputnik Electromagnetic Dipole Transmitter | Sputnik	max. depth
M87/2-741-1	Sputnik P2 position 7	2012-05-20 18:27:00.0	64°45.10’	5°04.59’		Sputnik Electromagnetic Dipole Transmitter | Sputnik	start transmitting
M87/2-741-1	Sputnik P2 position 7	2012-05-20 18:33:00.0	64°45.10’	5°04.59’		Sputnik Electromagnetic Dipole Transmitter | Sputnik	start heaving
M87/2-741-1	Sputnik P2 position 7	2012-05-20 18:33:00.0	64°45.10 ‘	5°04.59’		Sputnik Electromagnetic Dipole Transmitter | Sputnik	end transmitting
M87/2-741-1	Sputnik P2 position 8	2012-05-20 18:44:00.0	64°45.16’	5°04.59’		Sputnik Electromagnetic Dipole Transmitter | Sputnik	position 8
M87/2-741-1	Sputnik P2 position 8	2012-05-20 18:50:00.0	64°45.16’	5°04.59’		Sputnik Electromagnetic Dipole Transmitter | Sputnik	max. depth
M87/2-741-1	Sputnik P2 position 8	2012-05-20 18:51:00.0	64°45.16’	5°04.59’		Sputnik Electromagnetic Dipole Transmitter | Sputnik	start transmitting
M87/2-741-1	Sputnik P2 position 8	2012-05-20 18:55:00.0	64°45.16’	5°04.59’		Sputnik Electromagnetic Dipole Transmitter | Sputnik	start heaving
M87/2-741-1	Sputnik P2 position 8	2012-05-20 18:55:00.0	64°45.16’	5°04.59’		Sputnik Electromagnetic Dipole Transmitter | Sputnik	end transmitting
M87/2-741-1	Sputnik P2 position 9	2012-05-20 19:06:00.0	64°45.21’	5°04.59’		Sputnik Electromagnetic Dipole Transmitter | Sputnik	position 9
M87/2-741-1	Sputnik P2 position 9	2012-05-20 19:14:00.0	64°45.21’	5°04.59’		Sputnik Electromagnetic Dipole Transmitter | Sputnik	start transmitting
M87/2-741-1	Sputnik P2 position 9	2012-05-20 19:14:00.0	64°45.21’	5°04.59’		Sputnik Electromagnetic Dipole Transmitter | Sputnik	max. depth
M87/2-741-1	Sputnik P2 position 9	2012-05-20 19:18:00.0	64°45.21’	5°04.59’		Sputnik Electromagnetic Dipole Transmitter | Sputnik	start heaving
M87/2-741-1	Sputnik P2 position 9	2012-05-20 19:18:00.0	64°45.21’	5°04.59’		Sputnik Electromagnetic Dipole Transmitter | Sputnik	end transmitting
M87/2-741-1	Sputnik P2 position 10	2012-05-20 19:29:00.0	64°45.26’	5°04.59’		Sputnik Electromagnetic Dipole Transmitter | Sputnik	position 10
M87/2-741-1	Sputnik P2 position 10	2012-05-20 19:35:00.0	64°45.26’	5°04.59’		Sputnik Electromagnetic Dipole Transmitter | Sputnik	start transmitting
M87/2-741-1	Sputnik P2 position 10	2012-05-20 19:35:00.0	64°45.26’	5°04.59’		Sputnik Electromagnetic Dipole Transmitter | Sputnik	max. depth

METEOR Station	Event	Time [UTC]	Latitude [°N]	Longitude [°E]	Water Depth [mbsl]	Gear	Remarks
M87/2-741-1	Sputnik P2 position 10	2012-05-20 19:40:00.0	64°45.26’	5°04.59’		Sputnik Electromagnetic Dipole Transmitter | Sputnik	end transmitting
M87/2-741-1	Sputnik P2 position 10	2012-05-20 19:40:00.0	64°45.26’	5°04.59’		Sputnik Electromagnetic Dipole Transmitter | Sputnik	start heaving
M87/2-741-1	Sputnik P2 position 11	2012-05-20 19:51:00.0	64°45.32’	5°04.59’		Sputnik Electromagnetic Dipole Transmitter | Sputnik	position 11
M87/2-741-1	Sputnik P2 position 11	2012-05-20 19:57:00.0	64°45.32’	5°04.59’		Sputnik Electromagnetic Dipole Transmitter | Sputnik	start transmitting
M87/2-741-1	Sputnik P2 position 11	2012-05-20 19:57:00.0	64°45.32’	5°04.59’		Sputnik Electromagnetic Dipole Transmitter | Sputnik	max. depth
M87/2-741-1	Sputnik P2 position 11	2012-05-20 20:00:00.0	64°45.32’	5°04.59’		Sputnik Electromagnetic Dipole Transmitter | Sputnik	end transmitting
M87/2-741-1	Sputnik P2 position 11	2012-05-20 20:01:00.0	64°45.32’	5°04.59’		Sputnik Electromagnetic Dipole Transmitter | Sputnik	start heaving
M87/2-741-1	Sputnik P2 position 12	2012-05-20 20:13:00.0	64°45.37’	5°04.59’		Sputnik Electromagnetic Dipole Transmitter | Sputnik	position 12
M87/2-741-1	Sputnik P2 position 12	2012-05-20 20:28:00.0	64°45.37’	5°04.59’		Sputnik Electromagnetic Dipole Transmitter | Sputnik	max. depth
M87/2-741-1	Sputnik P2 position 12	2012-05-20 20:28:00.0	64°45.37’	5°04.59’		Sputnik Electromagnetic Dipole Transmitter | Sputnik	start transmitting
M87/2-741-1	Sputnik P2 position 12	2012-05-20 20:42:00.0	64°45.37’	5°04.59’		Sputnik Electromagnetic Dipole Transmitter | Sputnik	end transmitting
M87/2-741-1	Sputnik P2 position 12	2012-05-20 20:42:00.0	64°45.37’	5°04.59’		Sputnik Electromagnetic Dipole Transmitter | Sputnik	start heaving
M87/2-741-1	Sputnik P2 position 13	2012-05-20 20:54:00.0	64°45.43’	5°04.59’		Sputnik Electromagnetic Dipole Transmitter | Sputnik	position 13
M87/2-741-1	Sputnik P2 position 13	2012-05-20 20:58:00.0	64°45.43’	5°04.59’		Sputnik Electromagnetic Dipole Transmitter | Sputnik	max. depth
M87/2-741-1	Sputnik P2 position 13	2012-05-20 20:58:00.0	64°45.43’	5°04.59’		Sputnik Electromagnetic Dipole Transmitter | Sputnik	start transmitting
M87/2-741-1	Sputnik P2 position 13	2012-05-20 21:03:00.0	64°45.43’	5°04.59’		Sputnik Electromagnetic Dipole Transmitter | Sputnik	start heaving
M87/2-741-1	Sputnik P2 position 13	2012-05-20 21:03:00.0	64°45.43’	5°04.59’		Sputnik Electromagnetic Dipole Transmitter | Sputnik	end transmitting
M87/2-741-1	Sputnik P2 position 14	2012-05-20 21:18:00.0	64°45.48’	5°04.59’		Sputnik Electromagnetic Dipole Transmitter | Sputnik	position 14
M87/2-741-1	Sputnik P2 position 14	2012-05-20 21:25:00.0	64°45.48’	5°04.59’		Sputnik Electromagnetic Dipole Transmitter | Sputnik	max. depth

METEOR Station	Event	Time [UTC]	Latitude [°N]	Longitude [°E]	Water Depth [mbsl]	Gear	Remarks
M87/2-741-1	Sputnik P2 position 14	2012-05-20 21:26:00.0	64°45.48’	5°04.59’		Sputnik Electromagnetic Dipole Transmitter | Sputnik	start transmitting
M87/2-741-1	Sputnik P2 position 14	2012-05-20 21:29:00.0	64°45.48’	5°04.59’		Sputnik Electromagnetic Dipole Transmitter | Sputnik	start heaving
M87/2-741-1	Sputnik P2 position 14	2012-05-20 21:29:00.0	64°45.48’	5°04.59’		Sputnik Electromagnetic Dipole Transmitter | Sputnik	end transmitting
M87/2-741-1	Sputnik P2 position 15	2012-05-20 21:42:00.0	64°45.56’	5°04.59’		Sputnik Electromagnetic Dipole Transmitter | Sputnik	position 15
M87/2-741-1	Sputnik P2 position 15	2012-05-20 21:48:00.0	64°45.56’	5°04.59’		Sputnik Electromagnetic Dipole Transmitter | Sputnik	start transmitting
M87/2-741-1	Sputnik P2 position 15	2012-05-20 21:50:00.0	64°45.56’	5°04.59’		Sputnik Electromagnetic Dipole Transmitter | Sputnik	end transmitting
M87/2-741-1	Sputnik P2 position 15	2012-05-20 21:50:00.0	64°45.56’	5°04.59’		Sputnik Electromagnetic Dipole Transmitter | Sputnik	start heaving
M87/2-741-1	Sputnik P2 position 16	2012-05-20 22:04:00.0	64°45.64’	5°04.59’		Sputnik Electromagnetic Dipole Transmitter | Sputnik	position 16
M87/2-741-1	Sputnik P2 position 16	2012-05-20 22:09:00.0	64°45.64’	5°04.59’		Sputnik Electromagnetic Dipole Transmitter | Sputnik	max. depth
M87/2-741-1	Sputnik P2 position 16	2012-05-20 22:10:00.0	64°45.64’	5°04.59’		Sputnik Electromagnetic Dipole Transmitter | Sputnik	start transmitting
M87/2-741-1	Sputnik P2 position 16	2012-05-20 22:12:00.0	64°45.64’	5°04.59’		Sputnik Electromagnetic Dipole Transmitter | Sputnik	start heaving
M87/2-741-1	Sputnik P2 position 16	2012-05-20 22:12:00.0	64°45.64’	5°04.59’		Sputnik Electromagnetic Dipole Transmitter | Sputnik	end transmitting
M87/2-741-1	Sputnik P2 position 17	2012-05-20 22:27:00.0	64°45.75’	5°04.59’		Sputnik Electromagnetic Dipole Transmitter | Sputnik	position 17
M87/2-741-1	Sputnik P2 position 17	2012-05-20 22:33:00.0	64°45.75’	5°04.59’		Sputnik Electromagnetic Dipole Transmitter | Sputnik	max. depth
M87/2-741-1	Sputnik P2 position 17	2012-05-20 22:34:00.0	64°45.75’	5°04.59’		Sputnik Electromagnetic Dipole Transmitter | Sputnik	start transmitting
M87/2-741-1	Sputnik P2 position 17	2012-05-20 22:39:00.0	64°45.75’	5°04.59’		Sputnik Electromagnetic Dipole Transmitter | Sputnik	end transmitting
M87/2-741-1	Sputnik P2 position 17	2012-05-20 22:39:00.0	64°45.75’	5°04.59’		Sputnik Electromagnetic Dipole Transmitter | Sputnik	start heaving
M87/2-741-1	Sputnik P2 position 18	2012-05-20 22:54:00.0	64°45.86’	5°04.59’		Sputnik Electromagnetic Dipole Transmitter | Sputnik	position 18
M87/2-741-1	Sputnik P2 position 18	2012-05-20 23:00:00.0	64°45.86’	5°04.59’		Sputnik Electromagnetic Dipole Transmitter | Sputnik	max. depth

METEOR Station	Event	Time [UTC]	Latitude [°N]	Longitude [°E]	Water Depth [mbsl]	Gear	Remarks
M87/2-741-1	Sputnik P2 position 18	2012-05-20 23:01:00.0	64°45.86’	5°04.59’		Sputnik Electromagnetic Dipole Transmitter | Sputnik	start transmitting
M87/2-741-1	Sputnik P2 position 18	2012-05-20 23:04:00.0	64°45.86’	5°04.59’		Sputnik Electromagnetic Dipole Transmitter | Sputnik	start heaving
M87/2-741-1	Sputnik P2 position 18	2012-05-20 23:04:00.0	64°45.86’	5°04.59’		Sputnik Electromagnetic Dipole Transmitter | Sputnik	end transmitting
M87/2-741-1	Sputnik P2 position 18	2012-05-20 23:29:00.0	64°45.85’	5°04.60’		Sputnik Electromagnetic Dipole Transmitter | Sputnik	on deck
M87/2-742-1	Sputnik P3 position 1	2012-05-20 23:53:00.0	64°44.70’	5°03.79’		Sputnik Electromagnetic Dipole Transmitter | Sputnik	position 1, surface
M87/2-742-1	Sputnik P3 position 1	2012-05-21 00:30:00.0	64°44.71’	5°03.79’		Sputnik Electromagnetic Dipole Transmitter | Sputnik	max. depth
M87/2-742-1	Sputnik P3 position 1	2012-05-21 00:31:00.0	64°44.71’	5°03.79’		Sputnik Electromagnetic Dipole Transmitter | Sputnik	start transmitting
M87/2-742-1	Sputnik P3 position 1	2012-05-21 00:35:00.0	64°44.71’	5°03.79’		Sputnik Electromagnetic Dipole Transmitter | Sputnik	end transmitting
M87/2-742-1	Sputnik P3 position 1	2012-05-21 00:35:00.0	64°44.71’	5°03.79’		Sputnik Electromagnetic Dipole Transmitter | Sputnik	start heaving
M87/2-742-1	Sputnik P3 position 2	2012-05-21 00:48:00.0	64°44.82’	5°03.79’		Sputnik Electromagnetic Dipole Transmitter | Sputnik	position 2
M87/2-742-1	Sputnik P3 position 2	2012-05-21 00:57:00.0	64°44.82’	5°03.79’		Sputnik Electromagnetic Dipole Transmitter | Sputnik	max. depth
M87/2-742-1	Sputnik P3 position 2	2012-05-21 00:58:00.0	64°44.82’	5°03.79’		Sputnik Electromagnetic Dipole Transmitter | Sputnik	start transmitting
M87/2-742-1	Sputnik P3 position 2	2012-05-21 01:01:00.0	64°44.82’	5°03.79’		Sputnik Electromagnetic Dipole Transmitter | Sputnik	start heaving
M87/2-742-1	Sputnik P3 position 2	2012-05-21 01:01:00.0	64°44.82’	5°03.79’		Sputnik Electromagnetic Dipole Transmitter | Sputnik	end transmitting
M87/2-742-1	Sputnik P3 position 3	2012-05-21 01:15:00.0	64°44.92’	5°03.79’		Sputnik Electromagnetic Dipole Transmitter | Sputnik	position 3
M87/2-742-1	Sputnik P3 position 3	2012-05-21 01:20:00.0	64°44.93’	5°03.79’		Sputnik Electromagnetic Dipole Transmitter | Sputnik	max. depth
M87/2-742-1	Sputnik P3 position 3	2012-05-21 01:21:00.0	64°44.93’	5°03.79’		Sputnik Electromagnetic Dipole Transmitter | Sputnik	start transmitting
M87/2-742-1	Sputnik P3 position 3	2012-05-21 01:31:00.0	64°44.93’	5°03.79’		Sputnik Electromagnetic Dipole Transmitter | Sputnik	end transmitting
M87/2-742-1	Sputnik P3 position 3	2012-05-21 01:31:00.0	64°44.93’	5°03.79’		Sputnik Electromagnetic Dipole Transmitter | Sputnik	start heaving

METEOR Station	Event	Time [UTC]	Latitude [°N]	Longitude [°E]	Water Depth [mbsl]	Gear	Remarks
M87/2-742-1	Sputnik P3 position 4	2012-05-21 01:44:00.0	64°45.03’	5°03.79’		Sputnik Electromagnetic Dipole Transmitter | Sputnik	position 4
M87/2-742-1	Sputnik P3 position 4	2012-05-21 01:50:00.0	64°45.03’	5°03.79’		Sputnik Electromagnetic Dipole Transmitter | Sputnik	max. depth
M87/2-742-1	Sputnik P3 position 4	2012-05-21 01:51:00.0	64°45.03’	5°03.79’		Sputnik Electromagnetic Dipole Transmitter | Sputnik	start transmitting
M87/2-742-1	Sputnik P3 position 4	2012-05-21 01:56:00.0	64°45.03’	5°03.79’		Sputnik Electromagnetic Dipole Transmitter | Sputnik	end transmitting
M87/2-742-1	Sputnik P3 position 4	2012-05-21 01:56:00.0	64°45.03’	5°03.79’		Sputnik Electromagnetic Dipole Transmitter | Sputnik	start heaving
M87/2-742-1	Sputnik P3 position 5	2012-05-21 02:14:00.0	64°45.11’	5°03.79’		Sputnik Electromagnetic Dipole Transmitter | Sputnik	position 5
M87/2-742-1	Sputnik P3 position 5	2012-05-21 02:18:00.0	64°45.11’	5°03.79’		Sputnik Electromagnetic Dipole Transmitter | Sputnik	start transmitting
M87/2-742-1	Sputnik P3 position 5	2012-05-21 02:18:00.0	64°45.11’	5°03.79’		Sputnik Electromagnetic Dipole Transmitter | Sputnik	max. depth
M87/2-742-1	Sputnik P3 position 5	2012-05-21 02:21:00.0	64°45.11’	5°03.79’		Sputnik Electromagnetic Dipole Transmitter | Sputnik	end transmitting
M87/2-742-1	Sputnik P3 position 5	2012-05-21 02:21:00.0	64°45.11’	5°03.79’		Sputnik Electromagnetic Dipole Transmitter | Sputnik	start heaving
M87/2-742-1	Sputnik P3 position 6	2012-05-21 02:39:00.0	64°45.21’	5°03.75’		Sputnik Electromagnetic Dipole Transmitter | Sputnik	position 6
M87/2-742-1	Sputnik P3 position 6	2012-05-21 02:43:00.0	64°45.21’	5°03.75’		Sputnik Electromagnetic Dipole Transmitter | Sputnik	max. depth
M87/2-742-1	Sputnik P3 position 6	2012-05-21 02:44:00.0	64°45.21’	5°03.75’		Sputnik Electromagnetic Dipole Transmitter | Sputnik	start transmitting
M87/2-742-1	Sputnik P3 position 6	2012-05-21 02:53:00.0	64°45.21’	5°03.75’		Sputnik Electromagnetic Dipole Transmitter | Sputnik	end transmitting
M87/2-742-1	Sputnik P3 position 6	2012-05-21 02:53:00.0	64°45.21’	5°03.75’		Sputnik Electromagnetic Dipole Transmitter | Sputnik	start heaving
M87/2-742-1	Sputnik P3 position 7	2012-05-21 03:24:00.0	64°45.29’	5°03.74’		Sputnik Electromagnetic Dipole Transmitter | Sputnik	position 7
M87/2-742-1	Sputnik P3 position 7	2012-05-21 03:24:00.0	64°45.29’	5°03.74’		Sputnik Electromagnetic Dipole Transmitter | Sputnik	start transmitting
M87/2-742-1	Sputnik P3 position 7	2012-05-21 03:24:00.0	64°45.29’	5°03.74’		Sputnik Electromagnetic Dipole Transmitter | Sputnik	max. depth
M87/2-742-1	Sputnik P3 position 7	2012-05-21 03:35:00.0	64°45.29’	5°03.74’		Sputnik Electromagnetic Dipole Transmitter | Sputnik	end transmitting

METEOR Station	Event	Time [UTC]	Latitude [°N]	Longitude [°E]	Water Depth [mbsl]	Gear	Remarks
M87/2-742-1	Sputnik P3 position 7	2012-05-21 03:36:00.0	64°45.29’	5°03.74’		Sputnik Electromagnetic Dipole Transmitter | Sputnik	start heaving
M87/2-742-1	Sputnik P3 position 8	2012-05-21 03:51:00.0	64°45.37’	5°03.80’		Sputnik Electromagnetic Dipole Transmitter | Sputnik	position 8
M87/2-742-1	Sputnik P3 position 8	2012-05-21 03:53:00.0	64°45.37’	5°03.80’		Sputnik Electromagnetic Dipole Transmitter | Sputnik	max. depth
M87/2-742-1	Sputnik P3 position 8	2012-05-21 03:54:00.0	64°45.37’	5°03.80’		Sputnik Electromagnetic Dipole Transmitter | Sputnik	start transmitting
M87/2-742-1	Sputnik P3 position 8	2012-05-21 04:00:00.0	64°45.37’	5°03.80’		Sputnik Electromagnetic Dipole Transmitter | Sputnik	end transmitting
M87/2-742-1	Sputnik P3 position 8	2012-05-21 04:00:00.0	64°45.37’	5°03.80’		Sputnik Electromagnetic Dipole Transmitter | Sputnik	start heaving
M87/2-742-1	Sputnik P3 position 9	2012-05-21 04:16:00.0	64°45.45’	5°03.80’		Sputnik Electromagnetic Dipole Transmitter | Sputnik	position 9
M87/2-742-1	Sputnik P3 position 9	2012-05-21 04:21:00.0	64°45.45’	5°03.80’		Sputnik Electromagnetic Dipole Transmitter | Sputnik	max. depth
M87/2-742-1	Sputnik P3 position 9	2012-05-21 04:21:00.0	64°45.45’	5°03.80’		Sputnik Electromagnetic Dipole Transmitter | Sputnik	start transmitting
M87/2-742-1	Sputnik P3 position 9	2012-05-21 04:25:00.0	64°45.45’	5°03.80’		Sputnik Electromagnetic Dipole Transmitter | Sputnik	end transmitting
M87/2-742-1	Sputnik P3 position 9	2012-05-21 04:25:00.0	64°45.45’	5°03.80’		Sputnik Electromagnetic Dipole Transmitter | Sputnik	start heaving
M87/2-742-1	Sputnik P3 position 10	2012-05-21 04:37:00.0	64°45.56’	5°03.80’		Sputnik Electromagnetic Dipole Transmitter | Sputnik	position 10
M87/2-742-1	Sputnik P3 position 10	2012-05-21 04:44:00.0	64°45.56’	5°03.80’		Sputnik Electromagnetic Dipole Transmitter | Sputnik	max. depth
M87/2-742-1	Sputnik P3 position 10	2012-05-21 04:45:00.0	64°45.56’	5°03.80’		Sputnik Electromagnetic Dipole Transmitter | Sputnik	start transmitting
M87/2-742-1	Sputnik P3 position 10	2012-05-21 04:48:00.0	64°45.56’	5°03.80’		Sputnik Electromagnetic Dipole Transmitter | Sputnik	start heaving
M87/2-742-1	Sputnik P3 position 10	2012-05-21 04:48:00.0	64°45.56’	5°03.80’		Sputnik Electromagnetic Dipole Transmitter | Sputnik	end transmitting
M87/2-742-1	Sputnik P3 position 11	2012-05-21 05:06:00.0	64°45.66’	5°03.80’		Sputnik Electromagnetic Dipole Transmitter | Sputnik	position 11
M87/2-742-1	Sputnik P3 position 11	2012-05-21 05:10:00.0	64°45.66’	5°03.80’		Sputnik Electromagnetic Dipole Transmitter | Sputnik	max. depth
M87/2-742-1	Sputnik P3 position 11	2012-05-21 05:10:00.0	64°45.66’	5°03.80’		Sputnik Electromagnetic Dipole Transmitter | Sputnik	start transmitting

METEOR Station	Event	Time [UTC]	Latitude [°N]	Longitude [°E]	Water Depth [mbsl]	Gear	Remarks
M87/2-742-1	Sputnik P3 position 11	2012-05-21 05:15:00.0	64°45.66’	5°03.80’		Sputnik Electromagnetic Dipole Transmitter | Sputnik	end transmitting
M87/2-742-1	Sputnik P3 position 11	2012-05-21 05:15:00.0	64°45.66’	5°03.80’		Sputnik Electromagnetic Dipole Transmitter | Sputnik	start heaving
M87/2-742-1	Sputnik P3 position 12	2012-05-21 05:31:00.0	64°45.77’	5°03.80’		Sputnik Electromagnetic Dipole Transmitter | Sputnik	position 12
M87/2-742-1	Sputnik P3 position 12	2012-05-21 05:34:00.0	64°45.77’	5°03.80’		Sputnik Electromagnetic Dipole Transmitter | Sputnik	max. depth
M87/2-742-1	Sputnik P3 position 12	2012-05-21 05:34:00.0	64°45.77’	5°03.80’		Sputnik Electromagnetic Dipole Transmitter | Sputnik	start transmitting
M87/2-742-1	Sputnik P3 position 12	2012-05-21 05:41:00.0	64°45.77’	5°03.80’		Sputnik Electromagnetic Dipole Transmitter | Sputnik	end transmitting
M87/2-742-1	Sputnik P3 position 12	2012-05-21 05:41:00.0	64°45.77’	5°03.80’		Sputnik Electromagnetic Dipole Transmitter | Sputnik	start heaving
M87/2-742-1	Sputnik P3 position 13	2012-05-21 05:56:00.0	64°45.88’	5°03.80’		Sputnik Electromagnetic Dipole Transmitter | Sputnik	position 13
M87/2-742-1	Sputnik P3 position 13	2012-05-21 05:59:00.0	64°45.88’	5°03.80’		Sputnik Electromagnetic Dipole Transmitter | Sputnik	max. depth
M87/2-742-1	Sputnik P3 position 13	2012-05-21 06:00:00.0	64°45.88’	5°03.80’		Sputnik Electromagnetic Dipole Transmitter | Sputnik	start transmitting
M87/2-742-1	Sputnik P3 position 13	2012-05-21 06:01:00.0	64°45.88’	5°03.80’		Sputnik Electromagnetic Dipole Transmitter | Sputnik	start heaving
M87/2-742-1	Sputnik P3 position 13	2012-05-21 06:01:00.0	64°45.88’	5°03.80’		Sputnik Electromagnetic Dipole Transmitter | Sputnik	end transmitting
M87/2-742-1	Sputnik P3 position 13	2012-05-21 06:24:00.0	64°45.88’	5°03.80’		Sputnik Electromagnetic Dipole Transmitter | Sputnik	on deck
M87/2-743-1	deployment	2012-05-21 10:22:00.0	64°39.80’	5°03.91’	822.3	Deep-towed Active Source Instrument | DASI	end deployment
M87/2-743-1	Dasi line A	2012-05-21 12:59:00.0	64°43.56’	5°04.21’	732.8	Deep-towed Active Source Instrument | DASI	begin profile
M87/2-743-1	Dasi line A	2012-05-21 15:40:00.0	64°47.42’	5°04.40’	716.7	Deep-towed Active Source Instrument | DASI	end profile
M87/2-743-1	Dasi line B	2012-05-21 18:38:00.0	64°45.95’	5°00.81’	731.2	Deep-towed Active Source Instrument | DASI	begin profile
M87/2-743-1	Dasi line B	2012-05-21 21:09:00.0	64°44.29’	5°08.64’	710	Deep-towed Active Source Instrument | DASI	end profile
M87/2-743-1	Dasi line C	2012-05-21 23:13:00.0	64°45.87’	5°05.30’	717.4	Deep-towed Active Source Instrument | DASI	begin profile

METEOR Station	Event	Time [UTC]	Latitude [°N]	Longitude [°E]	Water Depth [mbsl]	Gear	Remarks
M87/2-743-1	Dasi line C	2012-05-22 00:17:00.0	64°46.65’	5°01.53’	731.2	Deep-towed Active Source Instrument | DASI	end profile
M87/2-743-1	Dasi line D	2012-05-22 02:36:00.0	64°44.82’	5°02.14’	730.6	Deep-towed Active Source Instrument | DASI	begin profile
M87/2-743-1	Dasi line D	2012-05-22 04:40:00.0	64°43.64’	5°08.55’	711.7	Deep-towed Active Source Instrument | DASI	alter course
M87/2-743-1	Dasi line D	2012-05-22 06:07:00.0	64°43.27’	5°13.40’	699.8	Deep-towed Active Source Instrument | DASI	alter course
M87/2-743-1	Dasi line D	2012-05-22 06:48:00.0	64°42.82’	5°15.65’	695.9	Deep-towed Active Source Instrument | DASI	end profile
M87/2-743-1	Dasi line E	2012-05-22 10:00:00.0	64°39.96’	5°15.81’	741.2	Deep-towed Active Source Instrument | DASI	begin profile
M87/2-743-1	Dasi line E	2012-05-22 11:33:00.0	64°42.26’	5°16.06’	697.3	Deep-towed Active Source Instrument | DASI	end profile
M87/2-743-1	recovery	2012-05-22 13:34:00.0	64°43.12’	5°19.46’	680.3	Deep-towed Active Source Instrument | DASI	end recovery
M87/2-744-1	OBEM G1	2012-05-22 14:34:00.0	64°45.21’	5°04.09’	718.6	Ocean bottom electro-magnetic receiver | OBEM	released
M87/2-744-1	OBEM G1	2012-05-22 14:47:00.0	64°45.22’	5°04.16’		Ocean bottom electro-magnetic receiver | OBEM	on surface
M87/2-744-1	OBEM G1	2012-05-22 15:06:00.0	64°45.42’	5°03.97’		Ocean bottom electro-magnetic receiver | OBEM	on deck
M87/2-745-1	OBEM G2	2012-05-22 15:23:00.0	64°45.28’	5°03.91’		Ocean bottom electro-magnetic receiver | OBEM	released
M87/2-745-1	OBEM G2	2012-05-22 15:42:00.0	64°45.28’	5°03.94’		Ocean bottom electro-magnetic receiver | OBEM	on surface
M87/2-745-1	OBEM G2	2012-05-22 15:59:00.0	64°45.46’	5°03.78’	716.3	Ocean bottom electro-magnetic receiver | OBEM	on deck
M87/2-746-1	OBEM G3	2012-05-22 16:16:00.0	64°45.23’	5°03.82’		Ocean bottom electro-magnetic receiver | OBEM	released
M87/2-746-1	OBEM G3	2012-05-22 16:35:00.0	64°45.24’	5°03.79’		Ocean bottom electro-magnetic receiver | OBEM	on surface
M87/2-746-1	OBEM G3	2012-05-22 16:50:00.0	64°45.33’	5°03.86’		Ocean bottom electro-magnetic receiver | OBEM	on deck
M87/2-747-1	OBEM G4	2012-05-22 16:55:00.0	64°45.32’	5°03.92’		Ocean bottom electro-magnetic receiver | OBEM	released
M87/2-747-1	OBEM G4	2012-05-22 17:11:00.0	64°45.28’	5°03.44’		Ocean bottom electro-magnetic receiver | OBEM	on surface

METEOR Station	Event	Time [UTC]	Latitude [°N]	Longitude [°E]	Water Depth [mbsl]	Gear	Remarks
M87/2-747-1	OBEM G4	2012-05-22 17:22:00.0	64°45.36’	5°03.70’		Ocean bottom electro-magnetic receiver | OBEM	on deck
M87/2-748-1	OBEM G5	2012-05-22 17:27:00.0	64°45.34’	5°03.68’		Ocean bottom electro-magnetic receiver | OBEM	released
M87/2-748-1	OBEM G5	2012-05-22 17:43:00.0	64°45.28’	5°03.44’		Ocean bottom electro-magnetic receiver | OBEM	on surface
M87/2-748-1	OBEM G5	2012-05-22 17:56:00.0	64°45.42’	5°03.68’		Ocean bottom electro-magnetic receiver | OBEM	on deck
M87/2-749-1	OBEM G6	2012-05-22 18:00:00.0	64°45.40’	5°03.64’		Ocean bottom electro-magnetic receiver | OBEM	released
M87/2-749-1	OBEM G6	2012-05-22 18:18:00.0	64°45.31’	5°03.35’		Ocean bottom electro-magnetic receiver | OBEM	on surface
M87/2-749-1	OBEM G6	2012-05-22 18:33:00.0	64°45.44’	5°03.31’		Ocean bottom electro-magnetic receiver | OBEM	on deck
M87/2-750-1	MB-PS profile 37	2012-05-22 19:07:00.0	64°45.26’	5°07.78’	705.9	Multibeam + Parasound | MB-PS	begin profile
M87/2-750-1	MB-PS profile 37	2012-05-22 20:46:00.0	64°48.50’	4°41.83’	826.8	Multibeam + Parasound | MB-PS	alter course
M87/2-750-1	MB-PS profile 37	2012-05-22 20:54:00.0	64°47.89’	4°40.58’	829.3	Multibeam + Parasound | MB-PS	alter course
M87/2-750-1	MB-PS profile 37	2012-05-22 22:34:00.0	64°44.20’	5°07.44’	719.3	Multibeam + Parasound | MB-PS	alter course
M87/2-750-1	MB-PS profile 37	2012-05-22 22:42:00.0	64°43.27’	5°07.40’	728.3	Multibeam + Parasound | MB-PS	alter course
M87/2-750-1	MB-PS profile 37	2012-05-23 00:22:00.0	64°46.65’	4°39.63’	832.1	Multibeam + Parasound | MB-PS	alter course
M87/2-750-1	MB-PS profile 37	2012-05-23 00:30:00.0	64°45.95’	4°38.89’	831.8	Multibeam + Parasound | MB-PS	alter course
M87/2-750-1	MB-PS profile 37	2012-05-23 02:13:00.0	64°42.20’	5°06.63’	743.1	Multibeam + Parasound | MB-PS	end profile
M87/2-751-1	OBEM S1	2012-05-23 02:37:00.0	64°44.48’	5°03.61’	731	Ocean bottom electro-magnetic receiver | OBEM	released
M87/2-751-1	OBEM S1	2012-05-23 02:52:00.0	64°44.48’	5°03.60’		Ocean bottom electro-magnetic receiver | OBEM	released
M87/2-751-1	OBEM S1	2012-05-23 03:31:00.0	64°44.51’	5°03.58’		Ocean bottom electro-magnetic receiver | OBEM	on surface
M87/2-751-1	OBEM S1	2012-05-23 03:56:00.0	64°44.72’	5°02.47’		Ocean bottom electro-magnetic receiver | OBEM	on deck
M87/2-752-1	OBEM S2	2012-05-23 03:58:00.0	64°44.70’	5°02.38’		Ocean bottom electro-magnetic receiver | OBEM	released
M87/2-753-1	OBEM S3	2012-05-23 04:47:00.0	64°45.28’	5°03.51’		Ocean bottom electro-magnetic receiver | OBEM	released
M87/2-752-1	OBEM S2	2012-05-23 04:52:00.0	64°45.28’	5°03.51’		Ocean bottom electro-magnetic receiver | OBEM	on surface

METEOR Station	Event	Time [UTC]	Latitude [°N]	Longitude [°E]	Water Depth [mbsl]	Gear	Remarks
M87/2-752-1	OBEM S2	2012-05-23 05:09:00.0	64°45.40’	5°02.92’		Ocean bottom electro-magnetic receiver | OBEM	on deck
M87/2-753-1	OBEM S3	2012-05-23 05:38:00.0	64°45.48’	5°03.20’		Ocean bottom electro-magnetic receiver | OBEM	on surface
M87/2-753-1	OBEM S3	2012-05-23 05:48:00.0	64°45.45’	5°03.19’		Ocean bottom electro-magnetic receiver | OBEM	on deck
M87/2-754-1	OBEM S4	2012-05-23 05:50:00.0	64°45.44’	5°03.14’		Ocean bottom electro-magnetic receiver | OBEM	released
M87/2-754-1	OBEM S4	2012-05-23 06:31:00.0	64°45.56’	5°03.06’		Ocean bottom electro-magnetic receiver | OBEM	on surface
M87/2-754-1	OBEM S4	2012-05-23 06:43:00.0	64°45.64’	5°03.24’		Ocean bottom electro-magnetic receiver | OBEM	on deck
M87/2-755-1	OBEM S5	2012-05-23 06:44:00.0	64°45.64’	5°03.24’		Ocean bottom electro-magnetic receiver | OBEM	released
M87/2-755-1	OBEM S5	2012-05-23 07:25:00.0	64°46.14’	5°02.73’		Ocean bottom electro-magnetic receiver | OBEM	on surface
M87/2-755-1	OBEM S5	2012-05-23 07:38:00.0	64°46.32’	5°03.39’		Ocean bottom electro-magnetic receiver | OBEM	on deck
M87/2-756-1	OBEM S6	2012-05-23 07:40:00.0	64°46.32’	5°03.39’		Ocean bottom electro-magnetic receiver | OBEM	released
M87/2-756-1	OBEM S6	2012-05-23 08:11:00.0	64°46.15’	5°03.56’		Ocean bottom electro-magnetic receiver | OBEM	on surface
M87/2-756-1	OBEM S6	2012-05-23 08:34:00.0	64°46.17’	5°01.23’		Ocean bottom electro-magnetic receiver | OBEM	on deck
M87/2-757-1	OBEM S7	2012-05-23 08:36:00.0	64°46.17’	5°01.18’		Ocean bottom electro-magnetic receiver | OBEM	released
M87/2-757-1	OBEM S7	2012-05-23 09:04:00.0	64°45.88’	5°02.55’		Ocean bottom electro-magnetic receiver | OBEM	on surface
M87/2-757-1	OBEM S7	2012-05-23 09:17:00.0	64°45.72’	5°03.16’		Ocean bottom electro-magnetic receiver | OBEM	on deck
M87/2-758-1	OBEM S8	2012-05-23 09:20:00.0	64°45.72’	5°03.11’		Ocean bottom electro-magnetic receiver | OBEM	released
M87/2-758-1	OBEM S8	2012-05-23 09:50:00.0	64°45.48’	5°04.57’		Ocean bottom electro-magnetic receiver | OBEM	on surface
M87/2-758-1	OBEM S8	2012-05-23 10:05:00.0	64°45.34’	5°05.23’		Ocean bottom electro-magnetic receiver | OBEM	on deck
M87/2-759-1	HyBIS transect 1	2012-05-23 11:11:00.0	64°39.05’	5°05.26’		Hydraulic Benthic Interactive Sampler | HyBIS	surface

METEOR Station	Event	Time [UTC]	Latitude [°N]	Longitude [°E]	Water Depth [mbsl]	Gear	Remarks
M87/2-759-1	HyBIS transect 1	2012-05-23 12:03:00.0	64°39.05’	5°05.25’	844.8	Hydraulic Benthic Interactive Sampler | HyBIS	on deck (problems)
M87/2-759-1	HyBIS transect 1	2012-05-23 15:43:00.0	64°39.05’	5°05.27’	838.6	Hydraulic Benthic Interactive Sampler | HyBIS	surface
M87/2-759-1	HyBIS transect 1	2012-05-23 16:37:00.0	64°39.06’	5°05.27’	841.4	Hydraulic Benthic Interactive Sampler | HyBIS	sea bottom visible
M87/2-759-1	HyBIS transect 1	2012-05-23 16:41:00.0	64°39.06’	5°05.27’	833.3	Hydraulic Benthic Interactive Sampler | HyBIS	begin profile
M87/2-759-1	HyBIS transect 1	2012-05-23 18:16:00.0	64°38.50’	5°05.35’	876.8	Hydraulic Benthic Interactive Sampler | HyBIS	end profile
M87/2-759-1	HyBIS transect 1	2012-05-23 18:17:00.0	64°38.49’	5°05.35’	876.8	Hydraulic Benthic Interactive Sampler | HyBIS	start heaving
M87/2-759-1	HyBIS transect 1	2012-05-23 18:56:00.0	64°38.36’	5°05.04’	884.4	Hydraulic Benthic Interactive Sampler | HyBIS	on deck
M87/2-759-1	HyBIS transect 2	2012-05-23 19:42:00.0	64°35.54’	4°51.97’	1073.9	Hydraulic Benthic Interactive Sampler | HyBIS	surface
M87/2-759-1	HyBIS transect 2	2012-05-23 20:33:00.0	64°35.40’	4°51.79’	1081.5	Hydraulic Benthic Interactive Sampler | HyBIS	sea bottom visible
M87/2-759-1	HyBIS transect 2	2012-05-23 20:36:00.0	64°35.39’	4°51.78’	1080.4	Hydraulic Benthic Interactive Sampler | HyBIS	max. depth
M87/2-759-1	HyBIS transect 2	2012-05-23 21:53:00.0	64°34.96’	4°51.23’	1100.7	Hydraulic Benthic Interactive Sampler | HyBIS	begin profile
M87/2-759-1	HyBIS transect 2	2012-05-23 22:21:00.0	64°34.82’	4°51.05’	1102.8	Hydraulic Benthic Interactive Sampler | HyBIS	end profile
M87/2-759-1	HyBIS transect 2	2012-05-23 23:03:00.0	64°34.84’	4°50.96’	1102.9	Hydraulic Benthic Interactive Sampler | HyBIS	on deck
M87/2-760-1	deployment	2012-05-24 00:45:00.0	64°30.17’	4°49.44’	1307.8	2D-Multi-Channel-Seismic | 2D-MCS	end deployment
M87/2-761-1	MB-PS profile 38	2012-05-24 01:12:00.0	64°30.38’	4°50.16’	1302.2	Multibeam + Parasound | MB-PS	begin profile
M87/2-760-1	2D seismic profile 08	2012-05-24 01:12:00.0	64°30.38’	4°50.16’	1302.2	2D-Multi-Channel-Seismic | 2D-MCS	begin profile
M87/2-760-1	2D seismic profile 08	2012-05-24 01:58:00.0	64°33.73’	4°49.63’	1165.9	2D-Multi-Channel-Seismic | 2D-MCS	alter course
M87/2-761-1	MB-PS profile 38	2012-05-24 01:58:00.0	64°33.73’	4°49.63’	1165.9	Multibeam + Parasound | MB-PS	alter course
M87/2-761-1	MB-PS profile 38	2012-05-24 02:26:00.0	64°35.39’	4°51.69’	1081.6	Multibeam + Parasound | MB-PS	alter course
M87/2-760-1	2D seismic profile 08	2012-05-24 02:26:00.0	64°35.39’	4°51.69’	1081.6	2D-Multi-Channel-Seismic | 2D-MCS	alter course

METEOR Station	Event	Time [UTC]	Latitude [°N]	Longitude [°E]	Water Depth [mbsl]	Gear	Remarks
M87/2-760-1	2D seismic profile 08	2012-05-24 02:50:00.0	64°36.93’	4°50.72’	1040.3	2D-Multi-Channel-Seismic | 2D-MCS	alter course
M87/2-761-1	MB-PS profile 38	2012-05-24 02:50:00.0	64°36.93’	4°50.72’	1040.3	Multibeam + Parasound | MB-PS	alter course
M87/2-761-1	MB-PS profile 38	2012-05-24 04:29:00.0	64°44.47’	4°51.54’	791.8	Multibeam + Parasound | MB-PS	end profile
M87/2-760-1	2D seismic profile 08	2012-05-24 04:29:00.0	64°44.47’	4°51.54’	791.8	2D-Multi-Channel-Seismic | 2D-MCS	end profile
M87/2-760-1	2D seismic profile 09	2012-05-24 04:47:00.0	64°44.46’	4°53.76’	771.9	2D-Multi-Channel-Seismic | 2D-MCS	begin profile
M87/2-761-1	MB-PS profile 39	2012-05-24 04:47:00.0	64°44.46’	4°53.76’	771.9	Multibeam + Parasound | MB-PS	begin profile
M87/2-761-1	MB-PS profile 39	2012-05-24 07:50:00.0	64°30.85’	4°52.74’	1263.5	Multibeam + Parasound | MB-PS	end profile
M87/2-760-1	2D seismic profile 09	2012-05-24 07:50:00.0	64°30.85’	4°52.74’	1263.5	2D-Multi-Channel-Seismic | 2D-MCS	end profile
M87/2-760-1	2D seismic profile 10	2012-05-24 08:12:00.0	64°30.80’	4°55.45’	1245.6	2D-Multi-Channel-Seismic | 2D-MCS	begin profile
M87/2-761-1	MB-PS profile 40	2012-05-24 08:12:00.0	64°30.80’	4°55.45’	1245.6	Multibeam + Parasound | MB-PS	begin profile
M87/2-760-1	2D seismic profile 10	2012-05-24 11:11:00.0	64°44.34’	4°56.06’	764.2	2D-Multi-Channel-Seismic | 2D-MCS	end profile
M87/2-761-1	MB-PS profile 40	2012-05-24 11:11:00.0	64°44.34’	4°56.06’	764.2	Multibeam + Parasound | MB-PS	end profile
M87/2-760-1	2D seismic profile 11	2012-05-24 11:32:00.0	64°44.38’	4°58.34’	756.9	2D-Multi-Channel-Seismic | 2D-MCS	begin profile
M87/2-761-1	MB-PS profile 41	2012-05-24 11:32:00.0	64°44.38’	4°58.34’	756.9	Multibeam + Parasound | MB-PS	begin profile
M87/2-760-1	2D seismic profile 11	2012-05-24 14:33:00.0	64°30.70’	4°58.15’	1219.8	2D-Multi-Channel-Seismic | 2D-MCS	end profile
M87/2-761-1	MB-PS profile 41	2012-05-24 14:33:00.0	64°30.70’	4°58.15’	1219.8	Multibeam + Parasound | MB-PS	end profile
M87/2-761-1	MB-PS profile 42	2012-05-24 14:53:00.0	64°30.75’	5°00.82’	1185.5	Multibeam + Parasound | MB-PS	begin profile
M87/2-760-1	2D seismic profile 12	2012-05-24 14:53:00.0	64°30.75’	5°00.82’	1185.5	2D-Multi-Channel-Seismic | 2D-MCS	begin profile
M87/2-760-1	2D seismic profile 12	2012-05-24 17:54:00.0	64°44.34’	5°00.64’	739.2	2D-Multi-Channel-Seismic | 2D-MCS	end profile
M87/2-761-1	MB-PS profile 42	2012-05-24 17:54:00.0	64°44.34’	5°00.64’	739.2	Multibeam + Parasound | MB-PS	end profile
M87/2-761-1	MB-PS profile 43	2012-05-24 18:14:00.0	64°44.28’	5°02.90’	732	Multibeam + Parasound | MB-PS	begin profile
M87/2-760-1	2D seismic profile 13	2012-05-24 18:14:00.0	64°44.28’	5°02.90’	732	2D-Multi-Channel-Seismic | 2D-MCS	begin profile
M87/2-761-1	MB-PS profile 43	2012-05-24 20:12:00.0	64°35.47’	5°02.96’	993.2	Multibeam + Parasound | MB-PS	end profile
M87/2-760-1	2D seismic profile 13	2012-05-24 20:12:00.0	64°35.47’	5°02.96’	993.2	2D-Multi-Channel-Seismic | 2D-MCS	end profile

METEOR Station	Event	Time [UTC]	Latitude [°N]	Longitude [°E]	Water Depth [mbsl]	Gear	Remarks
M87/2-760-1	2D seismic profile 14	2012-05-24 20:36:00.0	64°35.51’	5°05.99’	978.1	2D-Multi-Channel-Seismic | 2D-MCS	begin profile
M87/2-761-1	MB-PS profile 44	2012-05-24 20:36:00.0	64°35.51’	5°05.99’	978.1	Multibeam + Parasound | MB-PS	begin profile
M87/2-760-1	2D seismic profile 14	2012-05-24 22:09:00.0	64°42.46’	5°04.62’	748.5	2D-Multi-Channel-Seismic | 2D-MCS	alter course
M87/2-761-1	MB-PS profile 44	2012-05-24 22:09:00.0	64°42.46’	5°04.62’	748.5	Multibeam + Parasound | MB-PS	alter course
M87/2-760-1	2D seismic profile 14	2012-05-24 22:31:00.0	64°43.88’	5°06.46’	728	2D-Multi-Channel-Seismic | 2D-MCS	end profile
M87/2-761-1	MB-PS profile 44	2012-05-24 22:31:00.0	64°43.88’	5°06.46’	728	Multibeam + Parasound | MB-PS	end profile
M87/2-761-1	MB-PS profile 45	2012-05-24 22:40:00.0	64°44.43’	5°06.12’	723.3	Multibeam + Parasound | MB-PS	begin profile
M87/2-760-1	2D seismic profile 15	2012-05-24 22:40:00.0	64°44.43’	5°06.12’	723.3	2D-Multi-Channel-Seismic | 2D-MCS	begin profile
M87/2-760-1	2D seismic profile 15	2012-05-24 22:59:00.0	64°45.15’	5°03.25’	726.7	2D-Multi-Channel-Seismic | 2D-MCS	end profile
M87/2-761-1	MB-PS profile 45	2012-05-24 22:59:00.0	64°45.15’	5°03.25’	726.7	Multibeam + Parasound | MB-PS	end profile
M87/2-761-1	MB-PS profile 46	2012-05-24 23:35:00.0	64°44.88’	5°03.23’	725.5	Multibeam + Parasound | MB-PS	begin profile
M87/2-760-1	2D seismic profile 16	2012-05-24 23:35:00.0	64°44.88’	5°03.23’	725.5	2D-Multi-Channel-Seismic | 2D-MCS	begin profile
M87/2-761-1	MB-PS profile 46	2012-05-25 03:53:00.0	64°43.52’	5°48.72’	365.2	Multibeam + Parasound | MB-PS	end profile
M87/2-760-1	2D seismic profile 16	2012-05-25 03:53:00.0	64°43.52’	5°48.72’	365.2	2D-Multi-Channel-Seismic | 2D-MCS	end profile
M87/2-760-1	2D seismic profile 17	2012-05-25 04:08:00.0	64°42.79’	5°49.12’	360.7	2D-Multi-Channel-Seismic | 2D-MCS	begin profile
M87/2-761-1	MB-PS profile 47	2012-05-25 04:08:00.0	64°42.79’	5°49.12’	360.7	Multibeam + Parasound | MB-PS	begin profile
M87/2-760-1	2D seismic profile 17	2012-05-25 05:19:00.0	64°42.41’	5°36.06’	544.9	2D-Multi-Channel-Seismic | 2D-MCS	end profile
M87/2-761-1	MB-PS profile 47	2012-05-25 05:19:00.0	64°42.41’	5°36.06’	544.9	Multibeam + Parasound | MB-PS	end profile
M87/2-761-1	MB-PS profile 48	2012-05-25 05:37:00.0	64°41.39’	5°36.13’	543.4	Multibeam + Parasound | MB-PS	begin profile
M87/2-760-1	2D seismic profile 18	2012-05-25 05:37:00.0	64°41.39’	5°36.13’	543.4	2D-Multi-Channel-Seismic | 2D-MCS	begin profile
M87/2-761-1	MB-PS profile 48	2012-05-25 06:46:00.0	64°42.11’	5°48.87’	356.7	Multibeam + Parasound | MB-PS	end profile
M87/2-760-1	2D seismic profile 18	2012-05-25 06:46:00.0	64°42.11’	5°48.87’	356.7	2D-Multi-Channel-Seismic | 2D-MCS	end profile
M87/2-761-1	MB-PS profile 49	2012-05-25 07:04:00.0	64°41.12’	5°49.52’	355.1	Multibeam + Parasound | MB-PS	begin profile
M87/2-760-1	2D seismic profile 19	2012-05-25 07:04:00.0	64°41.12’	5°49.52’	355.1	2D-Multi-Channel-Seismic | 2D-MCS	begin profile

METEOR Station	Event	Time [UTC]	Latitude [°N]	Longitude [°E]	Water Depth [mbsl]	Gear	Remarks
M87/2-760-1	2D seismic profile 19	2012-05-25 10:43:00.0	64°32.53’	5°14.76’	984.6	2D-Multi-Channel-Seismic | 2D-MCS	end profile
M87/2-761-1	MB-PS profile 49	2012-05-25 10:43:00.0	64°32.53’	5°14.76’	984.6	Multibeam + Parasound | MB-PS	end profile
M87/2-761-1	MB-PS profile 50	2012-05-25 10:46:00.0	64°32.47’	5°14.23’	990	Multibeam + Parasound | MB-PS	begin profile
M87/2-760-1	2D seismic profile 20	2012-05-25 10:46:00.0	64°32.47’	5°14.23’	990	2D-Multi-Channel-Seismic | 2D-MCS	begin profile
M87/2-760-1	2D seismic profile 20	2012-05-25 12:00:00.0	64°32.44’	5°00.65’	1136.6	2D-Multi-Channel-Seismic | 2D-MCS	end profile
M87/2-761-1	MB-PS profile 50	2012-05-25 12:00:00.0	64°32.44’	5°00.65’	1136.6	Multibeam + Parasound | MB-PS	end profile
M87/2-760-1	recovery	2012-05-25 12:23:00.0	64°32.47’	4°59.27’	1147.1	2D-Multi-Channel-Seismic | 2D-MCS	end recovery
M87/2-762-1	SVP Nyegga-2	2012-05-25 12:40:00.0	64°32.54’	4°59.07’	1144.7	Sound Velocity Profiler | SVP	to water
M87/2-762-1	SVP Nyegga-2	2012-05-25 13:08:00.0	64°32.64’	4°59.06’	1143.7	Sound Velocity Profiler | SVP	at depth
M87/2-762-1	SVP Nyegga-2	2012-05-25 13:40:00.0	64°32.64’	4°58.77’	1146.5	Sound Velocity Profiler | SVP	on deck

8 Data and Sample Storage and Availability

A Cruise Summary Report (CRS) was compiled and submitted to DOD (Deutsches Ozeanographisches Datenzentrum), BSH, Hamburg, immediately after the cruise.

Concerning data storage a joint data management team of GEOMAR and Kiel University organizes and supervises data storage and publication by marine science projects in a web based multi-user system. In a first phase, data are only available to the project user groups. After a three year proprietary time the data management team will publish these data by dissemination to national and international data archives, i.e. the data will be submitted to PANGAEA no later than September, 2015. Digital object identifiers (DOIs) are automatically assigned to data sets archived in the PANGAEA Open Access library making them publically retrievable, citable and reusable for the future.

All metadata are immediately available publically via the following link pointing at the GEOMAR portal (https://portal.geomar.de/metadata/leg/show/316178).
In addition the portal provides a single downloadable KML formatted file (https://portal.geomar.de/metadata/leg/kmlexport/316178) which retrieves and combines up-to-date cruise (M87/2) related information, links to restricted data and to published data for visualization e.g. in GoogleEarth. Cruise related data can be found on PANGAEA at: http://www.pangaea.de/search?q=campaign%3A"M87/2"

Data availability

Data type	Database	Available	Contact
Seismic data	Pangaea/GEOMAR	01.08.2016	Dirk Klaeschen
Parasound data	Pangaea/GEOMAR	01.08.2016	Dirk Klaeschen
Multi-beam data	Pangaea/GEOMAR	01.08.2016	Ingo Klaucke
Sputnik CSEM data	Pangaea	01.08.2016	Marion Jegen
DASI CSEM data	Pangaea	01.08.2016	Karen Weitemeyer / NOCS

9 Acknowledgements

We like to thank captain Michael Schneider, his officers and crew of RV Meteor for their professional support of our science programme and for very pleasant company on board. We also thank our technical team Martin Wollatz-Vogt, Gero Wetzel and Torge Matthiessen for the many hours of relentless effort fixing the scientific equipment.

The ship time of RV Meteor was provided by the Deutsche Forschungsgemeinschaft within the core program METEOR/MERIAN. Financial support for the different projects carried out during the cruise was provided though the BMBF Sugar 2 project and funding through the institutions involved. We gratefully appreciate all this support.

10 References

Andreassen K., Berteussen K.A., Sognnes H., Henneberg, K., Langhammer, J., Mienert, J., 2003. Multicomponent ocean bottom cable data in gas hydrate investigation offshore of Norway, Journal of Geophysical Research-Solid Earth 108, B82399.

Ellis, M.A., Minshull, T.A., Sinha, M.C., Best, A.I., 2008. Joint seismic/electrical effective medium modelling of hydrate-bearing marine sediments and an application to the Vancouver Island margin. Proceedings of the 6th International Conference on Gas Hydrates, Vancouver, British Columbia, Canada, July 6-10, 2008.

Gay, A., Mourgues, R., Berndt, C., Bureau, D., Planke, S., Laurent, D., Gautier, S., Lauer, C., Loggia, D., 2012. Anatomy of a fluid pipe in the Norway Basin: initiation, propagation and 3D shape. Marine Geology 332-334, 75-88.

Hansen, J.P.V., Cartwright, J.A., Huuse, M., Clausen, O.R., 2005. 3D seismic expression of fluid migration and mud mobilization on the Gjallar Ridge, offshore Mid-Norway. Basin Research 17, 123-139.

Hensen, C., Nuzzo, M., Hornibrook, E., Pinheiro, L. M., Bock, B., Magalhães, V. H., & Brückmann, W. (2007). Sources of mud volcano fluids in the Gulf of Cadiz - indications for hydrothermal imprint. Geochimica Et Cosmochimica Acta, 71, 1232–1248.

Hjelstuen, B.O., Haflidason, H. Sejrup, H.-P., Nygård, A., 2010. Sedimentary and structural control on pockmark development—evidence from the Nyegga pockmark field, NW European margin. Geo-Marine Letters 30, 221–230.

Higgins, A., Schrag, D.P., 2006. Beyond methane: Towards a theory for the Paleocene-Eocene Thermal Maximum. Earth and Planetary Science Letters 245, 523-537.

Hovland, M. and Svensen, H., 2006. Submarine pingoes: Indicators of shallow gas hydrates in a pockmark at Nyegga, Norwegian Sea. Marine Geology 228, 15-23.

Hovland, M. and O. T. Gudmestad, 2001. Potential influence of gas hydrates on seabed installations. In: Paull, C.K., Dillon, W.P. (Eds.), Natural Gas Hydrates: Occurrence, Distribution, and Detection. AGU Monograph Series 24, pp. 300-309.

Ivanov, M., Mazzini A., Blinova V., Kozlova E., Laberg J.S., Mtveeva T., Taviani M. and Kskov N. 2010, Seep mounds on the Southern Vøring Plateau (offshore Norway), Marine and Petroleum Geology 27, pp 1235–1261.

Mienert, J., Vanneste, M., Haflidason, H., and Bünz, S. (2010) Norwegian margin outer shelf cracking: a consequence of climate-induced gas hydrate dissociation? International Journal for Earth Sciences, DOI 10.1007/s00531-010-0536-z.

Planke, S., Rassmussen, T., Rey, S.S. and Myklebust, R. (2005) Seismic characteristics and distribution of volcanic intrusions and hydrothermal vent complexes in the Vøring and Møre basins. In: Doré, A.G. & Vining, B. (eds) Petroleum Geology: North-West Europe and Global Perspectives—Proceedings of the 6th Petroleum Geology Conference. Geological Society, London, 833–844.

Schmale, O., Greinert, J., and Rehder, G. (2005) Methane emission from high-intensity marine gas seeps in the Black Sea into the atmosphere. Geophysical Research Letters 32, L07609, doi: 10.1029/2004GL021138.

Schwalenberg K., W. Wood., I. Pecher, S. Henrys, M. Jegen and R. Coffin (2009a) Geochemical Data for Gas Hydrate Distribution Across Porangahau Ridge, New Zealand, Marine Geology.

Schwalenberg, K., Häckel, M., Poort, J. and Jegen-Kulcsar, M. (2009b) Evaluation of gas hydrate deposits in an active seep using marine controlled source electromagnetics; results from Opouawe Bank, Hikurangi Margin, New Zealand. Marine Geology, doi:10.1016/j.margeo.2009.07.006

Svensen, H., Jamtveit, B., Planke, S. and Chevallier, L. (2006) Structure and evolution of hydrothermal vent complexes in the Karoo Basin, South Africa. Journal of the Geological Society, 163: 671-682.

Svensen, H., Planke, S. and Malthe-Sørensen, A. (2004). Release of methane from a volcanic basin as a mechanism for initial Eocene global warming. Nature, 429: 542-545.

Wallmann K, Linke P, Suess E, Bohrmann G, Sahling H, Schlüter M, Dählmann A, Lammers S, Greinert J, von Mirbach N (1997) Quantifying fluid flow, solute mixing, and biogeochemical turnover at cold vents of the eastern Aleutian subduction zone. Geochimica et Cosmochimica Acta 61, 5209-5219.

Weitemeyer K.A., S. C. Constable, K. W. Key, and J. P. Behrens (2006) First results from a marine controlled-source electromagnetic survey to detect gas hydrates offshore Oregon, Geophys Res. Lett., 33, doi:10.1029/2005GL024896.

Westbrook, G. K., R. Exley, T. Minshull, H. Nouzé, A. Gailler, T. Jose, S. Ker and A. Plaza (2008) High-resolution 3D seismic investigations of hydrate-bearing fluid escape chimneys in the Nyegga region of the Voring Plateau, Norway, Proc. 6th Int. Conf. on Natural Gas Hydrates, paper 5597.

Wood, W.T., Gettrust, J.F., Chapman, N.R., Spence, G.D., and Hyndman, R.D. (2002) Decreased stability of methane hydrates in marine sediments owing to phase-boundary roughness: Nature, v. 420, p. 656-660.

Zachos, J., M. Pagani, et al. (2001) Trends, rhythms, and aberrations in global climate 65 Ma to present. Science 292(5517): 686-693.